

Faculdade de Engenharia da Universidade do Porto



FEUP

**Veículo elétrico com interface para a rede
elétrica**

Grid interface for an electric vehicle

Luís Miguel Faria Miranda

Dissertation carried out under the
Master in Electrical and Computers Engineering
Branch: Automation

Supervisor: Prof. Doutor Rui Manuel Esteves Araújo

June 2011

A Dissertação intitulada

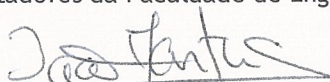
“veículo Eléctrico com Interface para a Rede Eléctrica”

foi aprovada em provas realizadas em 21-07-2011

o júri



Presidente Professor Doutor Luis Miguel Pinho de Almeida
Professor Associado do Departamento de Engenharia Electrotécnica e de
Computadores da Faculdade de Engenharia da Universidade do Porto

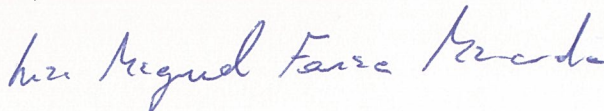


Professor Doutor João Francisco Alves Martins
Professor Auxiliar Departamento de Electrotécnica da Faculdade de Ciências e
Tecnologia da Universidade Nova de Lisboa



Professor Doutor Rui Manuel Esteves Araújo
Professor Auxiliar do Departamento de Engenharia Eletrotécnica e de Computadores
da Faculdade de Engenharia da Universidade do Porto

O autor declara que a presente dissertação (ou relatório de projeto) é da sua exclusiva autoria e foi escrita sem qualquer apoio externo não explicitamente autorizado. Os resultados, ideias, parágrafos, ou outros extractos tomados de ou inspirados em trabalhos de outros autores, e demais referências bibliográficas usadas, são corretamente citados.



Autor - Luis Miguel Faria Miranda

Abstract

The field of isolated DC-DC converter is an important area of power electronics and it is growing with electrical vehicles. The two main applications of these converters are related to the need of isolation between the power electronics system and grid during the charging period and the implementation of low voltage DC bus, used to supply auxiliary loads. This new requirements lead to a demand for new conversion architectures and solutions, with high values of efficiency and power density. These converters should avoid the usage of bulky low frequency transformers in the near term for low and medium-low power chargers. Topologies with soft-switching capability can be of particular interest for this application.

In this work is performed a study of the most common solutions for this purpose and a selection is carried out based on previously defined criteria. The development of the power converter is focused on the DC-DC stage whose topology is so called Dual Active Bridge. The converter structure, operation modes and particular aspects are presented and discussed. To conclude this analysis the converter was simulated in order to evaluate its performance. After that the main components which constitute the converter are selected and the high frequency power transformer is designed with special detail since it is the most critical part of the power stage.

The systems for interface with the power stage were then developed and implemented, i.e. a system to measure the variables and a system to act the converter according to the phase-shift control method. With all components working correctly, several tests were performed for modeling the power transformer and also in order to validate its operation as Dual Active Bridge.

Resumo

O campo dos conversores DC-DC isolados é uma área importante da electrónica de potência e está em crescimento com os veículos eléctricos. As duas principais aplicações destes conversores estão relacionadas com a necessidade de isolamento entre o sistema electrónico de potência do carro e a rede eléctrica durante o período de carga e a implementação de um barramento DC de baixa tensão, utilizado para alimentar as cargas auxiliares. Estes novos requisitos levam a uma procura por novas soluções e arquitecturas de conversão, com elevados valores de rendimento e densidade de potência. Tais conversores deverão evitar a utilização de volumosos transformadores de baixa frequência a curto prazo para carregadores de baixa ou média baixa potência. As topologias com capacidade de soft-switching podem ser de especial interesse para esta aplicação.

Neste trabalho é realizado um estudo das soluções mais comuns para esta aplicação e é feita uma selecção baseada em critérios previamente definidos. O desenvolvimento do conversor de potência é focado no andar DC-DC cuja topologia é chamada de Dual Active Bridge. A estrutura do conversor, modos de funcionamento e particularidades serão apresentadas e discutidas. Para concluir esta análise, o conversor foi simulado com o objectivo de estudar o seu desempenho. Após isso os principais componentes que constituem o conversor foram seleccionados e o transformador de alta frequência foi projectado de forma mais detalhada visto que é o componente mais crítico do andar de potência.

Os sistemas para interface com o andar de potência foram então desenvolvidos, i.e. o sistema para medição das variáveis e o sistema para comandar o conversor de acordo com o método de controlo por esfasamento. Com todos os componentes a funcionar correctamente, vários testes foram realizados para modelização do transformador de potência e também com o objectivo de validar o funcionamento do conversor como Dual Active Bridge.

Agradecimentos

Em primeiro lugar, gostaria de agradecer ao meu orientador, Prof. Doutor Rui Araújo pela confiança depositada nas minhas capacidades e por todo o seu empenho e disponibilidade na realização deste projecto e ao Engenheiro Ricardo Ferreira pela constante disponibilidade no desenvolvimento das tarefas reportadas neste documento.

Ao INESC Porto por ter suportado a realização deste trabalho, e mais em particular à equipa do projecto REIVE - Redes eléctricas inteligentes com veículos eléctricos com quem trabalhei directamente durante este tempo.

Aos meus colegas de curso, em particular aos finalistas da especialização em Electronica e Sistemas do major de Automação, com muitos dos quais partilho além do gosto pela área uma grande amizade.

À Joana, cujo o amor, apoio e compreensão estiveram sempre presentes, principalmente nos momentos mais difíceis.

E por último, mas de forma muito sincera, aos meus pais que sempre acreditaram em mim e que tornaram possível concluir a minha frequência no Mestrado Integrado em Engenharia Electrotécnica e de Computadores.

Contents

Abstract	iii
Resumo	v
Agradecimentos	vii
Contents	ix
List of Figures	xiii
List of Tables	xvii
Acronyms	xxi
Chapter 1	1
Introduction.....	1
1.1 The Electric Vehicle.....	1
1.2 Motivations and Challenges in Electric Vehicle Integration	3
1.3 The Vehicle-to-Grid (V2G) concept.....	4
1.4 Objectives of the work	5
1.5 Work plan	5
1.6 Map of the document	7
Chapter 2	9
State of the art.....	9
2.1 Modern Electric Vehicles	9
2.1.1 Storage systems	10
2.1.2 Traction Motors.....	11
2.1.3 Motor drives	12
2.1.4 Auxiliary Loads Supply.....	12
2.2 Electric Vehicles Market.....	12
2.2.1 V2G Market forecast for US.....	14
2.3 Standards.....	15
2.4 Charging systems	19
2.4.1 AC Charging Levels 1 and 2	19
2.4.2 DC Fast Charging	20
2.4.3 Commercial systems	21
2.5 Systematization of power converters	22
2.6 Summary	32

Chapter 3.....	33
Topology selection.....	33
3.1 Basic topologies.....	33
3.1.1 AC-DC.....	33
3.1.2 DC-DC	35
3.2 Association of AC-DC and DC-DC stages	37
3.3 Criteria	38
3.4 Comparative table.....	40
3.5 Discussion	40
3.6 Proposed architecture	41
3.7 Summary	41
Chapter 4.....	43
Dual active bridge converter	43
4.1 Introduction	43
4.2 Steady-state analysis	45
4.3 Boundaries for zero-voltage switching.....	49
4.4 Simulation.....	50
4.4.1 Model and parameters	51
4.4.2 Simulation results	53
4.4.3 Maximum leakage inductance estimation	54
4.4.4 Capacitors dimensioning	57
4.5 Summary	59
Chapter 5.....	61
Prototype design	61
5.1 Power switches	61
5.2 Drive circuit	63
5.2.1 Parameter setting.....	65
5.3 Interface board	70
5.4 Capacitors.....	72
5.4.1 Electrolytic capacitors	73
5.4.2 Metalized Polypropylene Film Capacitors (MKP).....	74
5.5 Transformer design.....	76
5.5.1 Core selection	78
5.5.2 Number of turns	79
5.5.3 Core losses	81
5.5.4 Wire	81
5.5.5 Windings	83
5.5.6 Mean turn length	85
5.5.7 Total wire length.....	85
5.5.8 Wire resistance	85
5.6 Summary	86
Chapter 6.....	87
Control system and results.....	87
6.1 Measurements	88
6.2 Acquisition	91
6.2.1 Error analysis.....	93
6.3 Phase-Shifted square wave generation	94
6.4 Transformer parameterization	95
6.4.1 Transformer model	95
6.4.2 DC winding resistance measurement	97
6.4.3 Short circuit test	98
6.4.4 Open circuit test	101

6.4.5 Model and validation	103
6.5 Experimental results	106
6.5.1 Transformer load tests	106
6.5.2 Converter operation	108
6.6 Summary	111
Chapter 7.....	113
Conclusions and future work.....	113
7.1 Conclusions	113
7.2 Future work.....	114
References	115
Annex A - Workplan	119

List of Figures

Figure 1.1 Basic diagram of Plug-in Hybrid Electric Vehicle (PHEV)	2
Figure 1.2 Basic diagram of Battery Electric Vehicle (BEV)	2
Figure 1.3 EV interface evolution	4
Figure 1.4 V2G based system	5
Figure 2.1 Conceptual architecture of a battery electric vehicle [8]	10
Figure 2.2 Annual global EV and PHEV sales in BLUE Map scenario [10]	13
Figure 2.3 Projected US Annual Sales of Light Duty PHEV/HEV's [11]	13
Figure 2.4 Battery costs through 2020 [10]	14
Figure 2.5 US V2G Unit Forecast [11]	14
Figure 2.6 US V2G Vehicle Market Value Forecast (US billions) [11].....	15
Figure 2.7 Mennekes® connector drawing and pinout [20].....	18
Figure 2.8 Commercial charging station [24]	21
Figure 2.9 Residential EVSE [24]	21
Figure 3.1 Full Bridge PWM rectifier/inverter	34
Figure 3.2 Single-phase multilevel rectifier/inverter	35
Figure 3.3 Half-Bridge converter (Buck/Boost).....	36
Figure 3.4 Dual active bridge converter [39]	37
Figure 3.5 Chart of alternatives for the converter architecture	38
Figure 3.6 System architecture.....	42
Figure 4.1 Circuit schematic of a single phase dual active bridge dc-to-dc converter [39]	44
Figure 4.2 Fundamental model [41]	44
Figure 4.3 Equivalent circuit 1	45

Figure 4.4 Equivalent circuit 2	45
Figure 4.5 Equivalent circuit 3	46
Figure 4.6 Equivalent circuit 4	46
Figure 4.7 Fundamental waveforms [41]	47
Figure 4.8 Output power vs. phase-shift [42].....	Error! Bookmark not defined.
Figure 4.9 Soft-switching boundaries [42].....	Error! Bookmark not defined.
Figure 4.10 Soft switching region vs. Phase-shift and M.....	50
Figure 4.11 Simulation model	51
Figure 4.12 Input bridge voltage, leakage inductance current and output bridge voltage in boost mode ($\phi=45^\circ$).....	53
Figure 4.13 Input bridge voltage, leakage inductance current and output bridge voltage in buck mode ($\phi=45^\circ$).....	53
Figure 4.14 Output current vs. phase-shift	55
Figure 4.15 Battery SoC, Current and Voltage with Input 400V, Output 360V, ϕ of 90° $L_\sigma = 1 \mu\text{H}$	55
Figure 4.16 Battery SoC, Current and Voltage with Input 400V, Output 400V, ϕ of 90° $L_\sigma = 1 \mu\text{H}$	56
Figure 4.17 Battery SoC, Current and Voltage with Input 400V, Output 355V, ϕ of -90° $L_\sigma = 1 \mu\text{H}$	56
Figure 4.18 Output current vs. Phase-shift - analytical and simulation results	57
Figure 4.19 Output voltage ripple	58
Figure 5.1 IGBT / MOSFET selection chart [43]	Error! Bookmark not defined.
Figure 5.2 Considered equivalent circuit.....	68
Figure 5.3 5 to 15V circuit	71
Figure 5.4 Internal equivalent circuit of HALT signal	71
Figure 5.5 HALT signal interface circuit	72
Figure 5.6 Simplified equivalent circuit diagram of an electrolytic capacitor [49].....	72
Figure 5.7 Transformer simplified equivalent model (primary referred).....	76
Figure 5.8 Transformer design flowchart.....	77
Figure 5.9 Voltage waveform applied to the transformer.....	80
Figure 5.10 Coil former drawing	83
Figure 5.11 Mean turn length identification	84

Figure 6.1 Power converter modules	88
Figure 6.2 Multiplexed analog inputs.....	91
Figure 6.3 Parallel analog inputs.....	91
Figure 6.4 Phase-shift generator	95
Figure 6.5 Practical transformer equivalent circuit (adapted from [57]).....	96
Figure 6.6 Practical transformer equivalent circuit (primary referred) (adapted from [57]) ..	96
Figure 6.7 Simplified transformer equivalent circuit (primary referred) (adapted from [57])	97
Figure 6.8 Equivalent circuit for DC resistance measurement.....	98
Figure 6.9 Equivalent circuit for shorted secondary.....	99
Figure 6.10 Primary winding voltage and current with sorted secondary	99
Figure 6.11 Step response with shorted secondary.	100
Figure 6.12 Equivalent circuit for open secondary	101
Figure 6.13 Input voltage and current with open circuit secondary	101
Figure 6.14 Magnetization current identification (dashed)	102
Figure 6.15 Slope estimation of magnetization current	102
Figure 6.16 Transformer model with parameters	104
Figure 6.17 Transformer transfer function	104
Figure 6.18 Simulated current with shorted secondary	105
Figure 6.19 Simulated magnetization current	105
Figure 6.20 Experimental setup for load tests.....	106
Figure 6.21 Light load test (120 W).....	107
Figure 6.22 Heavy load test (1.5 kW)	107
Figure 6.23 Converter schematic with external inductor.....	108
Figure 6.24 Transformer primary current $\phi=5^\circ$	110
Figure 6.25 Transformer primary current $\phi=10^\circ$	110
Figure 6.26 Transformer primary current $\phi=15^\circ$	110
Figure 6.27 Transformer primary current $\phi=20^\circ$	110
Figure 6.28 Transformer primary current $\phi=40^\circ$	110
Figure 6.29 Transformer primary current $\phi=60^\circ$	110

List of Tables

Table 2.1 Main characteristics of common battery types [9]	10
Table 2.2 NIST priority areas for standardization purpose [12]	15
Table 2.3 SAE Standards [13]	16
Table 2.4 SAE J2847 parts [13]	16
Table 2.5 Off-Board Standards from UL [14]	17
Table 2.6 On-Board Standards from UL [14]	17
Table 2.7 IEC Standards [15-18]	17
Table 2.8 Control pilot signal states [19]	18
Table 2.9 IEC 61851-1 Charging Modes [19]	19
Table 2.10 Yazaki single-phase AC charging connector specifications [22]	20
Table 2.11 Yazaki DC charging connector (CHAdeMO)	21
Table 2.12 Main features of GE WattStation™ [25]	22
Table 2.13 AeroVironment™ MODEL EV50-FS specifications [26]	22
Table 2.14 Desired features for V2G capable power conversion system	23
Table 3.1 Components list for rectifier/inverter	34
Table 3.2 Components list for multilevel rectifier/inverter	35
Table 3.3 Voltage range for Buck/Boost	36
Table 3.4 Components list for Buck/Boost	36
Table 3.5 Voltage range for dual active bridge	37
Table 3.6 Components list for dual active bridge	37
Table 3.7 SUR calculation	39
Table 3.8 Output voltage ranges	39

Table 4.1 Leakage inductance voltages in each time instant.....	47
Table 4.2 General simulation parameters.....	51
Table 4.3 Transformer parameters.....	51
Table 4.4 Battery pack parameters	52
Table 4.5 Considered scenario	54
Table 4.6 Capacitor dimensioning	58
Table 5.1 Input data for switch selection	62
Table 5.2 SKM100GB12V IGBT Half-Bridge main specifications [44]	63
Table 5.3 Main driver types comparison [45]	63
Table 5.4 Driver features.....	64
Table 5.5 Skyper 32 PRO R features [47]	65
Table 5.6 Minimum dead time estimation.....	66
Table 5.7 Dynamic short circuit protection parameters.....	68
Table 5.8 Input data for R_g calculation [44]	69
Table 5.9 Gate resistors calculation	69
Table 5.10 Electrolytic capacitors minimum requirements	73
Table 5.11 Epcos B43456A9158M Electrolytic capacitor specifications [50]	74
Table 5.12 Epcos B32656S8155 MKP capacitor specifications.....	75
Table 5.13 Core selection guide for a specific usage [54].....	78
Table 5.14 N27 UU 93/152/30 core magnetic characteristics [54]	79
Table 5.15 Primary voltage parameters	80
Table 5.16 Core losses estimation [54]	81
Table 5.17 Skin depth for Copper at 100°C [37]	82
Table 5.18 Coil former characteristics [54].....	83
Table 5.19 Turn segment dimensions	84
Table 5.20 Designed transformer full specifications	86
Table 6.1 Measured variables and nominal ranges.....	89
Table 6.2 LEM® LV 25-P voltage transducer data [55].....	89
Table 6.3 LEM® HY 15-P current transducer data [56]	90
Table 6.4 Analog to digital converters specifications.....	91

Table 6.5 Current acquisition parameterization	92
Table 6.6 Voltage acquisition parameterization	92
Table 6.7 Voltage measurement error	93
Table 6.8 Current measurement error	93
Table 6.10 Phase-shift generator resolution	95
Table 6.11 Transformer secondary to primary modification	96
Table 6.12 Simplified transformer equivalent circuit parameters	97
Table 6.14 Results from DC winding resistance measurement	98
Table 6.13 Parameters from the step response experiment	100
Table 6.15 Peak values of magnetization current	103

Acronyms and symbols

AC	<i>Alternating current</i>
ACIM	<i>Alternating current induction motor</i>
BJT	<i>Bipolar junction transistor</i>
BLDC	<i>Brushless direct current (motor)</i>
BMS	<i>Battery management system</i>
CAN	<i>Controller area network</i>
CHAdEMO	<i>Charge de Move</i>
DAB	<i>Dual active bridge</i>
DC	<i>Direct current</i>
DSP	<i>Digital signal processor</i>
ESL	<i>Equivalent self inductance</i>
ESR	<i>Equivalent series resistance</i>
EV	<i>Electric vehicle</i>
EVSE	<i>Electric vehicle supply equipment</i>
FPGA	<i>Field programmable gate array</i>
GE	<i>General electric</i>
HF	<i>High frequency</i>
IC	<i>Integrated circuit</i>
ICE	<i>Internal combustion engine</i>
IEA	<i>International energy agency</i>
IEC	<i>International Electrotechnical Commission</i>
IGBT	<i>Insulated gate bipolar transistor</i>
LF	<i>Low frequency</i>
MCU	<i>Microcontroller</i>
MOSFET	<i>Metal-oxide-semiconductor field-effect transistor</i>
NIST	<i>National Institute of Standards and Technology</i>
NTC	<i>Negative temperature coefficient (thermistor)</i>
PCB	<i>Printed circuit board</i>
PHEV	<i>Plug-in electric vehicle</i>

PLL	<i>Phase-locked loop</i>
PMSM	<i>Permanent magnet synchronous motor</i>
PTC	<i>Positive temperature coefficient (thermistor)</i>
PWM	<i>Pulse width modulation</i>
RMS	<i>Root mean square</i>
SAE	<i>Society of automotive engineers</i>
SoC	<i>State of charge</i>
SUR	<i>Switch utilization ratio</i>
UL	<i>Underwriters Laboratories</i>
UPS	<i>Uninterruptible power supply</i>
V2G	<i>Vehicle-to-grid</i>
XOR	<i>Exclusive OR (logic gate)</i>
ZVS	<i>Zero voltage switching</i>

ϕ	<i>Phase-shift angle</i>
$L\sigma$	<i>Leakage inductance</i>
L_m	<i>Magnetization inductance</i>
R_L	<i>Winding resistance</i>
V_{DC1}	<i>DC voltage of the input bridge (left side)</i>
V_{DC2}	<i>DC voltage of the output bridge (right side)</i>
ω	<i>Angular frequency</i>
I_0	<i>Average output current</i>
P_0	<i>Average transferred power</i>
$t_{d(on)}$	<i>Turn-on delay</i>
$t_{d(off)}$	<i>Turn-off delay</i>
t_r	<i>Rise time</i>
t_f	<i>Fall time</i>
V_{CEstat}	<i>Collector-emitter threshold static monitoring voltage</i>
V_{CEref}	<i>Collector-emitter reference voltage</i>
T_{bl}	<i>Blanking time</i>
C_{ies}	<i>Input to emitter capacity</i>
L_s	<i>Equivalent series inductance</i>
ψ	<i>Flux linkage</i>
B	<i>Induction</i>
Φ	<i>Magnetic flux</i>
\mathfrak{R}	<i>Magnetic reluctance</i>
δ	<i>Skin depth</i>
l_e	<i>Effective magnetic path length</i>
A_e	<i>Effective core cross section area</i>
μ_a	<i>Amplitude permeability</i>
Q	<i>Quantum</i>

Chapter 1

Introduction

This chapter represents a first approach to the subject under study. Three subchapters provide a successive approximation to the subject with a brief exposure of main parts.

At first, the basics about electric vehicles and the ones with interest for this work will be presented. Those are battery electric vehicles and plug-in hybrid electric vehicles.

The second part will be focused on one of the major issues related to widespread of electric vehicles - the grid interface. Some solutions will be presented and challenges will be identified as motivation for the proposed work.

Lastly the most promising interface system (Vehicle-to-Grid) will be presented with a rather deeper level of detail.

1.1 The Electric Vehicle

Along decades, cars with internal combustion engines (ICE) powered by fossil fuels have been widely used by almost all transportation segments like family cars, trucks, bus and even trains. This propulsion system found the success in a remarkable robustness and ease of refill the energy source - fuel tank.

The concern to find alternatives existed since the beginning but little was done until a few years ago. The conscience of sustainable growing and the approximation of the end of oil in a few decades were the two main concerns that boosted the demand for new technologies.

Most promising technology for now and for the near future is surely electricity. The knowledge gained over the years in electric power conversion (from and to electricity or between electricity and another energy types) have provided valuable input for success of Plug-In Hybrid Electric Vehicles and Battery Electric Vehicles.

Electric vehicles are usually divided in two main groups. The first one represents the Plug-In Hybrids, cars that combine at least two propulsion systems one of them electrical.

These cars are not viewed as the future of mobility but only the transition between ICE powered cars and electric vehicles. They are the current cost competitive solution to get

better fuel economy, lower emissions and the ones that can achieve interesting ranges, especially for huge and heavy cars [1].

The forthcoming solution is the other group, battery electrical vehicles. These cars are designed to be only electrical-powered, with energy stored in batteries or any other electrical storage system. One of the main advantages of electric cars is the fact that they can recharge the battery during braking. Anyway, battery should not receive pulsed power from abrupt braking what makes necessary the need for another energy storage system like super capacitors or flywheels.

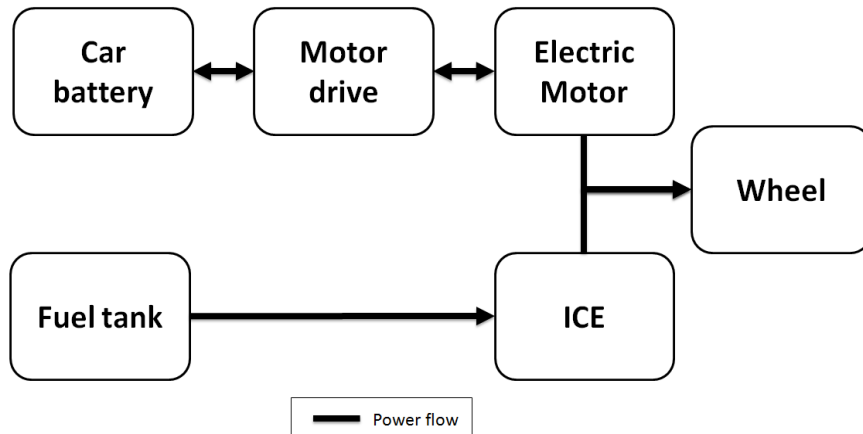


Figure 1.1 Basic diagram of Plug-in Hybrid Electric Vehicle (PHEV)

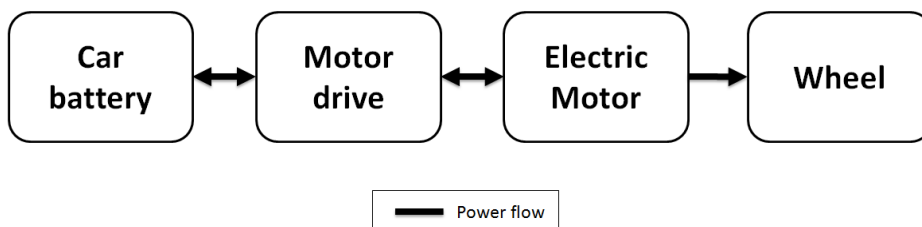


Figure 1.2 Basic diagram of Battery Electric Vehicle (BEV)

Most suitable electric motors for cars are AC induction motors (ACIM), synchronous motors such as permanent magnet synchronous motors (PMSM) or brushless DC motors (BLDC) and reluctance motors [2]. All of them have the great advantage of being brushless type requiring minimal maintenance. Very advanced variable frequency drives (VFD) and control schemes already developed for industrial applications are now used to improve performance from these electrical machines, with high efficiency levels.

Overall the control chances related to this motors are very promising when compared with ICEs. The ability to produce maximum torque in a wide speed range is a feature with special interest for electrical vehicle (EV) applications. Another advantage is related with noise and vibration generated by classic cars which are not present in modern EVs. Also in relation to

the traction system other advantages arises such as reduced external components needed (like cables, motor drives, cooling system) and even the gearbox can be dispensed.

Lack of pollutant emissions is certainly one of the advantages of electric vehicles because electricity is used only as mechanical power or wasted as heat.

Alongside these advantages other comfort-related can be found, whereas nowadays a car is not just an engine and four wheels. Ease in feeding the growing vehicle auxiliary loads like air conditioning or multimedia sets, electronic stability programs or traction control may be other factors with high potential.

Anyway, the widespread use of such vehicles is still bound by some problems. The main focus of research was around the storage system - batteries. They need to have high power density, able to fast charge and an expected lifetime that is near the duration of an ICE car. Expected range for cost competitive cars is still quite low which limits the utilization of EVs only for short distance trips. The charging systems are not yet standardized as well as the large-scale integration of this kind of vehicles with the existing power grids is still under study.

1.2 Motivations and Challenges in Electric Vehicle Integration

The usage of electric vehicles brings naturally to a question - how to recharge battery? People are used to recharge their mobile phones, notebooks and some other gadgets with no problem. In fact these loads do not represent anything significant to the grid due to their low stored energy.

With EVs this consideration cannot be done. Tens of kilowatt-hour batteries to be charged in a few hours or even less than an hour represent large amount of power to recharge each battery. With thousands of these loads coupled to grid serious problems would arise.

The results of such charging method are branch congestion and unacceptable voltage drops in some branches due to an uncontrolled peak of consumption that coincides with the time that everyone puts the vehicle to charge.

This problem creates a new research area and, above all, a new challenge in widespread EV integration. In this scope the lowest level charging method was called dumb charging. This method doesn't allow large scale integration with the existing power grid, motivating the appearance of increased intelligence systems such as smart charging or vehicle-to-grid (V2G) interface.

These more advanced systems claims for new power conversions systems with competence to exchange data with a centralized smart grid controller. With this system, users can set the desired time for car to be charged and the controller will choose the adequate period and possibly the charging ratio, therefore sends the command for the charger. These functionalities should be available in a smart charge system.

The next level consists in a full-featured vehicle to grid interface. In this case, system should be able to operate in inverter mode feeding power back to the grid. Proper control scheme will adjust charging/discharging ratio with respect not only to battery requirements but also grid constraints.

This feature can provide ancillary services like residential UPS system when Loss of Mains occurs or helping in recovery from a failure.

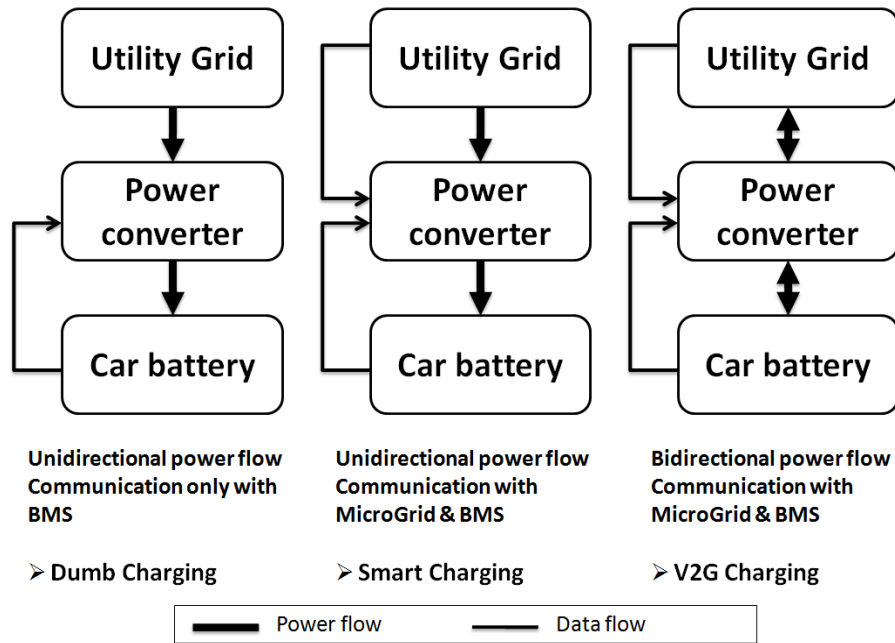


Figure 1.3 EV interface evolution

1.3 The Vehicle-to-Grid (V2G) concept

The V2G concept has been studied and can be seen as the future of charging systems. It is applied to on-board chargers or charging stations. It can offer great benefits for electric grid providing stability and load management but also for Plug-In owners.

Considering a first approach only grid would benefit from this strategy with owners being affected with longer charging periods and wasted battery cycles when a discharge takes place.

But on the other hand the vehicle owner can be able to be part of an open energy market, buying or selling energy with very different tariffs. The economical point of view can make this system attractive for users making money while the car is stopped.

Considering all these aspects, the system can become profitable to the owner and very helpful to the grid. The already identified benefits considering electric power system point of view are maximization of intermittent sources integration, reactive power compensation, branch congestion avoidance, auxiliary frequency regulation and assistance in failure recovery [3-5]. From the vehicle owner side some interesting opportunities have yet been identified such as residential UPS system or potential revenue from electricity market [6-7].

The data exchange with a smart grid controller allows this system to have remote operation and even as monitoring system sending local parameters back to smart grid controller if the charger has the ability to send back data.

In the simplest case, the grid might just switch the vehicle charger on and off in response to grid load. Grid could also send a message to the vehicle inhibiting it of charge during the peak period, which can be related to technological aspects like branch congestion or economical aspects like waiting for the cheaper tariff. In the most advanced scenario, grid controller might setup a periodic data exchange of messages to the charger, setting charging

rate or even changing charger operation mode to flow of energy back into the grid. These decisions can depend on several factors like statistical forecasts based on historical information or real-time data including grid load, amount of renewable generation, state of charge of the vehicle and energy pricing.

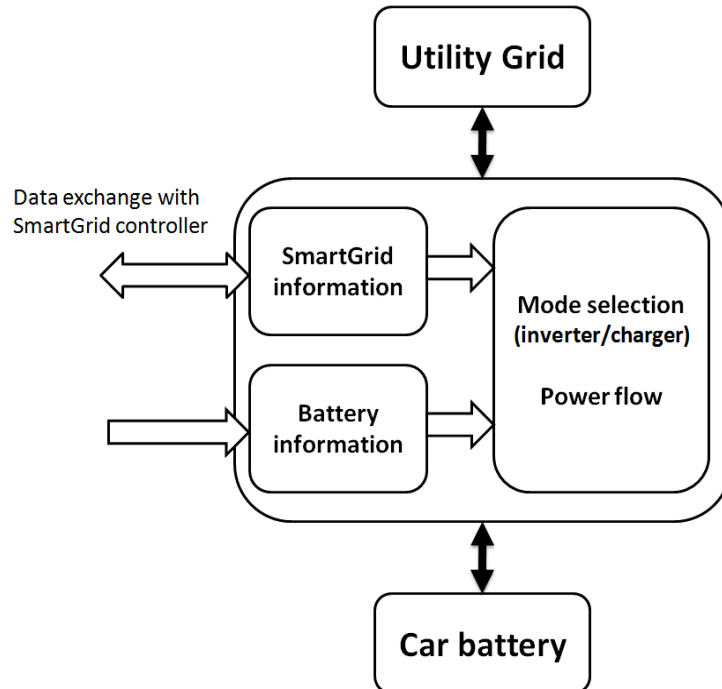


Figure 1.4 V2G based system

As seen so far this technology has a high potential representing a near term researching area. A full-featured interface can be configured to provide several services with interest for all stakeholders. Nevertheless some barriers like reliability and cost of overall communication system and impact on vehicle battery lifetime throw the feasibility of this solution to a medium term future.

1.4 Objectives of the work

The first objective for this work is to study relevant published knowledge about electric vehicles and respective charging systems, especially cars with grid interface (Plug-In).

Next, a suitable power electronic conversion solution must be defined with appropriate criteria in order to build a laboratory prototype. This hardware should allow getting valuable data and establishing a comparison between the proposed system and other currently available systems, which stands for the main objective of the work.

1.5 Work plan

To meet the objectives proposed for this work was developed a list of major tasks. These tasks were divided into subtasks and then were scheduled in a Gantt chart (Annex A). The justification and the results that are intended to achieve with each task are also presented.

1. Analysis of project requirements. Selection of the power structure and operation modes

This task has the main purpose of understand the main requirements that system should have, to implement a vehicle-to-grid interface. When completed, it should result in a technical specification of the power structure to be used, providing a comprehensive and feasible solution. The modes of operation required should also be defined at this stage to be contemplated in the prototype design.

2. Study, design and implementation of interface circuits for control and protection of power semiconductors. Study of different technologies available to implement electrical insulation.

At this stage should be considered different technologies to be used and chosen the most suitable for the requirements of the project. After that shall be designed and built a robust and modular hardware that allows the proper interconnection between the control and power modules. The various protections should also be built and tested. The result should be a drive and protection system that ensures a safe operation of all system components without compromising their operation.

3. Study, design and implementation of the measurement system

The measurement systems are of crucial importance for the proper functioning of the converter. Since it is a prototype, this system should be built in a modular way to ensure the future possibility of reorganization. The resulting hardware should have characteristics that do not compromise the closed-loop operation of the converter.

4. Assembly and testing of the power converter.

To accomplish this task the various power components must be assembled in a comprehensible structure resulting in a user friendly experimental setup. User safety must be ensured and it should be possible to collect data and make changes to the configuration easily.

5. Study and implementation of a control system based on digital signal processors, operating in real time.

The start of this task assumes that all the hardware is already assembled and tested. In this stage should be done a research of various algorithms and computing techniques and selected those with special interest for the controller to implement. After that, it should be a study of the capabilities of digital control system and implemented closed loop control scheme.

6. Exercise and develop the algorithms chosen based on numerical simulations.

The algorithms chosen should be implemented in numerical simulation and its results should be analyzed to verify if they correspond to the expected. Once validated, modifications can be made for the purpose of improving the performance of the control system. The completion of this task should allow a transition to a physical implementation with predictable results and stable operation.

7. Comparative testing between the developed algorithms and other technical solutions based on conventional methodologies.

The purpose of this task is to assess if the developed or modified algorithms permit better results than conventional or previously proposed. Performance measurements should be prior established in order to evaluate different solution comparatively. The task should allow produce valuable conclusions about this comparison.

8. Drafting of the dissertation.

Finishing the work, a detailed technical document should be produced with the aim of structuring and presenting the developed knowledge so as to present the methodologies adopted, the results achieved and relevant technical details.

1.6 Map of the document

This document is divided in seven chapters.

The first is a presentation of work. In it are first introduced the main concepts and objectives / tasks of this dissertation. In this chapter there is room for a brief introduction about the electric vehicle, for the presentation of the research motivations on grid integration of electric vehicles and to introduce the vehicle-to-grid concept.

Chapter two starts with a brief description of modern electric vehicle key components followed by an outer view of charging systems and its standards. Two commercial systems will be presented with main characteristics listed and finally an analysis of power converters to deal with vehicle-to-grid will take place.

In Chapter three are identified the basic topologies with interest to this application and possible associations in multiple stages. Afterwards, criteria are defined and one of the options is chosen. The proposed architecture for the system is then presented.

Chapter four is divided in two parts. The first aims to provide a description of the topology to design in terms of its constitution and how it works. In the second part is presented and described a simulation model for this converter and several simulations are made with clear objectives.

In Chapter five are reported the main aspects concerning the design of the converter power stage. The transformer design is presented with more detail, for being the most critical component.

Chapter five can be split in two parts. The first presents the development of the measurement and acquisition system and the converter command module. In the second part experimental results are obtained with the aim of parameterize and test the transformer and also results of the converter working as dual active bridge.

In the final chapter the main conclusions are taken and pointed orientations for future developments.

Chapter 2

State of the art

This chapter can be split in three significant parts. First, a brief description of modern electric vehicle key components will take place with some general remarks listed and the statistical data about electric vehicles market focusing on V2G market forecast with a given example for United States of America.

Second part will be focused in an outer view of charging systems with a short survey considering the main standard with interest for this purpose such as safety and connection requirements and after that the currently used charging levels will be described and a discussion of their features, constraints and applicability will take place. Lastly two commercial systems that together perform the three charging levels considered will be presented with main characteristics listed.

Finally the third part will be based in an inner view of the charger, i.e. considering electronics aspects only. A selection of recently published works matching this application will be analyzed based on standardized table with brief appreciation for each one. Based on these works will be performed an overall analysis identifying major trends and technological options for topologies and another critical hardware with relevance for system design.

2.1 Modern Electric Vehicles

Prior to moving to a detailed discussion of the various power converter topologies it is important to understand the reasons behind the ongoing development of electric vehicles.

In this context, the structure and key components of modern electric vehicles will be presented. The discussion will focus on battery electric vehicles since they are the most demanding in terms of performance and capabilities for all electrical components.

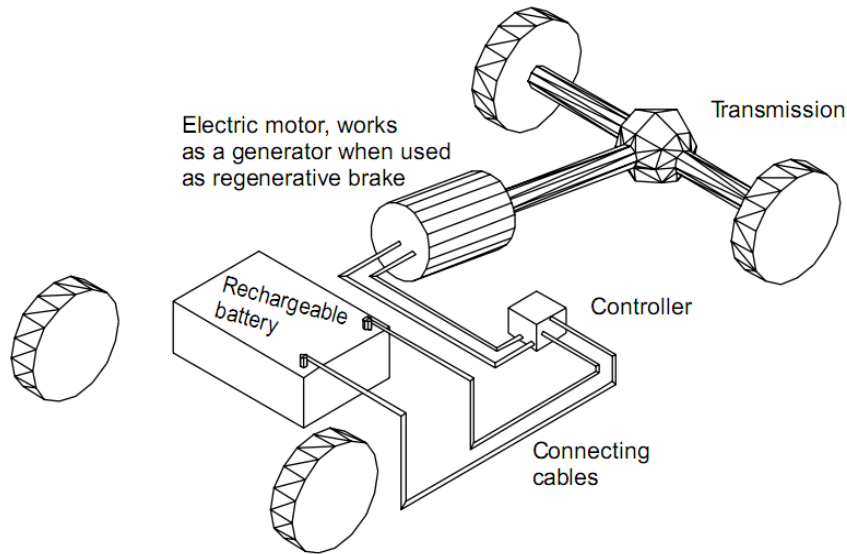


Figure 2.1 Conceptual architecture of a battery electric vehicle [8]

2.1.1 Storage systems

The main power storage systems for full electric vehicles are batteries. For this application several types of batteries can be used having rather different characteristics. In any way the batteries are sensitive equipment and do not allow peak charging power that is naturally generated by regenerative braking of vehicles. Due to this fact other technologies emerged to deal with this situation such as ultra capacitors or flywheels [8].

Referenced in Table 2.1 are the main characteristics of a battery and its values for different technologies. The theory associated with the batteries will not be presented because it does not fall within the scope of this work.

Table 2.1 Main characteristics of common battery types [9]

	Lead-Acid	Ni-Cd	Ni-MH	Li ion
Cost	Low	Medium	High	Very High
Specific Energy (Wh.kg ⁻¹)	30 - 50	50 - 80	40 - 100	160
Voltage per cell	2	1,25	1,25	3,6
Charge current	Low	Very Low	Moderate	High
Cycle number (charge/discharge)	200 - 500	1000	1000	1200
Autodischarge per month (% of total)	Low (5%)	Moderate-High (20%)	High (30%)	Low (10%)
Minimum time for charge (h)	8 - 16	1 - 1,5	2 - 4	2 - 4
Activity requirement	180 days	30 days	90 days	None
Environmental warning	High	High	Low	High

One of the critical issues related to battery usage is the charging process. The task of charging only one cell individually would be easy since the state of charge was known. A regulated power source with controlled output current or voltage can be used in order to

charge battery. In practice, battery packs are grouped in similar modules, with cells connected in series to provide a proper voltage level for car DC bus. Although the current is the same in all the cells, it does not mean that all were charged in the same way after a certain time. Different constructive parameters or even differences in cell temperature during charging can cause this situation. This phenomenon can also be observed in discharge process.

In practice the present charging systems use a normal rate of charge until the best-charged cells reach the full charge and thereafter switch to a reduced rate of charge mode and go on until the worst-charged cells are estimated to be fully charged. This method usually leads to a long time to go from near full charge to a real 100% state of charge in every cell [8].

There are various alternatives of energy storage devices including the flywheel and super capacitors. As a general rule both of these devices have increased specific power. However, the amount of energy they can store is currently rather small.

Flywheels are devices that are used for storing energy. A plane disc spinning about its axis would be an example of a simple flywheel. The kinetic energy of the spinning disc is released when the flywheel slows down. Connecting an electrical generator directly to the disc can capture the energy. The flywheel can be re-accelerated, acting as a regenerative brake.

An interesting alternative to flywheels is the use of large energy storing capacitors, so called super capacitors. In many ways the characteristics of super capacitors are like those of flywheels. They have relatively high specific power and relatively low specific energy. They can be used as the energy storage for regenerative braking. Super capacitors are inherently safer than flywheels as they avoid the problems of mechanical breakdown and gyroscopic effects [8].

2.1.2 Traction Motors

Electric motor is obviously one of the key parts of electric vehicles. His characteristics have serious influence on car weight, performance and reliability. The classic DC motor was widely used in traction applications over decades, with many control opportunities especially in separately excited configuration. The main problem associated with this motor is in its principle of operation - the brushes-collector set. For intensive usage the need for regular maintenance became a problem and other motor types emerged.

The alternative electrical machines used for electric vehicles are all brushless to not compromise the vehicle overall reliability. High power density and robustness are another key features pursuit for this application.

Two of them are very similar - the brushless DC and the permanent magnet synchronous motor. Based on a permanent magnet rotor and a wounded stator these motors have high power densities but also are more expensive than other options. The main difference between them is the voltage waveform applied to the stator windings - trapezoidal in the BLDC and sinusoidal in the PMSM. It is this fact that leads to the first being considered a DC motor and the second an AC motor. Disregarding the cost this motors have been widely used in modern all-electric and hybrid vehicles and represents a good solution for this purpose.

Another type of motor is called switched reluctance motor. This machine has basic operation principle of minimize the air gap of a magnetic circuit. The rotor can be only composed by a soft iron plate and two opposed stator windings. In practice a salient pole rotor and multiple stator coils are used in order to attenuate the torque pulsations and the

produced noise. The control of this motor is critical since it needs a measure or a precise estimation of the rotor position to produce torque and control speed correctly.

At last, the well known alternate current induction motor (ACIM) must be referred. The low cost and high reliability make this machine a very interesting solution in all kind of industrial or residential applications. Originally designed to be feed by a three-phase system, with the appearance of power electronic converters the application range has grown even more and now the motor can be supplied by AC or DC source easily using proper electronic drive [2, 8].

The control systems for this kind of motor are in a high state of development being this, one of the main advantages for this alternative. Despite this, the motor design has special design requirements for electric vehicle applications such as low weight and high power density compared to industrial applications.

2.1.3 Motor drives

Several parts of electrical machines were originally proposed to be supplied by a specific voltage system and many times at fixed speed. Early, mechanical systems were used to deal with speed regulation needs. In the last decades modern automation systems such as robotics, positioning systems etc have required precise speed regulated or torque regulated systems, working in closed loop. The power converters used are known as variable frequency drives and have the ability to deliver power at variable amplitude and variable frequency of current/voltage. This type of control is now very usual on ACIM and PMSM.

The motor drive is another critical component of vehicles because the power stored in car batteries are now very limited and the motor drive efficiency in both ways (acceleration or regenerative braking) should be very high. The technology available today allows building these drives with advanced control methods and power ratings in accordance with car needs (50-150kW) with reasonable size, weight, volume and reliability.

2.1.4 Auxiliary Loads Supply

Power converters in electric vehicles could have many other applications apart from battery charging or motor drive.

Currently high power density converters are studied to deal with this task. Loads like advanced multimedia systems, air conditioning, sunroof, electric windows, heating seats, cooling system pump, power steering and many other represents together a large amount of power and its operating voltage is by far lower than car DC bus. Some of these loads are also very sensitive, which leads to a converter with high power rating and well regulated output. These converters are usually DC-DC converters that create a low voltage DC bus from the car main bus, sometimes with electrical isolation due to safety aspects.

2.2 Electric Vehicles Market

So far, electric cars have not yet gained a significant market share. Despite the incentives of some governments, the price, range and uncertainty about the durability of the batteries fail to convince buyers. IEA has defined a technology roadmap for upcoming years with sales

forecast to next 40 years in a BLUE Map scenario for light duty vehicles. It is expected that sales will hit a substantially volume in 2015 and began to grow rapidly from there.

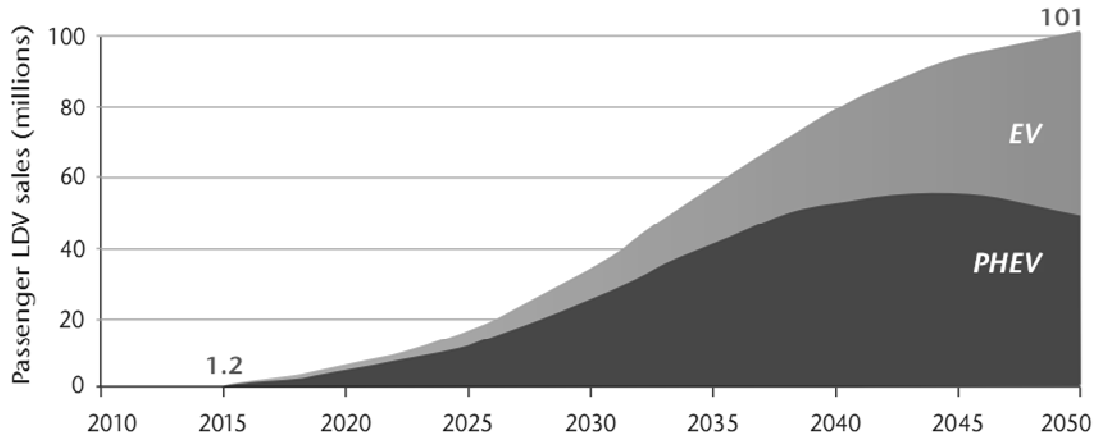


Figure 2.2 Annual global EV and PHEV sales in BLUE Map scenario [10]

According to the US Energy Information Agency’s Annual Energy Outlook 2010, annual unit sales of hybrid electric vehicles (HEVs) and plug-in hybrid electric vehicles (PHEVs) are expected to grow from 287,000 in 2010 to 2.2 million in 2035.

This represents a annual growth rate of 14.7% during this time period. The Annual Energy Outlook 2010 expects that PHEV/EV unit sales represent 2.8 percent of all light duty vehicle (LDV) sales in 2010 and 11.6 percent in 2035. [11]

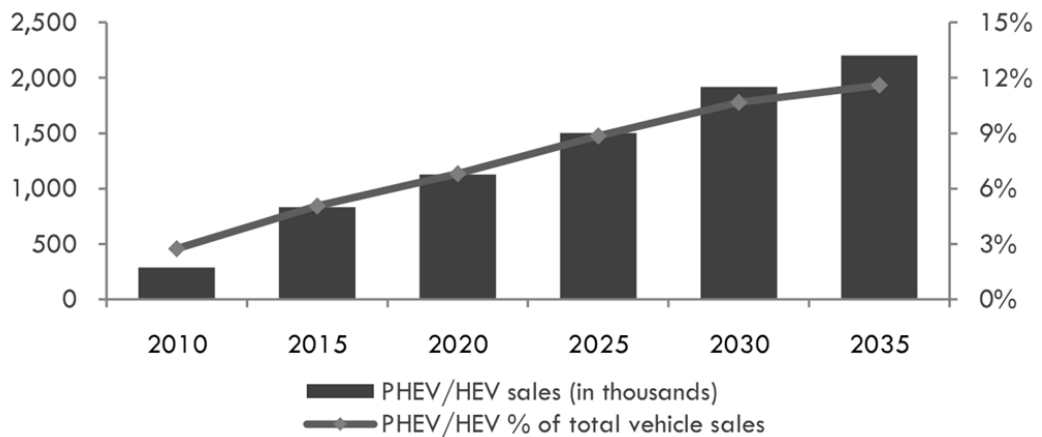


Figure 2.3 Projected US Annual Sales of Light Duty PHEV/HEV’s [11]

IEA have already identified the high battery packs cost to be the main obstacle for a large-scale appearance of these cars on the streets. Due this medium term target prices have been established in order to produce large battery packs with affordable cost. The achievement of these targets must enable to produce cost-competitive vehicles with ranges similar to those non electric vehicles on road today.

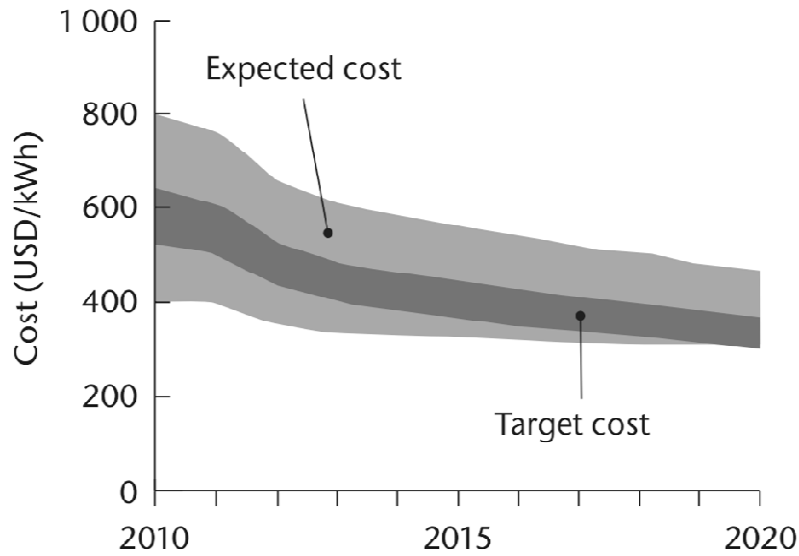


Figure 2.4 Battery costs through 2020 [10]

2.2.1 V2G Market forecast for US

Important data was recently published in a report made by Zpryme, where a market forecast for 2020 related to V2G was presented. United States, China, Germany, UK, South Korea and Denmark are the countries in this report.

United States market was presented has an example of V2G market potential.

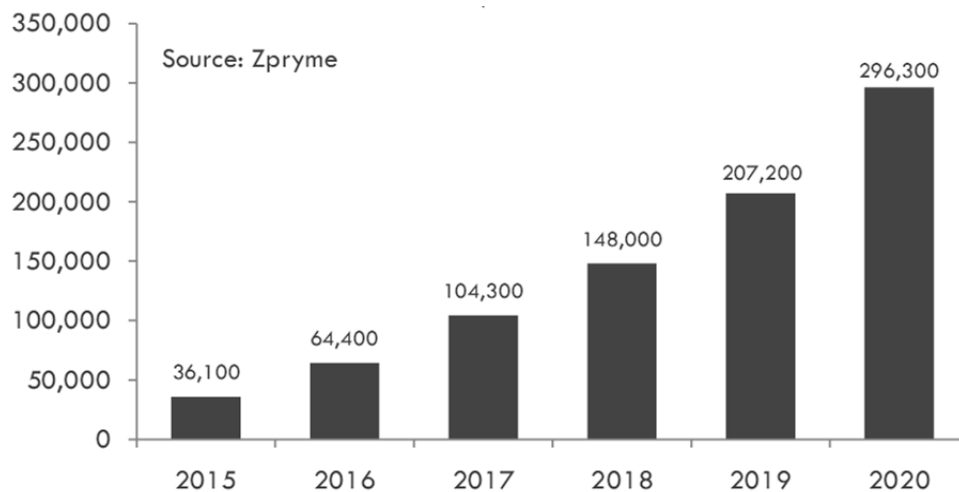


Figure 2.5 US V2G Unit Forecast [11]

Apart from the fact that being only forecasts the presented data with just a medium term range (ten years) should be able to make V2G an emerging market with significant value as can be seen in Figure 2.6 where within just ten years (2020) representing a market value of 8.2 billion dollars. [11]

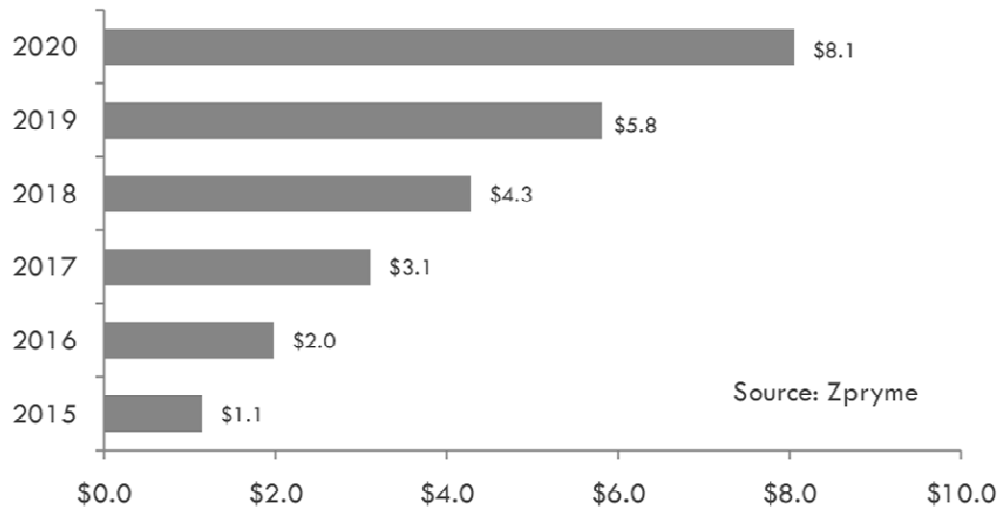


Figure 2.6 US V2G Vehicle Market Value Forecast (US billions) [11]

The above data should be able to encourage major players in areas such as power electronics and communication systems to increase their investments in this technology in coming years.

2.3 Standards

Standardization always represents a first step to guarantee the interoperability of whole systems and so the integration of plug-in vehicles onto the grid. Several organizations have been working on standards for electric vehicles.

Published in January 2010 by National Institute of Standards and Technology (NIST), the *NIST Framework and Roadmap for Smart Grid Interoperability Standards* set the priorities for standardization (Table 2.2).

Table 2.2 NIST priority areas for standardization purpose [12]

Demand Response and Consumer Energy Efficiency
Wide-Area Situational Awareness
Energy Storage
Electric Transportation
Advanced Metering Infrastructure
Distribution Grid Management
Cyber Security
Network Communications

The main organizations focused on writing standards for electric vehicles are the Society of Automotive Engineers (SAE), the International Electrotechnical Commission (IEC) and the Underwriters Laboratories (UL).

SAE Standards

One of the most popular standards is the SAE J1772 standard for conductive charge coupler which is now supported by GM, Chrysler, Ford, Toyota, Honda, Nissan, and Tesla Motors [12]. This standard allows the appearance of normalized connector which is now supplied by several manufacturers and can be easily found in commercial electric vehicles.

The SAE organization is working on other relevant standards (Table 2.3).

Table 2.3 SAE Standards [13]

J2293/1 & /2	Energy Transfer System for Electric Vehicles
Part 1	Functional Requirements and System Architectures
Part 2	Communication Requirements and Network Architecture
J2836	Use Cases & General Information
J2847	Detailed information (messages, state diagrams, etc.)

The J2847 standard is of great relevance for the purpose of this work, especially parts 1 and 3 (Table 2.4).

Table 2.4 SAE J2847 parts [13]

J2847/1	Communication between Plug-in Vehicles and the Utility Grid
J2847/2	Communication between Plug-in Vehicles and off-board DC Chargers
J2847/3	Communication between Plug-in Vehicles and the Utility Grid for Reverse Power Flow
J2847/4	Diagnostic Communication for Plug-in Vehicles
J2847/5	Communication between Plug-in Vehicles and their customers

In January 2011 only the part 1 of the SAE J2847 standard was published with the remaining parts reported as work in progress status, according to the SAE international website.

UL Standards

In this context, UL standards need to be referred too. The specifications are split in Off-Board and On-Board related. They are essentially safety standards for connectors, cables, power converters, traction motors, chargers and batteries.

Table 2.5 Off-Board Standards from UL [14]

UL 62	Standard for Safety of Electric Vehicle Cable
UL 2202	Standard for Safety of Electric Vehicle (EV) Charging System Equipment
UL 2231	Standard for Safety of Personnel Protection Systems for EV Supply Circuits
UL 2251	Standard for Safety of Plugs, Receptacles, and Couplers for EVs
UL Subject 2594	Subject Standard for Safety of Electric Vehicle (EV) Supply Equipment
UL Subject 2735	Subject Standard for Safety of Electric Utility (Smart) Meters

Table 2.6 On-Board Standards from UL [14]

UL Subject 458A	Subject Standard for Safety of Power Converters/Inverters for Electric Land Vehicles
UL Subject 1004-1	Subject Standard for Safety of On-board Electric Vehicle Equipment Traction Motors
UL 2202	Standard for Safety of Electric Vehicle (EV) Charging System Equipment
UL Subject 2733	Subject Standard for Safety of Surface Vehicle On-Board Cable
UL Subject 2734	Subject Standard for Safety of Connectors for Use with On-Board Electrical Vehicle (EV) Charging Systems

IEC standards

At last the well-known International Electrotechnical Commission (IEC) also published the some standards for electric vehicles. The most relevant standards for this work are the ones related to charging system, especially conductive charging.

The first standard is the IEC 61851/part 1 and describes the general requirements for on-board and off-board equipment used to charge electric road vehicles with up to 1000 V a.c. or up to 1500 V d.c.. Part 21 gives the electric vehicle requirements for conductive connection to a a.c. supply up to 690 V or a d.c. supply up to 1000 V. Part 22 gives the requirements for a.c. electric vehicle charging stations for conductive connection with a.c. supply voltages up to 690 V. [15-18]

Table 2.7 IEC Standards [15-18]

IEC 61851-1	Electric vehicle conductive charging system - Part 1: General requirements
IEC 61851-21	Electric vehicle conductive charging system - Part 21: Electric vehicle requirements for conductive connection to an a.c./d.c. supply
IEC 61851-22	Electric vehicle conductive charging system - Part 22: AC electric vehicle charging station
IEC 62196-1	Plugs, socket-outlets, vehicle couplers and vehicle inlets - Conductive charging of electric vehicles - Part 1: Charging of electric vehicles up to 250 A a.c. and 400 A d.c.

The IEC 62196/part 1 is applicable to plugs, socket-outlets, connectors, inlets and cable assemblies for electric vehicles, intended for use in conductive charging systems which incorporate control means, with a rated operating voltage not exceeding [18]:

- 690 V a.c., 50 - 60 Hz, at a rated current not exceeding 250 A;
- 600 V d.c., at a rated current not exceeding 400 A.

A connector/inlet set according to the IEC 62192-1 was proposed by MENNEKES® (Figure 2.7). The connector is suitable to supply on-board chargers with three-phase or single-phase input. It is composed by 5 power pins (3 phases, neutral and protective earth) and two additional control pins. These two control pins are the “plug present” pin which immobilizes the vehicle when the connector is attached and the “control pilot”. The communication through this pilot pin is used to exchange information between the electric vehicle on-board charger and the EVSE. The physical signal is pulse width modulated with a frequency of 1 kHz. IEC 61851-1 standard defined six distinct states depending on the average value of this signal.

Table 2.8 Control pilot signal states [19]

Vehicle state designation	Voltage (avg./DC level)	Description of vehicle state
State A	12.0 (a)	Vehicle not connected
State B	9.0 (b)	Vehicle connected / not ready to accept energy
State C	6.0 (b)	Vehicle connected / ready to accept energy / indoor charging area ventilation not required
State D	3.0 (b)	Vehicle connected / ready to accept energy / indoor charging area ventilation required
State E	0	EVSE disconnected, utility power not available, or other EVSE problem
State F	-12.0 (a)	EVSE not available, or other EVSE problem

Notes:

a) Static voltage

b) Positive portion of 1 kHz square wave, measured after transition has fully settled

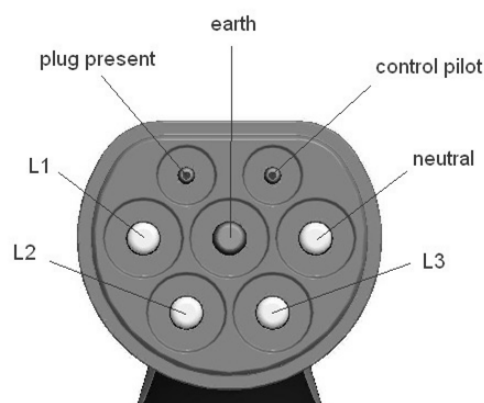


Figure 2.7 Mennekes® connector drawing and pinout [20]

2.4 Charging systems

Due to its limited range the electric vehicle charge is a serious concern for users. Desirable features for this task are a fast charge, to preserve battery lifetime and have the best tariff for energy. In fact, several options are currently offered by car manufacturers but often by third-party companies such as General Electric.

In this context the system that stands between the car and the power grid is called electric vehicle supply equipment (EVSE).

Table 2.9 IEC 61851-1 Charging Modes [19]

Level/Mode	Maximum current (A)	Maximum voltage (V)			Earth conductor
		Single-phase	Three-phase	DC	
1	16	250	480	-	Required
2	32	250	480	-	
3	connection of the EV to the a.c. supply network (mains) utilizing dedicated EVSE where the control pilot function extends to control equipment in the EVSE, permanently connected to the a.c. supply network (mains)				
4	connection of the EV to the a.c. supply network (mains) utilizing an off-board charger where the control pilot function extends to equipment permanently connected to the a.c. supply.				

2.4.1 AC Charging Levels 1 and 2

The first and at the same time less powerful systems are tagged as Level 1 charging systems, according to IEC 61851-1. This solution provides an up to 250V AC single-phase or 480V three-phase connection with current up to 16 A. The power rating is insufficient especially for 100% electric vehicles since nowadays battery packs have tens of kWh the charging time will be unacceptable. It is a good solution for cases of appeal, neighborhood vehicles, two-wheelers and hybrids with battery packs up to 10 kWh.

These EVSE systems can be supplied on the simplest form being just a cable with a connector on car side and a standard outlet on the other plus an additional very simple pilot circuit with specific safety/protection hardware between two connectors.

Single-phase connectors

The currently used connector (known as SAE J1172 connector) for single-phase charging is available from some major suppliers in the specific area of vehicle connectors and cabling. For instance, Yazaki corporation proposes a product rated up to 30 A (Table 2.10). A similar 1-Phase Connector is offered by REMA with 16 A and 30 A versions. As can be seen these connectors cover the AC Levels 1 and 2 full power range [21-22].

Table 2.10 Yazaki single-phase AC charging connector specifications [22]

Certification authority	JET / UL / TÜV Rheinland	
Certification standard	Electric Appliances and Material Safety Law / UL2251 / IEC62196-1	
Rated voltage	100 to 250V AC	120/240V AC
Rated current	20A (JPN/EU) / 30A (JPN)	20A / 30A (USA)
Cable type	POWER 2, GROUND 1, SIGNAL 1	
Operation temperature range	-40° to +60°	
Reference charging time (100%)	200V AC, 15A : 7h	100V AC, 15A : 14h
	* In case of a standard electric car	

Three-phase connectors

The use of on-board chargers is not limited to single-phase inputs. IEC 61851 standard predicts three-phase connections for AC charging levels 1 and 2. As seen so far a connector was proposed by Mennekes® according to this standard. Other manufacturers, such as REMA®, currently offer this connector. This solution may be of limited utility in a near term as three-phase outlets are more difficult to find than the single-phase outlets. On the other hand it is expected that with widespread use of electric vehicles, home or office parking places have available three-phase connections or even EVSE equipments.

There are no major differences between the single and three-phase connectors, apart from the two additional pins used to connect power lines. Connectors of such type are available with current ratings up to 63 A and usually split in three options: 16 A, 32 A and 63 A. [20-21]

2.4.2 DC Fast Charging

As seen the previous two levels have the capacity to meet different charging needs. Nevertheless these two levels do not meet all the user needs. Imagine if a trip away in the distance is beyond the range of the vehicle in which case you need to charge extremely quickly at least a significant portion of the battery. This failure to deliver enough power led to the emergence of the DC fast charge.

This is only possible using an external battery charger connected to the battery through a larger connector that came up together with the charging method presented by CHAdeMO. This Japanese association is formed by The Tokyo Electric Power Company, Nissan, Mitsubishi, Fuji Heavy Industries (the manufacturer of Subaru vehicles) and Toyota. Charging stations with the availability of DC charging currently in use provide CHAdeMO compliant connectors as well as the newer vehicles provide these connectors too. This connector is now available from industry-leader Yazaki Corporation.

Given that in this mode the charger is out of the vehicle, the on-board battery management system (BMS) should establish communication with the charger in order to transmit to it the required parameters for the charging process. This communication can be

performed by both analog signals and digital signal using CAN. Each connector has four analog signal pins, two CAN digital pins and a ground pin. [23]

Table 2.11 Yazaki DC charging connector (CHAdeMO)

Certification authority	UL / TÜV Rheinland
Certification standard	UL2251 / IEC62196-1
Rated voltage	500V DC
Rated current	120A
Cable type	POWER 2, SIGNAL 7, LED power supply 2
Operation temperature range	-40° to +60°
Reference charging time (100%)	500V DC, 120A : 30min * In case of a standard electric vehicle

2.4.3 Commercial systems

Several players from electric/electronic systems market have already proposed their solutions for electric vehicle charging. With WattStation™ trademark General Electric offers a range of chargers including charging stations and public EVSEs residential.



Figure 2.8 Commercial charging station [24]



Figure 2.9 Residential EVSE [24]

These charging systems are designed for Level 2 charge including a conductive coupled in accordance to SAE J1772 intended to be the commonly accepted solution for Level 1 and Level 2 AC charging. The built-in bidirectional communication system enables this system to be integrated in a Smart Grid infrastructure.

Table 2.12 Main features of GE WattStation™ [25]

UL Certified
Charger and vehicle communication in accordance with NEC 625
Cord connection in accordance with SAE J1772
Indoor and outdoor enclosures
Wall and pedestal mount
Commerce and card reader capability
User authentication
Network communications
Revenue grade metering with AMI communications
LED lights and display
Level 2 (208-240 VAC) charging capability

This proposal from General Electric fails to include even the capacity for DC fast charging. Other manufacturers like AeroVironment™ offer more powerful charging stations with power ratings of 30, 50, 60, 125 and 250 kW with public and fleet types. CHAdeMO association have certified until now 17 charging stations from multiple vendors. [23] One of these certified stations is the (fleet type) with a power rating up to 50 kW (Table 2.1).

Table 2.13 AeroVironment™ MODEL EV50-FS specifications [26]

Power Rating	50kW
Power Factor	0.95
Input Power	480V, 3 Phase AC (Other inputs available)
Input Current	68A
Frequency	50Hz / 60Hz
Efficiency Rating	>90%
Max. Output DC Current	120A
Max. Output DC Voltage	50-500V
Voltage Accuracy	1%
Current Accuracy (Lesser of the two)	.5A or 5%

A remarkable case study can be found in Portugal. The MOBI.E project is implementing a national charging network which provides all the services to allow the utilization of EVs. Users can subscribe this network and get access to 118 charging points throughout country.

2.5 Systematization of power converters

Prior to a first analyze of power converters do deal with V2G task the definition of some requirements should be done. These minimal requirements shouldn't be seen as constraints on the bellow presented research but rather as suitability measurements of the various alternatives.

Table 2.14 Desired features for V2G capable power conversion system

ID	Feature	Relevance
1	Bidirectional power flow	Needed
2	Close to unity power factor in rectifier or inverter mode	Desirable
3	Insulation between grid and car battery	Needed
4	Current control mode for battery charging	Desirable
5	Synchronous operation in inverter mode	Needed

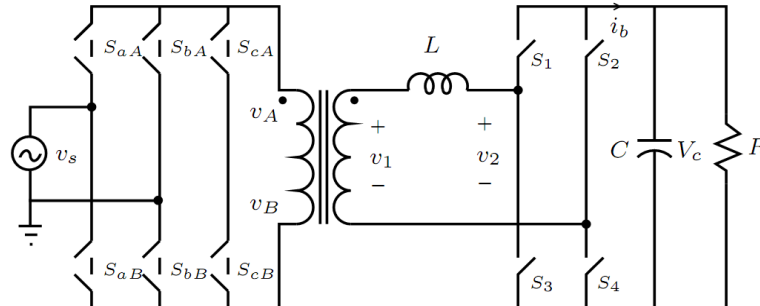
For this purpose a standard table was created in order to bring a better overview of all topologies and especially to provide a comparative analysis in an easy way.

Alongside with the verification of the previous features in each topology some other parameters are evaluated such as power and control scheme (if available), insulation method, the author's own conclusions about the work, control hardware used and the provenance of the results - analytical, numerical simulations or prototypes.

At the end of each table a brief analysis about each converter takes place.

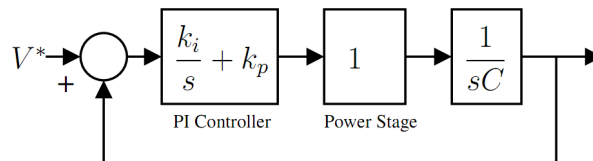
Author and year	Weise, N.D., K.K. Mohapatra, and N. Mohan, 2010 [27]
-----------------	--

Power schematic



AC-AC Stage	Single/Three Phase matrix converter
AC-DC Stage	Full bridge synchronous rectifier
Results provenance (s)	Simulation
Insulation method	High Frequency

Control scheme



Control platform/hardware	NA
Implemented features	(1)(2)(3)(4)(5)
Conclusions of the author (s)	Approximated models used are very acceptable, with errors studied and observed to be small. All the V2G requirements are satisfied. Usable with single or three phase source. Hardware being built to compare results.

Summary

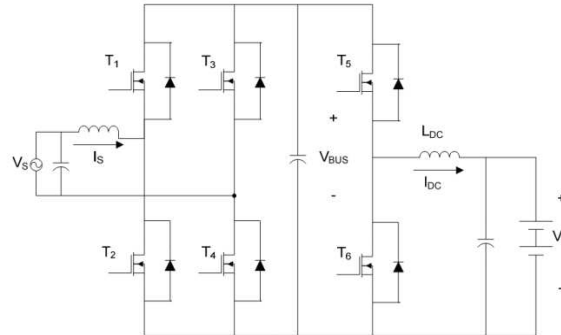
This solution is surely one of the most suitable for this application having potential to reach high power density levels with HF insulation but practical results awaited to proof the feasibility of this solution.

Low order harmonics present in current drawn from the source still need to be studied.

Interesting approach with control schemes and PWM generation done with low computational costs.

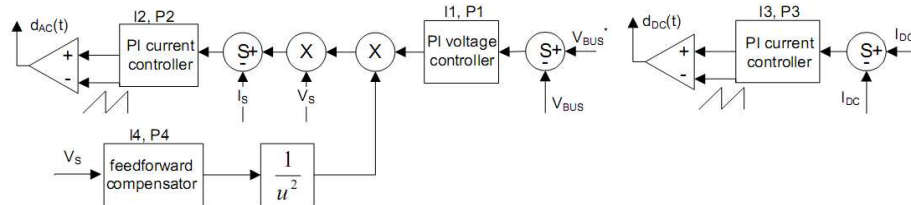
Author and year	Bilgin, B., A. Emadi, and M. Krishnamurthy, 2010 [28]
-----------------	---

Power schematic



AC-DC Stage	Single phase PWM rectifier/inverter
DC-DC Stage	Bidirectional Buck/Boost
Results provenance (s)	Simulation
Insulation method	None

Control scheme



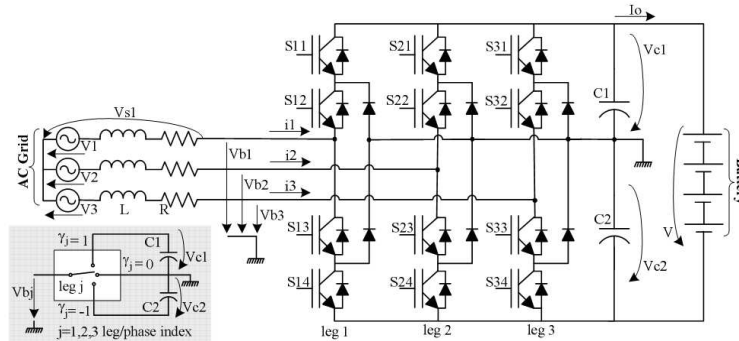
Control platform/hardware	NA
Implemented features	(2)(4)
Conclusions of the author (s)	Tests with maximum and minimum inputs (250V/50Hz and 90V/60Hz) shows good performance

Summary

Critical passive components have been designed based on analytical background. Design of feedback controller was done carrying the influence of DC bus capacitor and valuable observations relating feedback parameters and harmonic distortion generated and output current ripple.

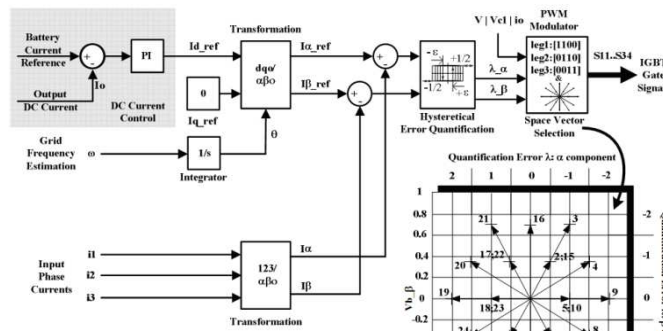
Author and year	Rei, R.J., et al., 2010 [29]
-----------------	---------------------------------

Power schematic



AC-DC Stage	Three-phase three-level PWM rectifier/inverter
DC-DC Stage	None
Results provenance (s)	Simulation
Insulation method	Low Frequency

Control scheme



Control platform/hardware	NA
Implemented features	(1)(2)(3)(4)(5)
Conclusions of the author (s)	Technical feasibility of charging strategies confirmed Developed a method handling coexistence of voltage and frequency droops

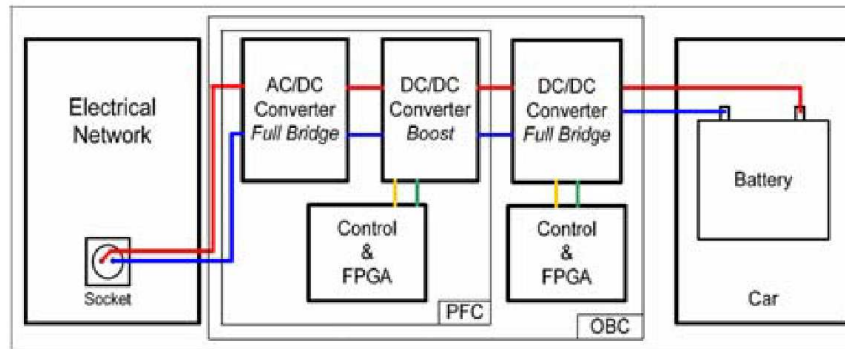
Summary

Interesting topology but voltage output with limited range due to inexistence of DC-DC stage. Suggested low frequency insulation transformer can create a bulky final system.

All features of the proposed control system validated with good results. Local grid condition estimation seems to be a promising short term solution for V2G feasibility.

Author and year	Grenier, M., M.G. Hosseini Aghdam, and T. Thiringer, 2010 [30]
-----------------	---

Power schematic



AC-DC Stage	PWM rectifier/inverter
DC-DC Stage	Bidirectional Full-bridge
Results provenance (s)	Simulation
Insulation method	High Frequency

Control scheme

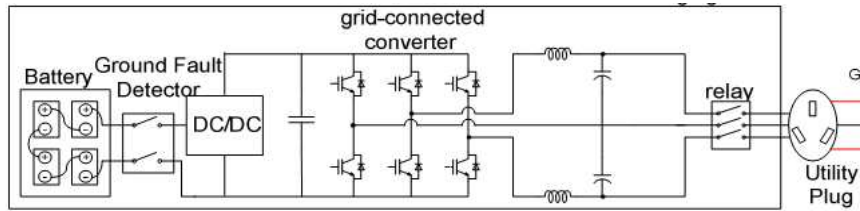
	NA
Control platform/hardware	FPGA
Implemented features	(1)(2)(3)(4)
Conclusions of the author (s)	Better efficiency with duty cycle control than phase shift control Efficiency increases as battery voltage increases Opting for an HEV could allow savings of 51% in energy costs

Summary

Significant data about efficiency study demonstrating linear relationship between drawn current and power losses.
 Estimation of weight and volume for the converter resulting in 4.75 Kg and 2.70 liter.
 Expected power density of 1.37 kW/liter with power rating considered in this paper
 Lack of details about resulting final system and also about control implementation

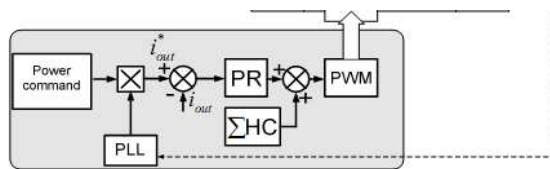
Author and year	Zhou, X., et al., 2009 [31]
-----------------	--------------------------------

Power schematic



AC-DC Stage	single-phase PWM rectifier/inverter
DC-DC Stage	Not specified
Results provenance (s)	Simulation
Insulation method	None

Control scheme



Control platform/hardware	NA
Implemented features	(1)(2)(5)
Conclusions of the author (s)	The PR and selective harmonics compensation method achieves good rejection of dominant harmonics in V2G mode. Capacitor current feedback method and PR controller guarantee low THD of output voltage for different types of loads in V2H mode. The proposed converter can greatly improve the performance of PHEV's integration with power grid.

Summary

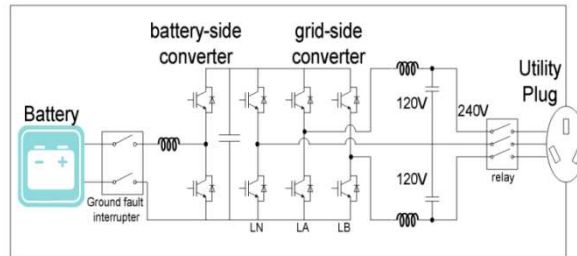
Remarkable results with the proposed proportional resonant + selective harmonic compensation controller when compared to classic PI

Good study about harmonic distortion in charger and V2G mode

Proposed vehicle-to-home operation mode (residential UPS) working as sinusoidal voltage source tested with several types of loads achieving good results due to capacitor current feedback strategy adopted

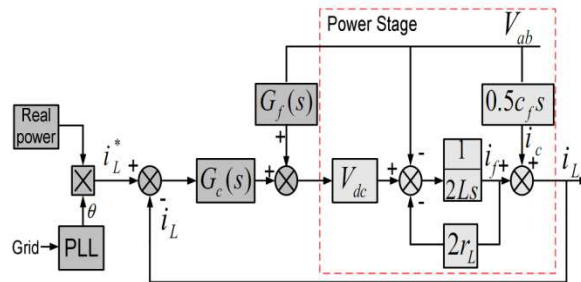
Author and year	Xiaohuz, Z., et al., 2009 [32]
-----------------	-----------------------------------

Power schematic



AC-DC Stage	Single phase PWM rectifier/inverter
DC-DC Stage	Bidirectional Buck/Boost
Results provenance (s)	Simulation and experimental setup
Insulation method	None

Control scheme



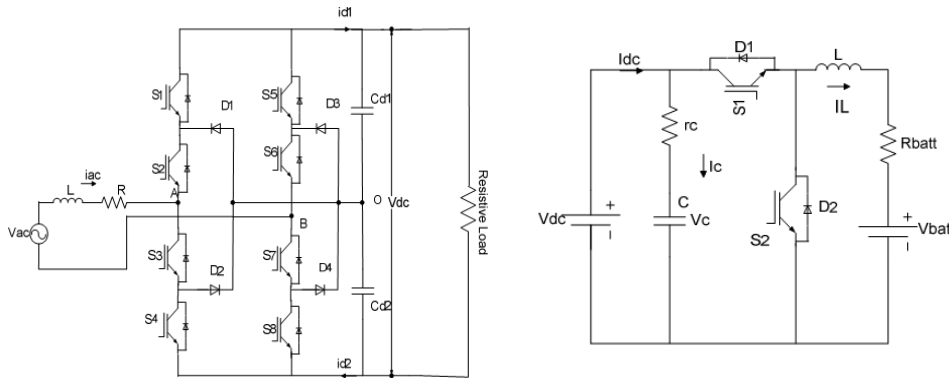
Control platform/hardware	TMS320F28335
Implemented features	(1)(2)(5)
Conclusions of the author (s)	Simulation and experimental results verify the functions and performance of the proposed charger. A household based PHEV charger can be used to implement multiple functions including battery charging, vehicle to grid and vehicle to home, which make the proposed charger promising for PHEV applications.

Summary

Lack of galvanic insulation studied and interesting techniques are presented to deal with possible safety issues. The small-scale prototype enables feasibility proof about the proposed topology and control strategies and acquisition of valuable data such as drawn current waveform and low order harmonics magnitude.

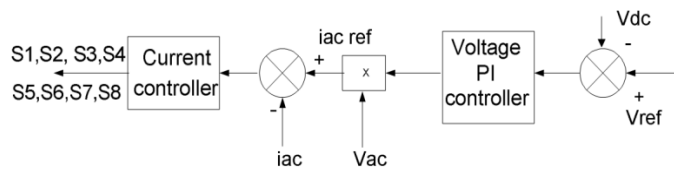
Author and year	Jaganathan, S. and G. Wenzhong., 2009 [33]
-----------------	---

Power schematic



AC-DC Stage	Single-phase three-level PWM rectifier/inverter
DC-DC Stage	Bidirectional Buck/Boost
Results provenance (s)	Simulation
Insulation method	

Control scheme



Control platform/hardware	NA
Implemented features	(1)(2)(4)(5)
Conclusions of the author (s)	The converter draws unity power factor from the grid. Also the harmonics of the system has shown to be greatly reduced and the charging system is shown to be utility friendly.

Summary

Option for a multilevel NPC resulting in low THD but practical implementation issues ignored. PI based control with detailed description of parameter calculation and converter model determination. Synchronization method not described.

The presented tables describe recently published work in charging systems technology for electric vehicles. Many options were discarded for not being minimally framed in the basic requirements defined earlier. Several simulation works has been presented recently but there are no many published experimental results. Some aspects like grid synchronization methods, passive components design and physical parameters like weight, size or even thermal management systems are still currently ignored by most authors. Apart from this some technological options start to become usual.

In AC-DC conversion is agreed the adoption of a force commutated rectifier with modern switches (especially IGBTs) and some PWM command technique. The variations are between single-phase and three-phase, with some alternative solutions for multilevel. If the topology does not expect much discussion, the control opens up many possibilities but always based on digital systems. The usage of controlled grid-connected systems implies the need for synchronization information like instant grid angle (Θ) commonly required for rotating frame based control systems or synchronized PWM generators. The most promising solution is the phase locked loop (PLL) block, prior known from analog communication systems. This method has become interesting for the control of synchronous electronic converters especially those based on digital control.

Another relevant issue is the passive component design. Some published works presents mathematical expressions essentially for line current filter inductor and DC bus filter capacitor and explicit their influence for system behavior. The signal acquisition implies some design cares but is not a particularity of this application and is not usually referred in this scope.

The analyzed solutions in some cases are built with just a single conversion stage but important features like galvanic insulation or battery pack voltage level matching are not possible unless a second DC-DC conversion stage is added. The discussion about the topology to use on this stage is still very open.

The simplest and more obvious option is the bidirectional buck/boost converter. This converter has a simple operation with only two controlled switches and an output voltage range between zero and DC bus voltage. Despite the continuous output current a large amount of power drawn from this leads to a high current ripple which could not be supported by batteries. This ripple needs to be attenuated with a filter inductor which certainly represents a large volume due to winding with large wire and the need for a huge core to handle magnetic saturation effect. In reverse mode the circuit operates as boost converter ensuring proper DC bus voltage to feed the AC-DC stage functioning as inverter.

Anyway the insulation requirement cannot be fulfilled with this solution. Considering this feature required prior to converter design the demand for a new topology has to be considered limiting the search to insulated DC-DC converters. Such converters are always based on magnetic elements (transformers) used to transfer power from one side to another through a magnetic circuit. Even with the need for bi-directionality options might include choice of half or full-bridge with several options for the control system such as controlled or uncontrolled rectification.

No relevant work has yet been proposed considering such insulated converters possibly due to a high level of abstraction used by the major part of authors when the feature is suggested to be implemented with a grid frequency transformer which not represents a practical solution to a physical system considering the large size and weight involved.

Apart from the conventional topologies a more sophisticated system using a AC-AC matrix converter was proposed in [27] to match the insulation requirement through a high frequency transformer with output rectified by a controlled full-bridge. The option for this converter will not be considered in this work due to control complexity and to not compromise the feasibility of the purposed work.

The main above referred alternatives are classified by [34] split in AC-DC stages ranging from single-phase half-bridge to three-phase multilevel full-bridge and DC-DC stages including dual active bridge, conventional bidirectional buck-boost and some other modified buck-boost designs.

An additional discussion is focused in which hardware should be used for power circuit - dedicated switches or the integration with motor drive using the existing power converter. It could be seen as a solution to reduce costs taking advantage from the high performance and power rating typical in such converters. In some approaches the motor windings are also properly arranged to perform a powerful input current filter or even used as power transformer providing insulation to charging system through some modifications in motor construction. The switching between charging/motor drive operation modes can be done easily through relays (solid state or mechanical) [35-36].

2.6 Summary

In this chapter the basic structure and components of modern electric vehicles have been described. The standards were also listed as they are essential in the evolution of electric vehicles, especially in charging systems.

After it, there were presented currently available charging systems. In the end it was analyzed recently published articles relating to electronic on-board charging, concluding with a discussion of the conversion topologies that have been used by several authors to the most relevant trends.

Chapter 3

Topology selection

The purpose of this chapter is to do a comparative analysis of suitable power converter structures to deal with vehicle-to-grid technology in the future. Due to the high amount of recent proposals and possibilities, an in-depth review of the state-of-art in bidirectional charger system was performed in the previous chapter.

After a survey of more appropriate solutions and analysis of current trends, is now important to identify the basic topologies of interest to this application and identify possible associations in multiple stages.

For the purpose of this work will be considered a single-phase connection to the grid. This restriction should not make the project less valuable since all the grid connected converters can be found in single and three phase configurations.

3.1 Basic topologies

3.1.1 AC-DC

Single Level

Surely the simplest way to make a bidirectional connection with grid is through a full bridge. This topology is far more interesting when compared with the conventional line commutated rectifiers due to its ability to shape a sinusoidal current waveform on grid interface and impose a unitary power factor.

Besides the active components (switches) in its simplest configuration also includes a filter on the DC side voltage generally consisting of one or more capacitors in parallel and a filter on the AC current, which can be a single inductor in its simplest version or a tuned LCL filter, with particular interest to major powers where the inductor size is very critical.

One of its main limitations is to have a minimum threshold for the DC bus voltage as a function of input voltage. This way can only be used as battery charger with high rated voltage batteries or there is a need to add another converter with voltage step down characteristic.

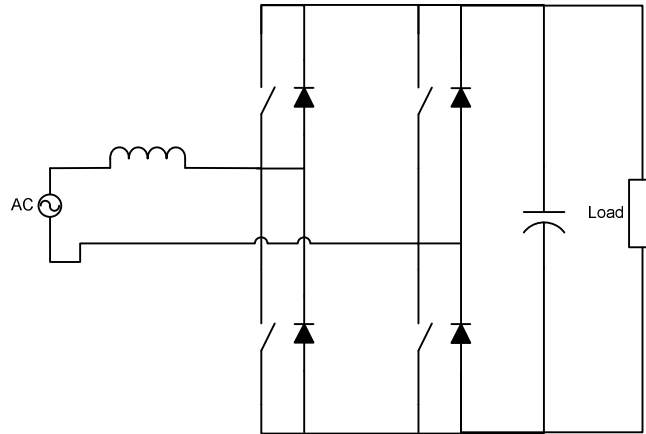


Figure 3.1 Full Bridge PWM rectifier/inverter

Table 3.1 Components list for rectifier/inverter

Component	Quantity	Observations
Switch	4	Fully-controlled
Inductor	1	Large for high currents or low switching frequencies
Capacitor	1	Large for a DC bus with low ripple Many times split in series/parallel associations

The control of this converter is also strongly studied and described in literature [37-38]. The vector control techniques based on rotational frame are the most sophisticated at this level although the computational resources used nowadays for the control of power electronics can already perform it with relative efficiency.

Multi Level

In systems with considerable power where AC power quality is a relevant factor, the option for a multilevel topology can be considered interesting. Multilevel converters make use of switches associated in series that allow beyond the usual levels $+V_{DC}$, $-V_{DC}$ and 0, put on the AC terminals other intermediate voltage levels, thus making it easier to shape a sinusoidal waveform and reducing the harmonic content for a similar conditions of operation when compared with single level configuration. These intermediate voltage levels can be produced by voltage sources isolated from each other or by series association of capacitors in the DC bus.

Their main difficulties are: first, the added complexity in the control circuit due to the need of twice the control signals and a more complex interlock system and the second relates to the balancing of voltages in capacitors responsible for generating the intermediate voltage levels. This management is usually done through the redundant states so that for long periods of time the energy extracted from various capacitors is the same. In a low power converter can be difficult to justify the choice for this solution.

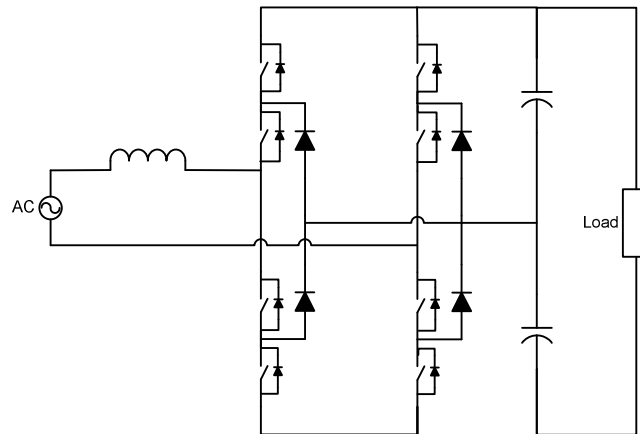


Figure 3.2 Single-phase multilevel rectifier/inverter

Table 3.2 Components list for multilevel rectifier/inverter

Component	Quantity	Observations
Switch	8	Fully-controlled
Inductor	1	Large for high currents or low switching frequencies
Capacitor	2	At least but can be rated to half DC bus voltage

3.1.2 DC-DC

Half-Bridge converter (Buck/Boost)

This DC-DC converter can be viewed as nearly universal as long as viewed from both sides. It consists of half-bridge with two fully controlled switches and an inductor connected between the two switches and the load (battery pack in this case).

Thus when the power is transferred from the DC bus to the load it works in buck mode, i.e. allows charging any battery whose maximum voltage during charging process does not exceed the DC bus voltage. This operation is possible by controlling the top switch and with bottom switch keeps functioning as free-wheeling diode.

Inversely enables to discharge the battery transferring energy to the DC bus and operating the circuit as a boost. This mode is achieved by switching the bottom switch and holding the top switch to act as a diode. So in this mode only voltages higher than the battery voltage can be achieved on the DC bus.

For purposes of this application can be pointed out two obstacles to the use of this topology. First the battery is not electrically isolated from the DC bus or from the mains, which violates a requirement of the project. Secondly a very large inductive filter would have to be used in series with the batteries due to magnetic saturation phenomena since the current has a strong DC component at this component.

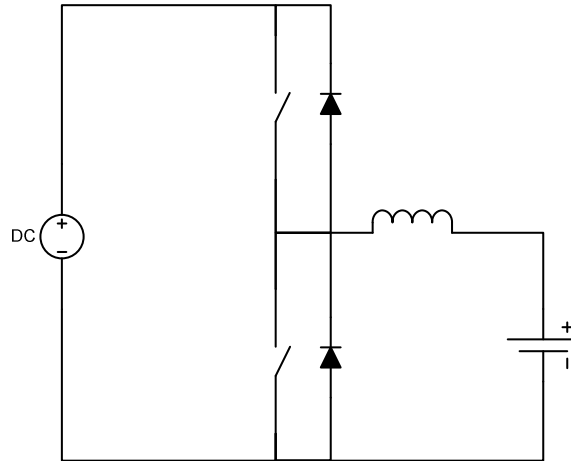


Figure 3.3 Half-Bridge converter (Buck/Boost)

Table 3.3 Voltage range for Buck/Boost

Limit	Value
Minimum	0
Maximum	V_{DC} (DC bus voltage)

Table 3.4 Components list for Buck/Boost

Component	Quantity	Observations
Switch	2	Fully-controlled
Inductor	1	Large for high currents or low switching frequencies

Dual Active Bridge converter (Buck/Boost)

To meet the insulation requirement many DC-DC topologies could be considered but the majority (Forward, Flyback, etc.) are not suited to power levels that rise above 1 kW. The only common options that can be taken into account for these levels are the half-bridge and full-bridge in combination with a high frequency transformer. These topologies are widely used in commercially available power supplies to power levels over 500 W but cannot be entered into the project by not having characteristics bidirectionality.

An interesting variant of the full-bridge called dual active bridge can be introduced to meet these two requirements: isolation and bidirectionality. This topology is certainly the more versatile DC-DC converter as it can be controlled in order to operate as a buck or boost, in either direction. Another of its interesting characteristics it's the low ripple produced at DC terminals. Still an advantage should be pointed out that relates to their characteristics of ZVS (zero-voltage switching) over nearly the entire operating range. Unlike Buck/Boost has a

perfect symmetry, i.e. the control can be performed exactly the same way to transfer power in either direction.

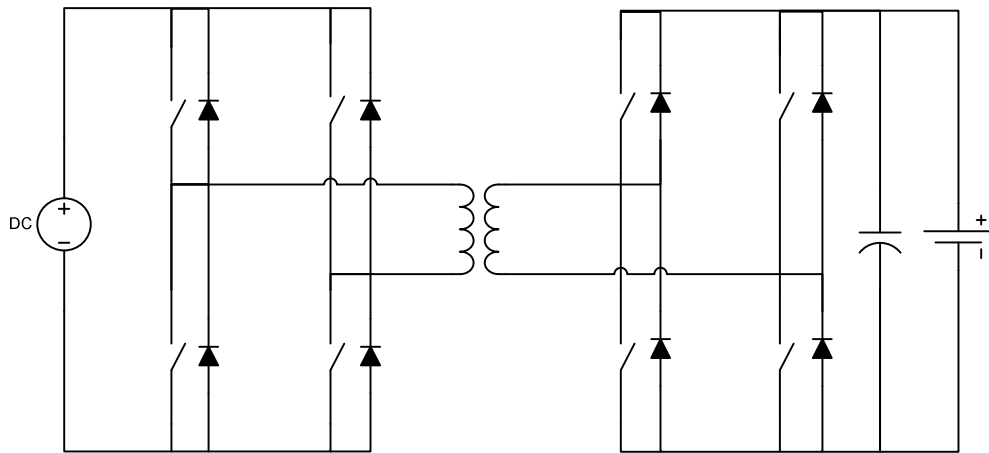


Figure 3.4 Dual active bridge converter [39]

Table 3.5 Voltage range for dual active bridge

Limit	Value
Minimum	0
Maximum	∞

Table 3.6 Components list for dual active bridge

Component	Quantity	Observations
Switch	8	Fully-controlled
Transformer	1	High-frequency. Expected to be small and light
Capacitor	1	At least one on the batteries side. The other is already on the DC bus

3.2 Association of AC-DC and DC-DC stages

As can be seen the total matching of all requirements is not possible with any of the basic topologies presented previously. The solution lies in involving two or more of them with the aim of forming a conversion architecture with multiple stages so that all requirements can be fulfilled.

One of the more immediate solutions is the combination of PWM inverter / rectifier with a buck / boost that would implement all the requirements except for the isolation of which cannot renounce. If this hypothesis were taken would be a need to put a low frequency isolation transformer in the grid interconnection.

Another solution would be to use the dual active bridge again associated with the PWM inverter / rectifier. This solution although more technically complex offers electrical isolation through a high frequency transformer which is certainly more interesting than the solution of the low frequency isolation.

A variant of these solutions would be to use a multilevel inverter / rectifier which would optimize the interface for the network and even if the option does not fall on it at this stage will always be considered as a future improvement.

To make all this range of options more comprehensive a diagram was made with available options for each stage. Note that with regard to the DC-DC converter the hypothesis of no use at all is also taken into account.

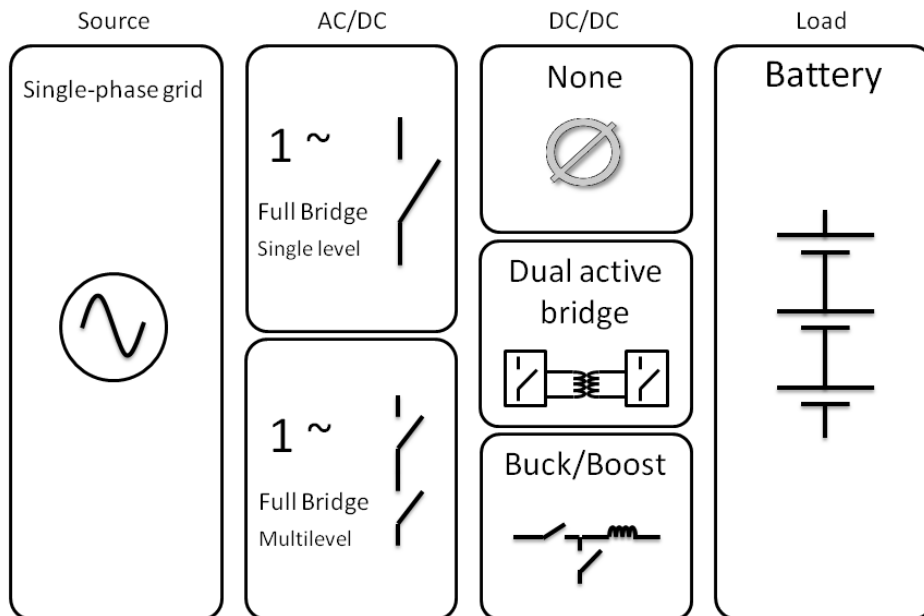


Figure 3.5 Chart of alternatives for the converter architecture

3.3 Criteria

After studied a range of alternatives for the converter implementation is time to establish criteria for a justified choice. Although at this stage still a conceptual design the criteria will have the most practical concern since the project is to be realized in fact. It is still necessary to take into account the final application of the system, which is an on-board charger so the volume available for such a device is limited being the power density of a winning criteria.

Following will be established the considered criteria as well as brief remarks on each.

Power density - the amount of power (time rate of energy transfer) per unit volume. A key criterion in this choice taking into account the application. In this field high values can be achieved by two factors: first the demand for converters with very high efficiency and secondly to avoid the use of large passive elements.

Cost - final cost of the whole system. Always an important factor when there is the possibility of becoming a commercial product. In this study, only a comparative evaluation can be made since at this stage the project still far from the physical system design.

Control complexity - a comparative measurement considering amount of computational requirements involved and the control circuit complexity. A very high level may affect the system on several factors such as cause the need for a higher performance control hardware (more expensive), add components to the measurement and act systems increasing the total

cost of the product and also last but not less important increase the engineering costs due to longer development and debugging time of both software or hardware, which sometimes can represent a significant part of total cost.

Switch utilization ratio - is the total switch utilization ratio defined as $SUR = \frac{P_{out}}{n \times V_{max} \times I_{max}}$, where n is the number of power switches in the circuit, V_{max} and I_{max} are their peak voltage and current. Can be understood as the ratio between the total converter power and the sum of the power ratings of all switches used by the topology. This criterion serves as a measure of wasted capacity of switches and usually prejudice complex topologies with large numbers of switches. The calculation of this parameter for the different solutions is shown in Table 3.7.

Table 3.7 SUR calculation

Solution	Calculation	Result	Rating
1-ph PWM Rectifier	$\frac{V_{out} \times I_{out}}{4 \times V_{out} \times I_{out}}$	0.25	++
1-ph PWM Rectifier + Buck-Boost	$\frac{V_{out} \times I_{out}}{6 \times V_{out} \times I_{out}}$	0.17	+
1-ph PWM Rectifier + Dual active bridge	$\frac{V_{out} \times I_{out}}{12 \times V_{out} \times I_{out}}$	0.08	-
1-ph multilevel PWM Rectifier	$\frac{V_{out} \times I_{out}}{8 \times \frac{V_{out}}{2} \times I_{out}}$	0.25	++
1-ph multilevel PWM Rectifier + Buck-Boost	$\frac{V_{out} \times I_{out}}{8 \times \frac{V_{out}}{2} \times I_{out} + 2 \times V_{out} \times I_{out}}$	0.17	+
1-ph multilevel PWM Rectifier + Dual active bridge	$\frac{V_{out} \times I_{out}}{12 \times V_{out} \times I_{out}}$	0.08	-

Output voltage range - range of the output voltage at which the convert has the capacity to deliver power to the battery. Since this design is not targeted to any particular battery pack is important to have a voltage range as wide as possible. At this point the battery packs that can be found in electric vehicles are not yet stabilized at a particular value which makes the project more difficult. This way to create a charger with high practical value is important being compatible with several packages of batteries. Even for a given battery, voltage may vary considerably for different state of charge values and a good regulation is desirable in the whole process.

For this purpose was an estimate of each converter output voltage range as is described above. These data are presented in Table 3.8.

Table 3.8 Output voltage ranges

DC-DC stage	Range	Rating
None	(output of the AC-DC stage)	0
Buck-Boost	0 to V_{DC}	+
Dual active bridge	0 to ∞ *	++

* It means that there is no theoretical limit.

3.4 Comparative table

Once established the criteria it was considered as very useful to put all data in a table to allow a choice for the most interesting solution for this application. In fact a few options were left out for various reasons but the most rational choices are the ones that do have interest in this phase. The purpose of this table is to support a comparative analysis and allow proposing a solution.

Solution	Switch Utilization Ratio	Power density	Cost	Control complexity	Output voltage range	Total
Single-phase						
LF* transformer + PWM rectifier	++	-	-	++	0	+2
LF transformer + PWM rectifier + Buck-Boost	+	--	-	+	+	0
PWM rectifier + Dual active bridge	-	++	++	0	++	+5
LF transformer + PWM multi-level rectifier	++	-	-	-	0	-1
LF transformer + PWM multi-level rectifier + Buck-Boost	+	--	-	-	+	-2
PWM multi-level rectifier + Dual active bridge	-	++	+	-	++	+3

*LF stands for low frequency.

3.5 Discussion

This study has covered a few different power converter topologies for bidirectional battery charger for electric vehicle application. According to the criteria defined so far the chosen topology is the association of a conventional single-phase PWM inverter/rectifier with the dual active bridge DC-DC converter.

The feature of providing insulation without penalizing the power density and cost was the main advantages of this solution. A reasonable control scheme can also be design to this converter with any of the conversion stages handling the task of controlling the rate of charge/discharge.

A proper voltage output level can be achieved not only with the transformation ratio but also with the proper control of any of the converters.

For power density classification the LF transformer was the determinant factor, but not the only one. In buck-boost the need for an output filter built through large and heavy passive elements may still penalize more the classification.

In relation to costs was understood that the LF transformer would represent a substantially larger amount than all other components.

All multilevel topologies got a bad rate essentially on control complexity. The need for a monitoring of half-bus capacitors to keep they balanced along operation are a critical

requirement. Considering the switching scheme these converters appear again with more switching states and an inherent more complex control algorithm. They need twice more drive circuits and a more complex protection circuit.

The rest were ranked in descending order starting with only a single-phase converter, after associated with the Buck-Boost and finally the association with the Dual Active Bridge.

A wide range of output voltages is important not only to make the solution applicable to a wide range of batteries, but mainly to allow for a proper control of the load current in all states of charge of the battery. Either the buck-boost or the dual active bridge allows a wide range of output voltage levels. In theory the buck-boost is upper limited and will charge the battery with output voltages ranging from the maximum voltage DC bus down to zero. On the other hand the dual active bridge doesn't have a theoretical upper limit and can the minimum voltage output is also zero.

In summary, the problem of transferring energy between a Grid and a high voltage DC bus in Electric Vehicle has been addressed. This work seeks to answer the following question: What is the best structure of the power converters to charge the batteries of electric vehicles with smart grid concept? The answer is of course not unique, given that not all requirements are known. However, this study points to a direction based on the single-phase Dual Active Bridge topology. The dual active bridge converter have attractive features in terms of reasonable number of components, low switching losses, high-power density and simple first-order stable dynamics. The main design issue is the transformer design.

3.6 Proposed architecture

This section provides the proposed structure for the charging system. For a better understanding of the framework a diagram is presented in Figure 3.6.

The first level is only conceptual and presents the main components of the car electrical system. This level is important to understand where the charging system takes place into the overall electric system. Then the proposed architecture for the charger is presented according to the selection made above. In the last level appears an electrical circuit of the converter that is proposed to be developed in this work.

3.7 Summary

In this chapter were presented basic topologies considered more relevant to the implementation of this charging system. Its voltage ranges as well as an assessment of their feasibility and complexity are also discussed.

After that are defined criteria for a reasoned selection and are data unified to make way for a discussion and a consequent choice for one of the alternatives. The converter architecture is presented and detailed for three levels.

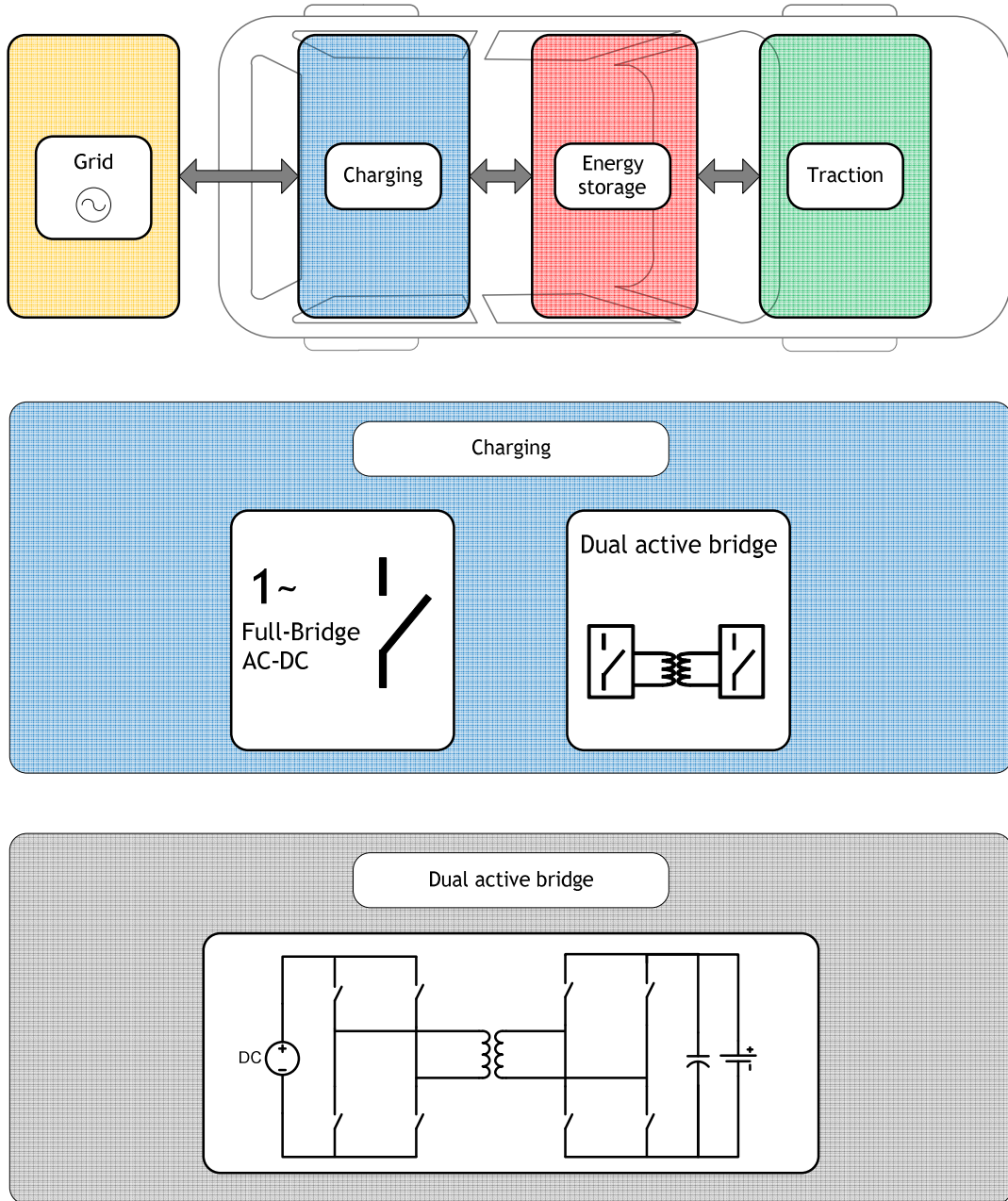


Figure 3.6 System architecture

Chapter 4

Dual active bridge converter

This chapter is divided into two parts. The first merely theoretical in nature aims to provide a description of the converter to design in terms of its constitution and how it works. It also examined the operation in steady state supported with basic waveforms and equivalent circuits. The most basic expressions are also presented as well as defining the boundaries for soft-switching operation. The limits for soft switching are also mentioned.

In the second part is presented and described a simulation model for this converter and several simulations are made with clear objectives. The first is to demonstrate the proper functioning of the converter in buck and boost modes presenting its key waveforms. The second objective is to determine a maximum value for the leakage inductance and perform various simulations for comparison with analytical results. In this phase should also be evaluated the suitability of the converter to the specific application. Finally there will be an estimate of the minimum capacitor to be placed on the batteries side to meet predefined ripple amplitude.

4.1 Introduction

The Dual-Active Bridge (DAB) topology is inserted in the group of bidirectional isolated DC-DC converters. It was firstly proposed by Kheraluwala et al. in [39-40] and consists essentially in two full bridges and a high frequency power transformer.

The ac terminals of each bridge are connected to each side of a high frequency transformer and the dc sides connected to different DC bus. Bridges are controlled in order to generate a symmetrical bipolar square wave with high frequency. The converter has a total symmetry, i.e. whether seen from primary to secondary or from secondary to primary, is exactly the same. This feature allows controlling power flow on both directions in the same manner and can operate in buck or boost mode.

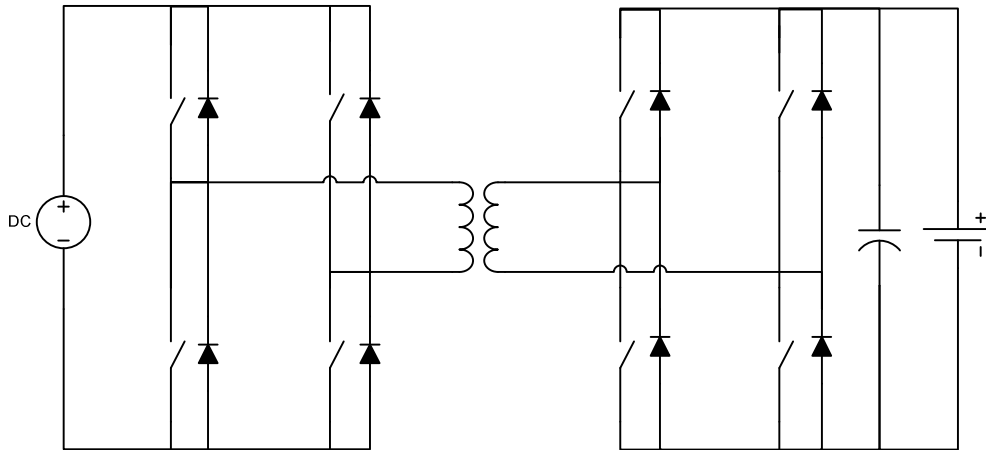


Figure 4.1 Circuit schematic of a single phase dual active bridge dc-to-dc converter [39]

The most common control method for this converter consists in control both bridges so as to create phase-shifted waveforms. When phase-shift is null there is no active power transfer in any direction and with 90° of phase shift the maximum power flow is achieved. In a range of 0 to 90° power flow can be controlled being always delivered from the bridge with leading square wave. The amount of power flow not only depends on the phase-shift but also on other parameters such as the DC voltages on both sides, the switching frequency and leakage inductance of power transformer. This last one, the leakage inductance, is generally seen as a transformer parasitic and implies the transformer design to be very careful with the aim of obtaining a particular value.

In order to realize its principle of operation is usually presented a fundamental model with two square wave energy sources connected by means of an inductor. This is a classic model has been used to represent the basic principle of energy transfer between to alternating sources, but with the difference of sources producing sinusoidal waveforms.

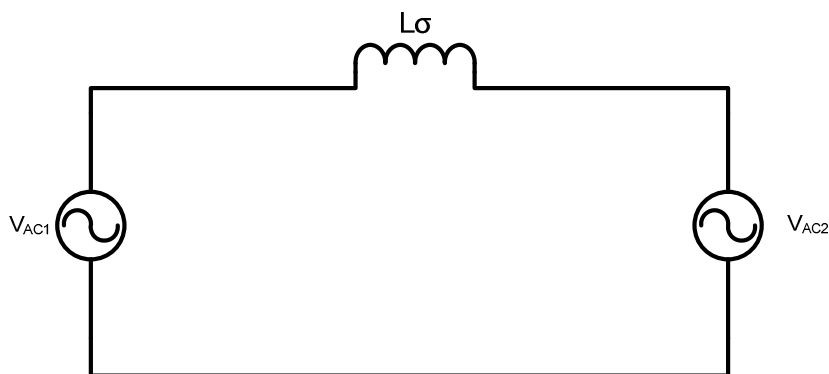


Figure 4.2 Fundamental model [41]

One of the most interesting features of this converter is that it allows the switches to be operated in zero voltage switching (ZVS) mode for a wide load range, which allows implementing converters with high efficiency and power density. Another advantage of DAB over other topologies is the potential for size reduction of the passive components, by using

integrated magnetics. These characteristics are of great added value when application is an electric vehicle battery charger.

4.2 Steady-state analysis

Equivalent circuits

One of the methods to analyze switching circuits is representing the equivalent circuits for each state. In this case the analysis will be conducted only for half cycle due to the characteristics of symmetry of its operation.

For this analysis we assume that the switching sequence begins with current flowing through the devices D_{A+} , D_{S3} and D_{S2} as shown in Figure 4.3. As the current is flowing by the diodes, the voltage drop on the switches is zero. Thus the switching of T_{A+} and after a certain phase-shift of T_{S2} and T_{S3} will take place on zero voltage.

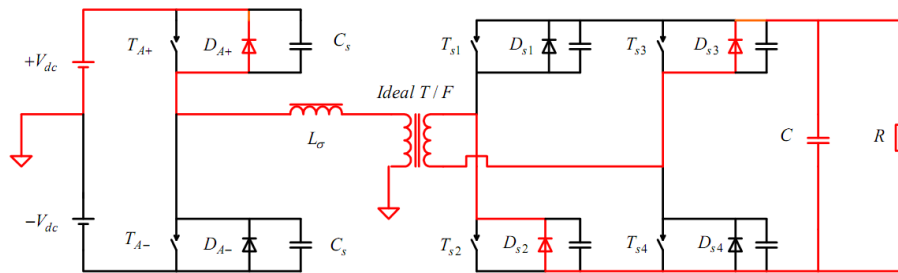


Figure 4.3 Equivalent circuit 1

When current reverse will begins to flow by T_{A+} , D_{S2} and D_{S3} as can be seen in Figure 4.4.

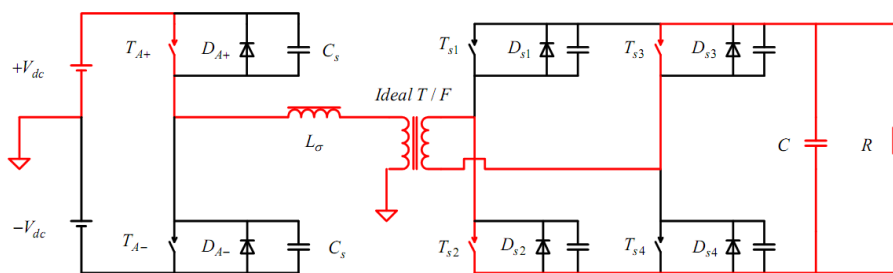


Figure 4.4 Equivalent circuit 2

After that is the time for the switches and T_{S2} T_{S3} turn off and forcing the current flow and by D_{S1} and D_{S4} . This is represented in Figure 4.5.

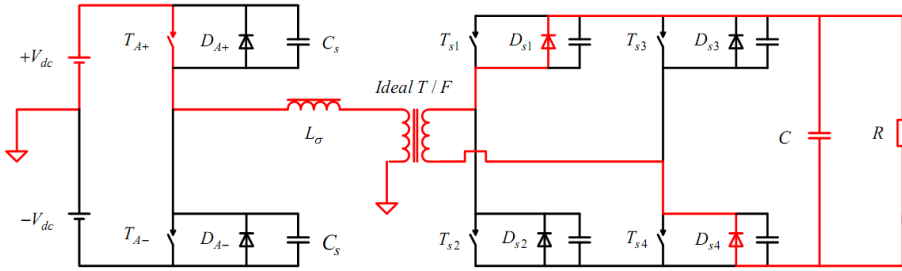


Figure 4.5 Equivalent circuit 3

When the switch T_{A+} is turned off the energy stored in the inductance is transferred to the snubber capacitors. The snubber capacitor placed across T_{A+} will take over the current, and the switch turn-off occurs under ZVS conditions and when the device is carrying a certain minimum current. Additionally, the snubber capacitor connected across the T_{A-} will be discharged and will force the diode D_{A-} to be forward-biased. Therefore, the inductor current starts flowing through the diode D_{A-} and diodes D_{s1} and D_{s4} , as shown in Figure 4.6.

Similarly, the switch T_{A-} is turned on at zero voltage and the commutation sequence will be repeated as above[42].

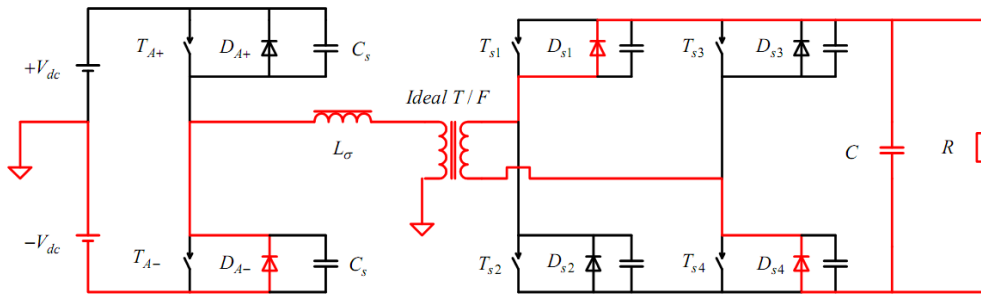


Figure 4.6 Equivalent circuit 4

An alternative analysis can be made to this circuit through its main waveforms. This analysis is then performed and allowed to identify the modes of operation of the converter.

Voltage across the leakage inductance terminals ($V_{L\sigma}$) can be seen as the difference between the ac terminals voltage in at any moment.

Recalling that the bridges are switched with a bipolar pattern only two different values of output voltage at the ac terminals can be obtained ($+V_{DC}$ and $-V_{DC}$).

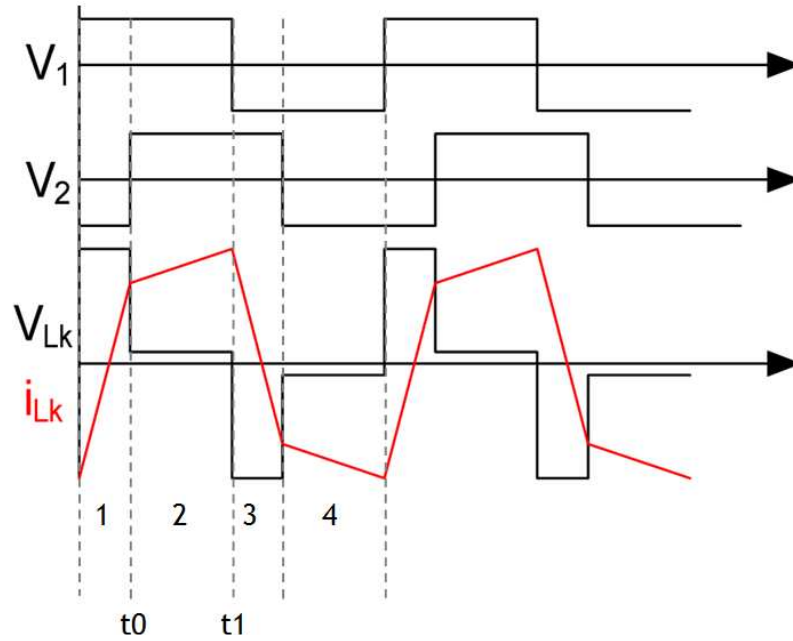


Figure 4.7 Fundamental waveforms [41]

Table 4.1 Leakage inductance voltages in each time instant

Instant (Figure 4.7)	Primary bridge	Secondary bridge	Leakage inductance
1	+ V_1	- V_2	V_1+V_2
2	+ V_1	+ V_2	V_1-V_2
3	- V_1	+ V_2	$-(V_1+V_2)$
4	- V_1	- V_2	$-(V_1-V_2)$

From Figure 4.7 can now be identified two operation modes, each consisting of two instants that the current has the same behavior but with inverted slope.

In this way will be established mode 1 that includes the instants 1 and 3, where voltages have different polarity, and mode 2 in which are inserted instants 2 and 4 and where voltages have the same polarity.

Mode 1:

$$0 \leq \omega t \leq \omega t_0 \tag{4.1}$$

$$i_{L\sigma}(\omega t) = \frac{V_{DC1} + V_{DC2}}{\omega L\sigma} \omega t + i_{L\sigma}(0) \tag{4.2}$$

Mode 2:

$$\omega t_0 \leq \omega t \leq \omega t_1 \quad (4.3)$$

$$i_{L\sigma}(\omega t) = \frac{V_{DC1} - V_{DC2}}{\omega L\sigma} (\omega t - \omega t_0) + i_{L\sigma}(\omega t_0) \quad (4.4)$$

Considering that the steady state current waveform is perfectly symmetrical the current at the end of a half-cycle can be expressed as:

$$i_{L\sigma}(0) = -i_{L\sigma}(\omega t_1) \quad (4.5)$$

The initial current ($i_{L\sigma}$) can now be calculated. From (4.2) $i_{L\sigma}(\omega t_0)$ is determined by considering $\omega t = \omega t_0$. From (4.4) $i_{L\sigma}(\omega t_1)$ is determined by setting $\omega t = \omega t_1$ and the $i_{L\sigma}(\omega t_0)$ found on (4.2). Rearranging and defining $M = \frac{V_{DC2}}{V_{DC1}}$ in combination with the (4.5) results:

$$i_{L\sigma}(0) = \frac{V_{DC1}}{2\omega L\sigma} [(1 - M)(\omega t_1 - \omega t_0) + (1 + M)\omega t_0] \quad (4.6)$$

In a similar way, $i_{L\sigma}(\omega t_0)$ can now be determined from (4.2) by insertion of $i_{L\sigma}(0)$ expression found in (4.6).

$$i_{L\sigma}(\omega t_0) = \frac{V_{DC1}}{2\omega L\sigma} [(1 + M)\omega t_0 - (1 - M)(\omega t_1 - \omega t_0)] \quad (4.7)$$

From Figure 4.7 is visible that $\omega t_1 - \omega t_0 = \pi - \phi$ and $\omega t_0 = \phi$, being ϕ the phase-shift of two voltage waveforms in radians. Rewriting the equations:

$$i_{L\sigma}(0) = \frac{V_{DC1}}{2\omega L\sigma} [(1 - M)(\pi - \phi) + (1 + M)\phi] \quad (4.8)$$

$$i_{L\sigma}(\phi) = \frac{V_{DC1}}{2\omega L\sigma} [(1 + M)\phi - (1 - M)(\pi - \phi)] \quad (4.9)$$

The converter output power is then given by [39]:

$$P_O = \frac{2V_{DC1}^2}{\omega L\sigma} M\phi \left(1 - \frac{|\phi|}{\pi}\right) \quad (4.10)$$

Average output current:

$$I_O = \frac{P_O}{V_{DC2}} = \frac{2V_{DC1}}{\omega L\sigma} \phi \left(1 - \frac{|\phi|}{\pi}\right) \quad (4.11)$$

4.3 Boundaries for zero-voltage switching

As mentioned earlier, this conversion topology has a large load range where the switches can be operated under zero-voltage switching and ways to identify the limits of this area is crucial when high efficiency is pursued. Thus it is necessary that a certain minimum current is circulating through the circuit ensuring that every time a switch occurs in a particular switching cell, the current is circulating through anti-parallel diodes in that moment.

These conditions can then be represented analytically by:

$$i_{L\sigma}(0) \leq 0 \quad (4.12)$$

$$i_{L\sigma}(\phi) \geq 0 \quad (4.13)$$

Gathering information from, (4.8), (4.9), (4.12) and (4.13) the soft switching region can be delimited as a relationship between M and ϕ .

$$M \leq \frac{\pi}{\pi - 2\phi} \quad (4.14)$$

$$M \geq 1 - \frac{2\phi}{\pi} \quad (4.15)$$

An important conclusion can be made based on (4.14) and (4.15). For $M=1$ the soft-switching conditions are fulfilled with any phase-shift angle.

This feature can gain a special interest when the converter is used in combination with another such as a grid-connected inverter / rectifier. This way you can adjust the input voltage to meet the output voltage of the converter and thus ensure a soft-switching operation throughout the operating range.

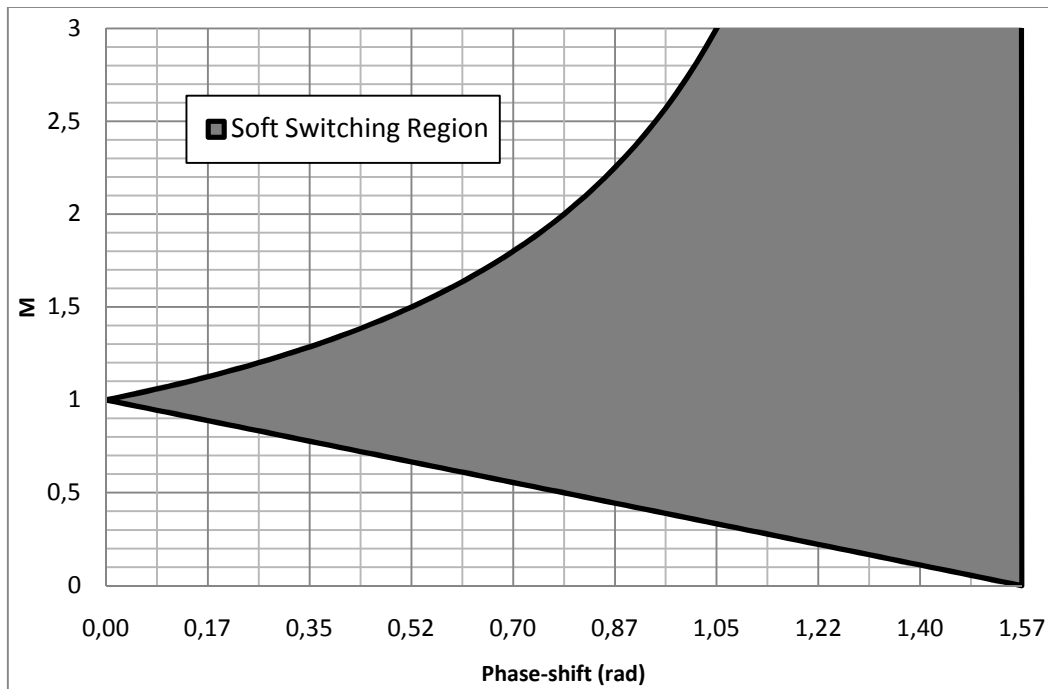


Figure 4.8 Soft switching region vs. Phase-shift and M

Once plotted the region where the converter operates in soft-switching mode is proven the above conclusion and can still be made other comments. The higher the phase-shift (which means a higher power transferred) is the widest area of soft-switching which is very favorable since losses increase with power level.

In the limit can be observed that for a maximum phase-shift corresponding to maximum power point ($\phi = \frac{\pi}{2}$), zero voltage transitions are guaranteed.

4.4 Simulation

After studied in detail the topology of the converter to be used and their modes of operation it was felt interesting perform some modeling and numerical simulation tasks. The simulation will allow easily gaining skills in the operation of this topology and assessing their potential for integration into the complete system.

At this stage equipment to be connected on both sides of the prototype are already known, so it is of great interest to include them as part of this simulation.

Another added value of simulation is to allow easily evaluate some parameters of passive components especially and point to a provisional acceptable values at this stage.

The simulation model is thus constituted by an ideal DC voltage source that represents DC-bus interconnection with the converter AC-DC, two full bridges with ideal switches, an ideal transformer with a turn's ratio of 1:1 and externally added leakage inductance, and a Lead-Acid battery pack with almost 400 V. A capacitor was also added in parallel with the battery pack in benefit of reducing the ripple voltage.

Open loop control system for validation of the convert is implemented by a square wave generator and the variable time delay. This solution can only be used for simulation because it's of very limited phase-shift resolution. When the system is implemented in a real-time

platform, the phase-shift generating mechanism must be done by dedicated hardware, so that the phase-shift step can be much faster than the cycle time of the control program.

The simulation will be carried out in Simulink® from MathWorks. The choice of this software is based on the fact of its large availability of blocks, whether for modeling the control system or power system, high control over the simulation process and also due to its comprehensive graphical user interface. For power blocks SimPowerSystems library will be used.

Measurements selected at this stage are very important. Measure the voltage output of the ac terminals of each bridge is essential as well as the current in the leakage inductance. This form will then be possible to establish a comparative analysis with the waveforms shown in the theoretical introduction previously made to this converter. Another critical component is the battery pack. The battery model provided by Simulink® already has a port of measures to that purpose. At that port is provided a vector with three signals: state of charge, current and voltage on battery terminals. Monitoring these signals is essential to assess whether this converter delivers energy in a way appropriate to charge / discharge batteries.

4.4.1 Model and parameters

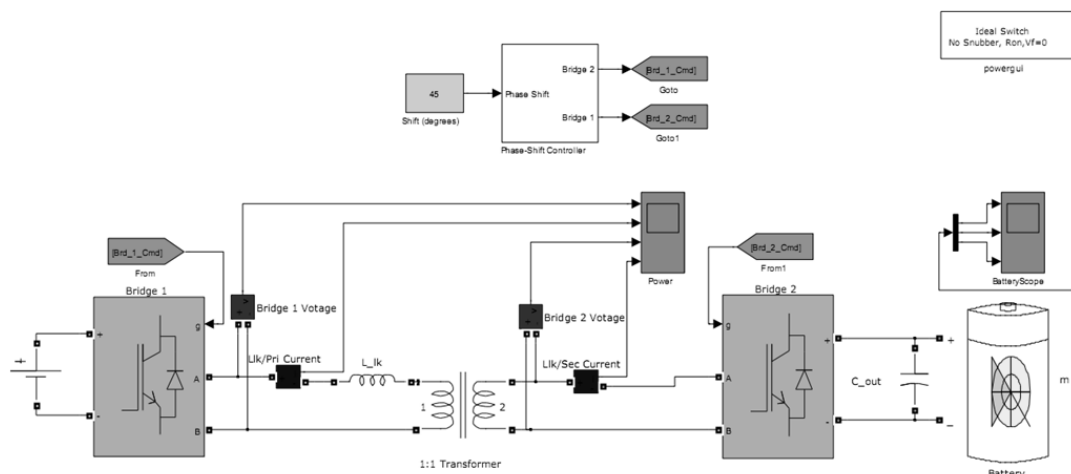


Figure 4.9 Simulation model

Table 4.2 General simulation parameters

DC voltage (left side)	400 V
Switching frequency	10 kHz

Table 4.3 Transformer parameters

Turns ratio	1:1
Primary winding resistance	5 mΩ
Secondary winding resistance	5 mΩ
Magnetization reactance	50 mH
Equivalent Leakage inductance	1000 μH

Table 4.4 Battery pack parameters

Battery type	Lead-Acid
Nominal voltage	384 V (12 V x 32)
Rated capacity	7 Ah

4.4.2 Simulation results

As mentioned earlier the primary objective of the simulation was to verify and evaluate its proper operation in association with the DC power supply and battery pack. Figure 4.10 and Figure 4.11 representing the typical waveforms of this converter in both buck and boost modes allow to ensuring correct operation of the converter. These first results allow also verifying the proper functioning of the command system implemented.

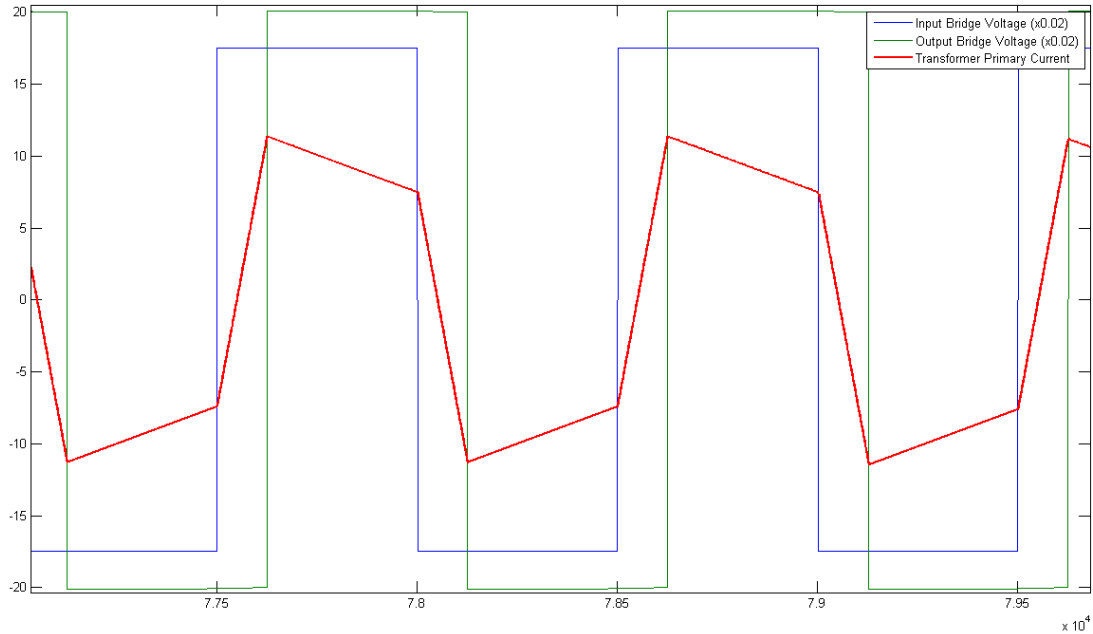


Figure 4.10 Input bridge voltage, leakage inductance current and output bridge voltage in boost mode ($\phi=45^\circ$)

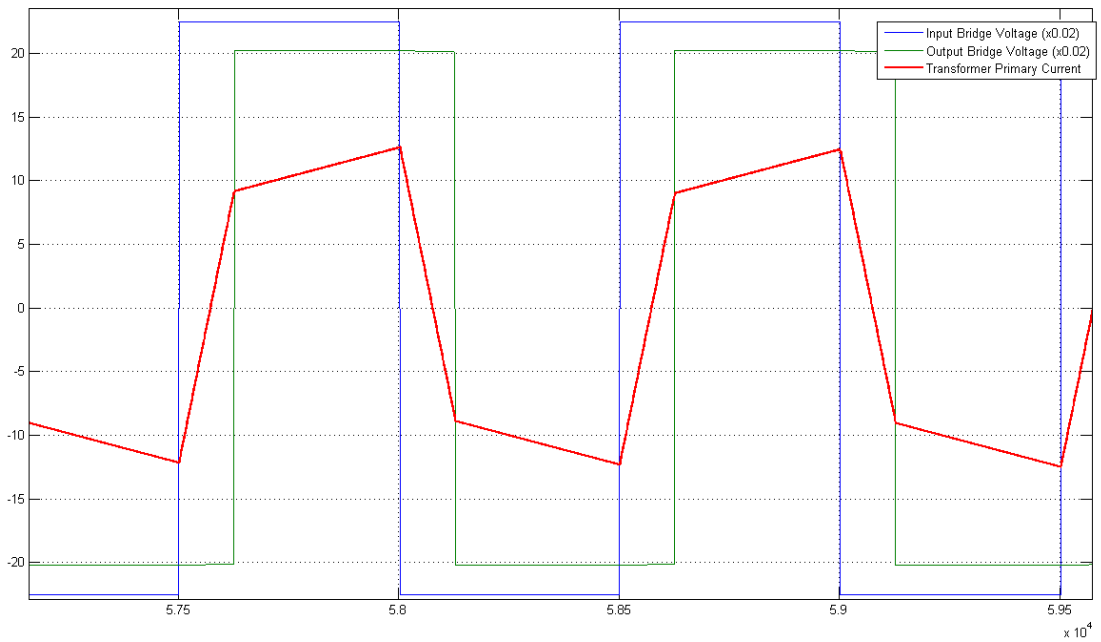


Figure 4.11 Input bridge voltage, leakage inductance current and output bridge voltage in buck mode ($\phi=45^\circ$)

4.4.3 Maximum leakage inductance estimation

At this point a critical task must be performed. As previously seen the power transmitted by this converter as well as the current is limited by several parameters such as input voltages and output phase-shift, frequency switching and leakage inductance of the transformer.

Some of these parameters are already established at this stage being them the DC bus voltage, minimum allowed voltage for the battery pack and the switching frequency.

The goal is to charge or discharge the batteries with a current of 10 A at the point of maximum power in any conditions. Since the phase-shift is the system control variable, there remains only the leakage inductance. The challenge now is to find the maximum acceptable value for this parameter to ensure the desired level of power transferred.

Table 4.5 Considered scenario

Parameter	Value
Input voltage (DC bus)	400 V
Battery pack voltage (Minimum)	360 V
Switching frequency	10 kHz
Phase-shift (maximum power transfer)	90° or $\frac{\pi}{2}$

$$I_o = \frac{2V_{DC1}}{\omega L_\sigma} \phi \left(1 - \frac{|\phi|}{\pi} \right) \quad (4.16)$$

$$10 \leq \frac{2 \times 400}{2 \times \pi \times 10 \times 10^3 \times L_\sigma} \times \frac{\pi}{2} \left(1 - \frac{1}{2} \right) \quad (4.17)$$

$$10 \leq \frac{800\pi}{80\pi \times 10^3 \times L_\sigma} \quad (4.18)$$

$$L_\sigma \leq \frac{800\pi}{80\pi \times 10^3 \times 10} \quad (4.19)$$

$$L_\sigma \leq 1 \times 10^{-3} \text{ H} \quad (4.20)$$

After determined a maximum value for leakage inductance a plot based on Table 4.5 scenario is now presented in Figure 4.12. As expected the maximum current is 10 A, corresponding to a shift of 90° .

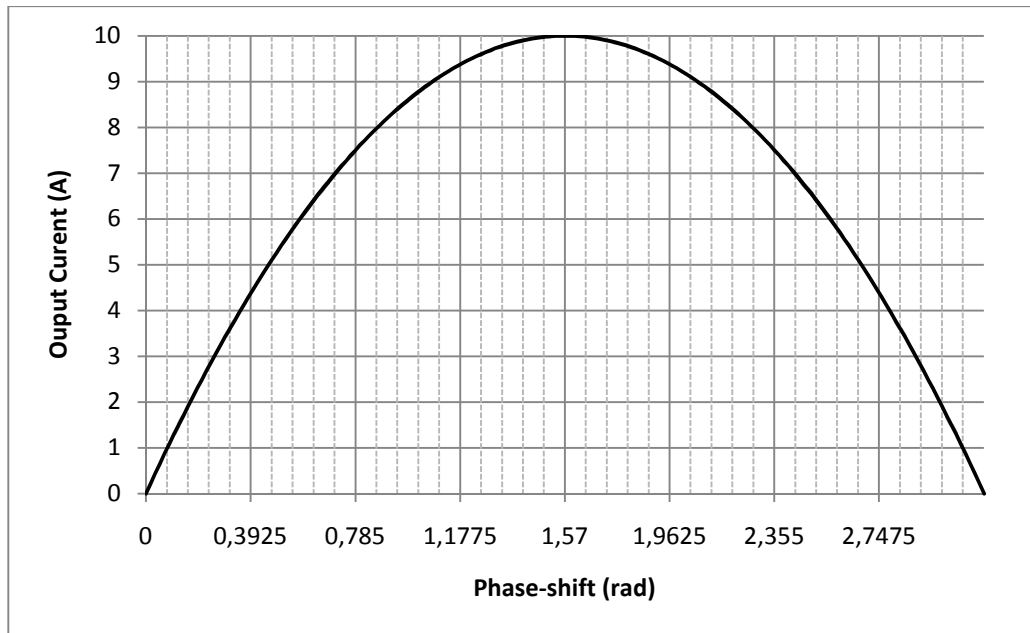
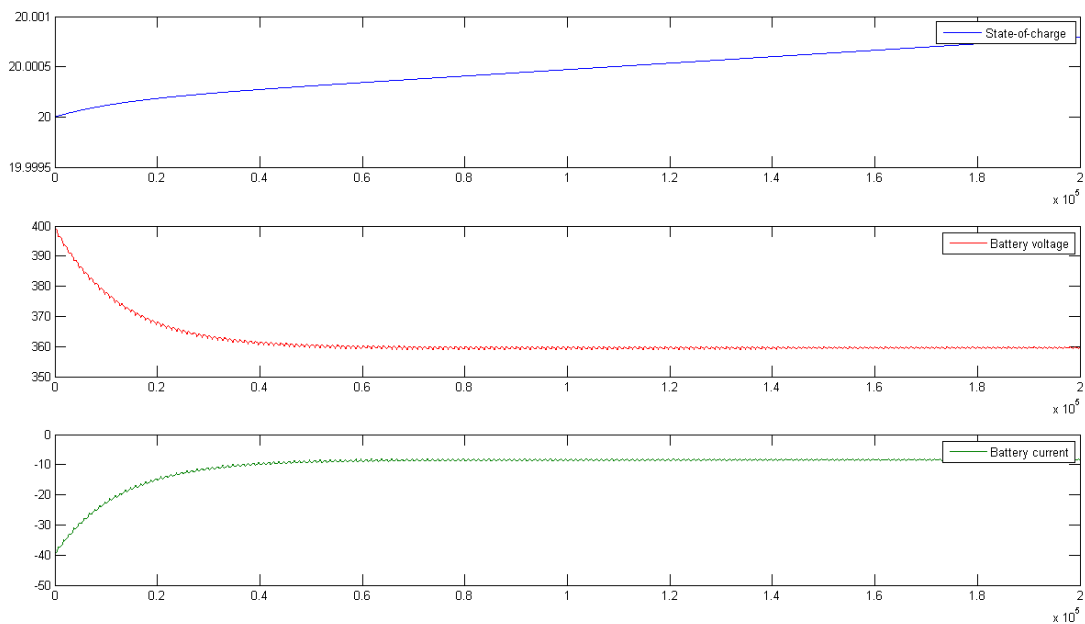


Figure 4.12 Output current vs. phase-shift

Achieved a value is now inserted into the simulation model to validate the calculation. It is important to refer that this value is an upper limit for the leakage inductance. Lower inductance values can be used to fulfill the desired power range. For instance, an equivalent leakage inductance of 500 μH allow to achieve a maximum output current of 20 A. This way controlling the phase-shift angle between zero and a certain value below 90° , a (0 - 10) A range can be performed. Such characteristic can avoid the need for an external inductor.

The first simulation will be carried out exactly to the proposed dimensioning, i.e. with the battery at a voltage near 360 V and a phase-shift of 90° or $\frac{\pi}{2}$.

Figure 4.13 Battery SoC, Current and Voltage with Input 400V, Output 360V, ϕ of 90° $L_\sigma = 1 \mu\text{H}$

One of the important conclusions that can be taken from (4.16) is that the average output current does not depend on the output voltage. Thus the output voltage was then modified by establishing a new initial value for the SoC of the battery, which increased from 20% to 80%. The aim is to verify that conclusion based on the analytical expression.

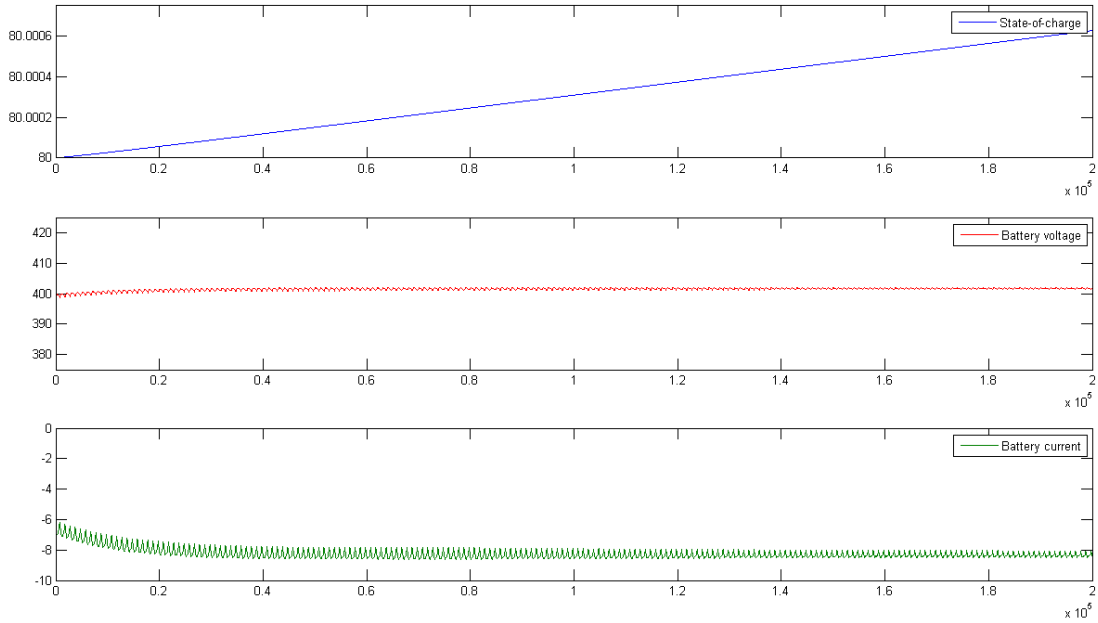


Figure 4.14 Battery SoC, Current and Voltage with Input 400V, Output 400V, ϕ of 90° $L_\sigma = 1 \mu\text{H}$

Another important task to be undertaken during the simulation is to verify the characteristics of symmetry relative to bidirectionality. This will be confirmed expeditiously by changing the phase shift of 90 degrees to 270 degrees (which corresponds to -90°).

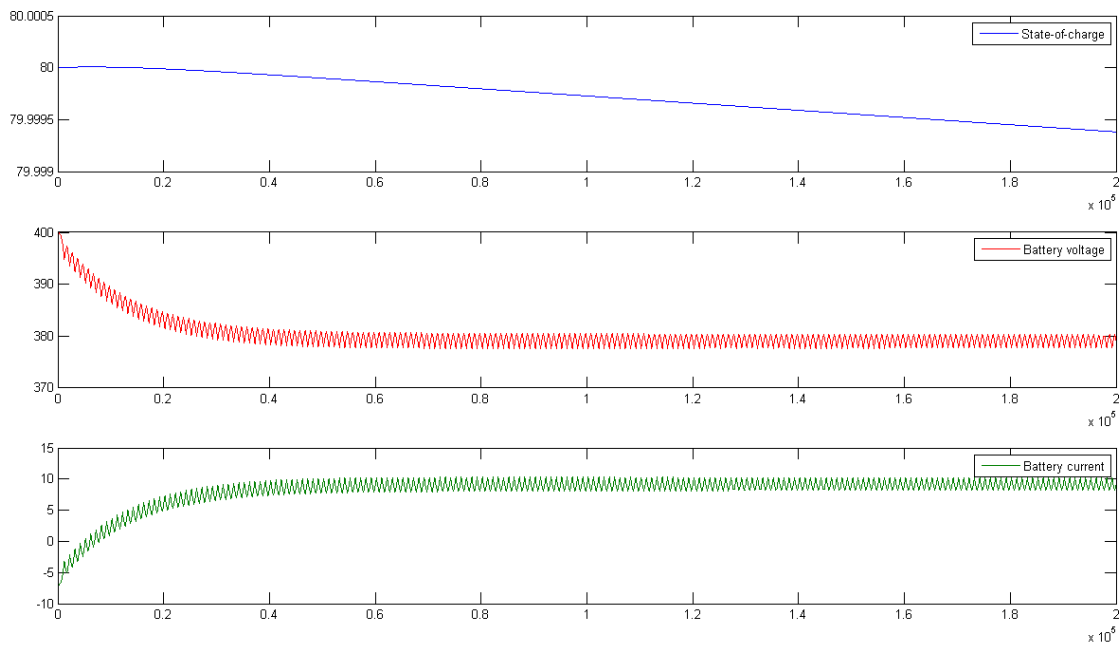


Figure 4.15 Battery SoC, Current and Voltage with Input 400V, Output 355V, ϕ of -90° $L_\sigma = 1 \mu\text{H}$

At this stage we already checked some important conclusions about the operation of this converter in steady state. Although it is still important to characterize the converter as a function of phase-shift for a particular operating point and compare with the analytical values of Figure 4.12.

To this purpose several simulations were carried out and will not appear obviously the plots of them all. Instead the current values in the battery for several values of phase-shift will be plotted on a new chart together with the analytical values. These values are measured in steps corresponding to five degrees.

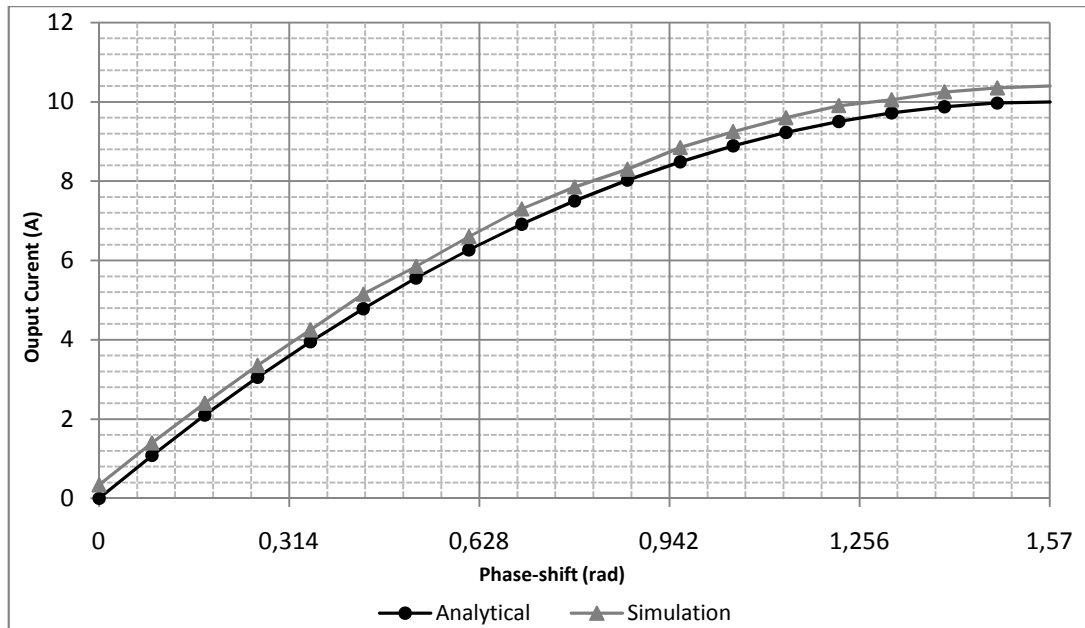


Figure 4.16 Output current vs. Phase-shift - analytical and simulation results

Obtained these results the converter was characterized for steady state operation in simulation aspects. The values are approximate although affected by an offset error. This same procedure could be carried out for a variation of output current vs. input voltage, but with a reduced interest by two factors: first the input voltage is assumed that does not vary significantly during the operation and second the relationship between input voltage and output current is linear.

4.4.4 Capacitors dimensioning

Another important task that can be carried out during the simulation is a first approximation to a reasonable value for the capacitors. This procedure can be divided in two phases: the first one will justifiably determine what the worst scenario for a particular ripple signal is and the second set a maximum allowable ripple (usually in percentage).

Besides all this, find a reasonable value cannot have only a lower limit, but also upper. Usually in applications of power electronics capacitors come with high capacity values generally associated to high voltage ratings, which means large capacitors. In this phase must have sense and balance all these factors to achieve an appropriate solution.

Surely the worst scenario for the ripple in the output voltage is at the moment when the voltage is lower and output is coupled to heaviest load.

For this specific application, that scenario occurs when the battery pack is at minimum state-of-charge and the allowable output current is the highest, since as previously shown the output current is independent of voltage.

One of the features that make this topology very feasible for charge / discharge batteries is its low ripple on the output. Enjoying this fact may be given a very low limit for the ripple.

In the simulation model was placed a resistive component (ESR) in series with the capacitor otherwise ripple observed would be unrealistic. This value was approximated at 100 m Ω by excess given that electrolytic capacitors in this range and of high quality should be a value somewhat less.

The maximum value for the ripple was then set at $\pm 1\%$ of the average output voltage for this stage and already includes that resistive component for the capacitor.

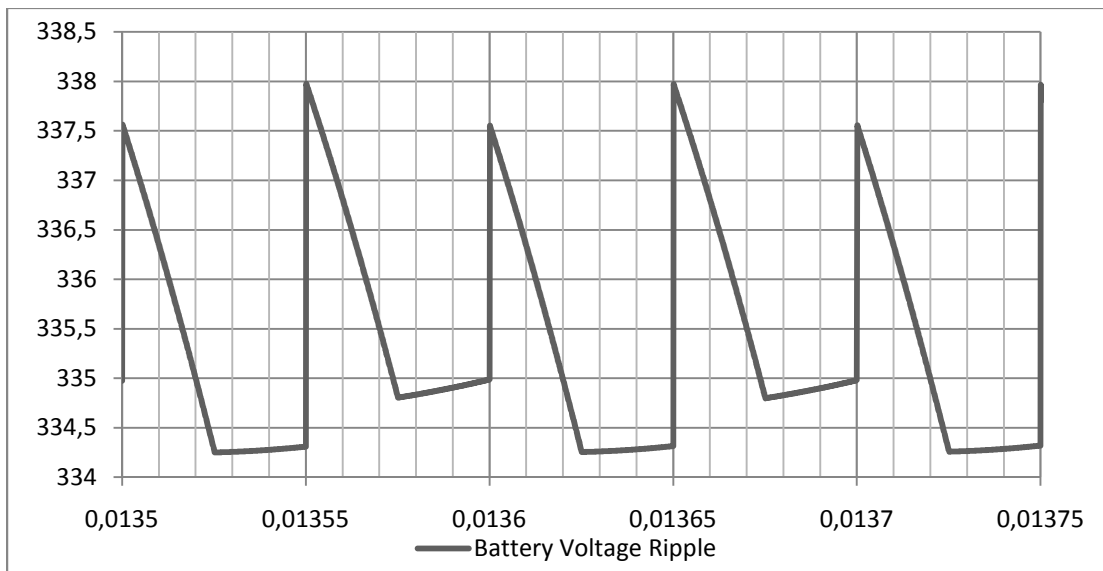


Figure 4.17 Output voltage ripple

Considering the conditions mentioned above were then performed simulations with an output of about 10 A and a phase-shift of 90 ° and typical values of commercially available capacities (470 μ F, 1000 μ F, 1500 μ F and 2200 μ F). The lowest value capable of fulfilling the requirement of $\pm 1\%$ of the DC voltage was the value of 1000 μ F and the signal for that capacity is plotted in Figure 4.17.

Table 4.6 Capacitor dimensioning

Parameter	Value
Output voltage (average)	335,7 V
Output voltage (minimum)	334,2 V
Output voltage (maximum)	338,0 V
Ripple voltage	3,8 V
Ripple in %	1,13 %
	$\pm 0,57$ %

This value should ensure safe operation of the batteries. Considering the total size of the converter this capacity should not represent a high volume. If a safety margin is desired the capacity can be increased without major problem for a 1500 μ F capacitor to deal with higher ESR or even to reduce the voltage ripple.

4.5 Summary

This chapter is an introduction to the topology to be implemented, describing the basics of his theory. Their average expressions are also presented as well as the limits for operation in soft switching.

In the second part a simulation work is performed with the objectives to understand the operation of the converter as well as assess the influence of various parameters in its operation.

Chapter 5

Prototype design

All aspects of the hardware power are described in this chapter being the discussion always focused on practical issues. In each of the parts there is a brief introduction to the most relevant options for this application and then are there defined criteria / measures of performance in which the choice is based. The procedure will always result in choice of a real component to be used in the prototype.

In the choice of switches there is a brief comparison of the most common types used in power electronics for this application and the specification of minimum requirements that the devices must have. Lastly, the chosen power module is presented taking into account all the aspects discussed. After choosing the switches a study is made about the appropriate drive circuits and a list of requirements is presented.

For capacitors the design procedure starts with a brief discussion of the types with relevance for this application and the reference to performance measures for each type with a choice of specific components in the end.

The transformer design is discussed in the last section, with a greater level of detail. Issues such as physical structure, dimensioning of magnetic and electric circuit, estimation of losses and other parameters and choice of all the components are presented.

5.1 Power switches

First step in active components selection is to find out the voltage and current ratings involved, as well as the switching frequency range.

In this specific case the frequency used for the converter switching is constant and defined as 10 kHz. The voltage rating is pointed to be twice the maximum voltage that each switch will block. Considering the input data presented in Table 5.1 the selected switches must have a blocking voltage of at least 800 V. Major types of switches are designed with just a few values of blocking voltages. For instance IGBTs are easily found on the market with typical levels of 600, 1200 or 1700 V.

Another critical parameter is the current supported by the switch under continuous operation. This value should be oversized respecting to the one calculated during circuit

analysis or measured in simulation environment, especially in a first prototype. If too short an accurate thermal protection must be designed and the transient overload intervals have to be studied in order to prevent critical overheating or possibly destruction. Considering the typical applications a scale factor of two can be inserted to the defined nominal value, resulting in a quite robust solution. In this converter the nominal power is set to 4 kW which means a DC bus current up to 10 A. Using the scale factor mentioned above concludes that the current rating of the switches to be used must be at least 20 A.

Table 5.1 Input data for switch selection

Parameter	Value
Maximum voltage	$2 \times 400 \text{ V}$
Rated power	4 kW
Maximum current (continuous)	$2 \times 10 \text{ A}$

Once defined the minimum values of the most basic parameters (Table 5.1), the switch type must be selected. The main types with interest to implement such converter are MOSFET and IGBT.

MOSFET - They have very high input impedance (capacitive) which allows to no power consumption under steady state conditions - power is only required to switch the device. The on-state resistance has no physical limit so that devices with very low on-state losses can be found. A positive temperature coefficient prevents thermal runaway and makes them suitable to use in parallel.

IGBT - They combine the advantages of the MOSFET including the ease and efficiency of the command with high voltage and current ratings of bipolar transistors. Its negative temperature coefficient makes its utilization in parallel difficult to implement. Commercially available devices provide a built-in anti-parallel diode [43].

Considering these aspects the most suitable switches type for this application are IGBTs. The voltage and current ratings offered along with an easy command make this technology particularly interesting for such applications.

Another relevant issue is the case where the semiconductor is supplied. IGBT are available in cases ranging from a small D²-PAK for PCB surface mount to large non-PCB devices that can be small blocks to mount on heatsinks with standard 80 or 93 mm rails or manufacturer proprietary case types. These large devices are usually found on the market with a single IGBT on each case or in power modules. These modules can be half-bridges, full-bridges or six-packs. Some of these modules integrate a temperature sensor.

The selected device is a block-type IGBT with two transistors per case. Its main advantages are high mechanical robustness, ease of mount due to standard distance between fixation screw holes (80 mm), ease of electrical connection in power (M5 screw) and

command terminals (Fast-on) and the high availability of accessories like DC bus bars and snubber capacitors. Unlike PCB assemblies this one can be easily reconfigured to future work. The selected component was SKM100GB12V IGBT Half-Bridge from Semikron®.

Table 5.2 SKM100GB12V IGBT Half-Bridge main specifications [44]

Parameter	Value
Blocking voltage (V_{CES})	1200 V
Nominal current (I_{Cnom})	100 A

5.2 Drive circuit

In power electronics, the so called driver is an electronic circuit that has the functionality to operate the main power switch in a correct manner. In most cases this circuit includes protection functions. These protections may be over and under voltage, over current, short circuit and over temperature. Drivers for multiple switches can include also interlock and dead time features.

Nowadays there is a wide commercial availability of drivers for power switches. They can range from small integrated circuits (IC driver) to high-end products known as hybrid drivers that include many of the above described features. The main differences between both types are listed in Table 5.3.

Table 5.3 Main driver types comparison [45]

Driver type	Driver IC	Hybrid driver	
		Midrange	High-end
Available configurations	Single, Halfbridge, Sixpack etc.	Single, Halfbridge, Sixpack etc.	
Insulation	no galvanic insulation	galvanic insulation	
Signal transmission	Level shifter (mainly for high side)	Opto-coupler	Pulse transformer Fibre optic
Energy transmission	Bootstrap-circuit (for high side)	Switch mode DC-DC converter	
Application	low power (<5 kW)	medium power (5...100 kW)	high power (>100 kW)

The most interesting devices are undoubtedly the hybrid drivers due not only to features which typically include, but also its performance. For that reason this type of drivers will be chosen for this design, improving the robustness and safety of the prototype and reducing the development time.

In order to select the most interesting product the performance measurements have to be identified as well as the required/desired features. Its performance measurement is usually made based on some essential characteristics which are:

Peak output current: Should be as high as possible. This characteristic can be achieved with very low output impedance on the secondary side. Currently available drivers reach values as high as 50 A (Skyper 52 R from Semikron®) [46].

Maximum switching frequency: At least the converter maximum switching frequency. In most cases this frequency is dependent on the gate charge of the power switch and ambient temperature where the component is placed. Its value is typically in the range of tens of kHz, depending on the range. Higher frequencies are of limited interest for high power converters, resonant converters unless.

Table 5.4 Driver features

Feature	Relevance	Explanation
Short-circuit protection	Needed	Implemented generally by continuous V_{CEsat} monitoring detects when this value goes above a previously defined voltage. It's indispensable to protect the integrity of power hardware.
Top/bottom interlock	Needed	Although it can be managed by the control platform, cannot be sufficiently robust to ensure that commands will never short-circuit the DC bus.
Error output	Needed	It is necessary to have access to an error signal so the control platform can manage it in right manner.
Reset input	Needed	At system start-up or after a recovery from a failure is required to reset the drivers to resume normal converter operation.
Over current protection	Desirable	Required to ensure that the power switch limits are respected. Needs to be configured according to the power modules or other hardware limitations.
Over and under voltage protection	Desirable	Required to ensure that the power switch limits are respected. Needs to be configured according to the power modules or other hardware limitations.
Over temperature protection	Desirable	It can be as simple as a voltage comparator with an adjustable limit to allow a sensing with an NTC or it can be configurable to use PTC or NTC. This feature can be implemented by an external dedicated circuit.

Holding these all the selected driver is the model Skyper 32 PRO R from Semikron®. Besides all the features mentioned above, this driver include some more advanced. All of them are represented on Table 5.5.

Table 5.5 Skyper 32 PRO R features [47]

Two output channels
Integrated potential free power supply
Under voltage protection
Drive interlock top/bottom
Dynamic short circuit protection
Half logic signal (reset + error signals)
Failure management
Soft turn-off
External error input (secondary side)

Some of these features are partially implemented on an evaluation board that interfaces between the driver core and power hardware. For the same driver core there are several different boards for direct connect to proprietary power modules or alternatively a universal adapter for a wired connection to any other power module is available.

This driver solution supplied it's almost ready to use. Although, it's necessary assemble a few components to configure some parameters. A technical document related to the device has detailed information on how to determine the values of these components.

5.2.1 Parameter setting

The parameter setting and board configuration is made through some components soldered on the evaluation board and based in [48].

5.2.1.1 Dead time setting

Dead time is an important parameter since the two or more fully controlled switches are series associated in the same DC bus. In most cases they are turned ON/OFF in a complementary way. This process is not instantaneous and transient short circuits may occur on the DC bus.

Merging the data from the driver core and the evaluation board technical documents is possible to find that the dead time is controlled by means of four external pins, one to enable/disable dead time e three to select from 8 different values.

The simplest approach to establish a value for the dead time is to ensure that a transistor is turned on right after the process of shutting down the other is fully completed. In other words, the dead time will be equal to or greater than the sum of the turn-off delay with the fall time.

Table 5.6 Minimum dead time estimation

Parameter	Value
Turn-off delay ($t_{d(off)}$)	418 ns
Fall time (t_f)	62 ns
Minimum dead time	0,48 μ s

Considering this value any of the values available from the drive could be used but in fact is not so, as the parameters present in the technical document refer to tests carried out with a gate resistance of 1Ω , which is quite low. A higher value of gate resistance will lead to a higher fall time and this made a need to have a value of dead time also higher. For this reason, it will be used for the dead time a higher value until the gate resistance is set and fall time is accurately determined. The value used in this phase will be the default on the evaluation board, 3.3 μ s.

5.2.1.2 Dynamic short circuit protection

This protection feature is implemented through a parallel connection of a resistance and a capacitor. These two basic components are intended to generate a time constant that has a behavior similar to the V_{CE} voltage during normal operation of the circuit. The analytical expressions to determine these values are given in [47].

$$R_{CE}[k\Omega] = -15,5k\Omega \times \ln \left(1 - \frac{V_{CEstat} + R_{VCE} \times \frac{V}{k\Omega}}{8V} \right) \quad (5.1)$$

$$C_{CE}[pF] = \frac{t_{bl}[\mu s] - 2,1 - 0,11 \frac{\mu s}{\Omega} \times R_{CE}}{0,00323 \frac{\mu s}{pF}} \quad (5.2)$$

Expressions (5.1) and (5.2) have two input parameters and they are the Collector-emitter threshold static monitoring voltage (V_{CEstat}) and the blanking time (t_{bl}).

The V_{CEstat} is the maximum allowed V_{CE} value in steady state mode when the switch is turned on that is not seen as a short-circuit. In the selected transistor the maximum value of V_{CE} with the nominal current is 2.65 V, which means that the value of V_{CEstat} expected to be always above this value. If this parameter has a value too low the transistor will be better protected but the protection can be activated unexpectedly during transient overload. On the other hand, if the value is too high the transistor may be subject to weak short-circuits, which do not act the protection.

The t_{bl} is the time between a turn-on command and the first monitoring of the transistor V_{CE} voltage. To correctly choose this value the switching characteristics have to be studied in detail. When the switch is turned on the V_{CE} voltage falls from the prior blocking voltage to $V_{CEonsat}$ value with an exponential behavior. To handle with this characteristic is required that V_{CE} reference fall more slowly than the true value of V_{CE} , or at limit at the same speed to do not trigger the comparator and hence the protection.

For being beyond the scope of the work was decided to use a reference value for a typical 1200V IGBT application, suggested in [47]. These values for V_{CEref} and t_{bl} are presented on Table 5.7.

Table 5.7 Dynamic short circuit protection parameters

Parameter	Value
V_{CEref}	5,5 V
t_{bl}	5,1 μs
R_{CE}	18 k Ω
C_{CE}	330 pF

5.2.1.3 Collector Series Resistance

As seen earlier, short-circuit protection is done by monitoring of the voltage VCE, which implies the need for sensing the voltage at the collector of the transistors. The connection between the drive circuit pin which makes this measure and the collector of the transistor is done with a reverse biased high voltage diode, which is already assembled on the evaluation board.

When using a 1200 V IGBT only the diode should be placed in series and with 1700 V IGBT should be placed the diode in series with a resistance of 1 k Ω with a minimum power dissipation of 0.4 W. The place should be assembled with a shunt or a 0 Ω resistor.

5.2.1.4 Adaptation Gate Resistors

The gate resistance is a very critical parameter for the operation of the circuit, especially with concerns to the switching characteristics. A very low value should be able to fast commutation of the transistor, but with higher dv/dt and di/dt values and a higher current absorbed from the driver. In most cases the semiconductor has some different turn on and turn off times. This leads to the need to use different resistors to switch on and off the transistor. This driver provides such optimization and contemplates separate spaces for assembling turn on and turn off resistors for each transistor.

Considering the transistor datasheet and collecting the values of the gate input capacity, rise and fall time and approaching the command circuit for an RC network is possible to estimate an optimized value for the gate resistance.

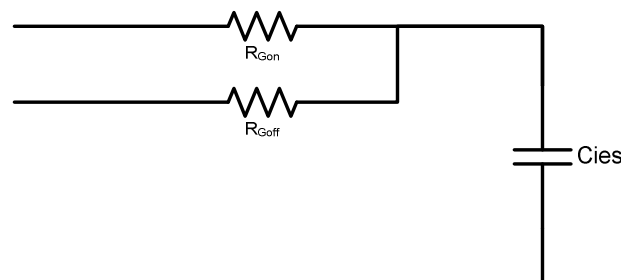


Figure 5.1 Considered equivalent circuit

Table 5.8 Input data for R_g calculation [44]

Parameter	Value
C_{ies}	6.01 nF
t_r	38 ns
t_f	62 ns

As a series RC circuit has a time constant τ given by $R \times C$. The C value is given in the datasheet of the transistor, and approaching the rise and fall times by 5τ is possible to determine the resistance value to place in series with the IGBT gate.

The on resistance is calculated using the rise time and the OFF resistance is based on the fall time.

Table 5.9 Gate resistors calculation

Parameter	Value
Rising time constant	$\tau_r = \frac{38}{5} = 7,6 \text{ ns}$
Falling time constant	$\tau_f = \frac{62}{5} = 12,4 \text{ ns}$
Gate resistor (ON)	$R_{GON} = \frac{C_{ies}}{\tau_r} = 0,79\Omega$
Gate resistor (OFF)	$R_{GOFF} = \frac{C_{ies}}{\tau_f} = 0,48\Omega$

The gate resistors are not only limited by the characteristics of the transistor. The value of peak current supplied by the driver must also be considered as a restriction on the minimum resistance that can be used.

The driver has the output voltage level of +15 V when to turn on the transistor and -7V when to turn it off. This represents an almost instantaneous change of 22 V when the command changes. Recalling that the peak current provided by the driver is 15 A, and considering the transition to be instantaneous, the resistance should ensure that this current limit is never exceeded.

Despite the current limit of the driver is high it was understood that at this stage would not be necessary to achieve its maximum value. Thus the value of desired maximum current was set at one-third the maximum current, i.e. 5 A.

$$R_{GMIN} = \frac{V_{ON} - V_{OFF}}{I_{pkMAX}} = \frac{22}{5} = 4,4 \Omega \quad (5.3)$$

Considering all these factors the selected value was 4.7Ω , since it is the closest value above 4.4Ω found in E12 resistor table.

5.2.1.5 Soft Turn-Off

The functionality of soft turn off is the one that distinguishes this version (PRO) of the normal version of the same product. This mechanism doesn't allow an abrupt turn off the transistor in case of a short circuit. Thus when a fault occurs the transistor is switched off smoothly (gradually increasing the resistance in series) through its transient operation in the linear region. This form voltage spikes due to very high di/dt will not be generated, especially in the presence of inductive elements with very high inductance values.

The speed of this process of soft turning off the transistor is related to a resistance that can be mounted on the evaluation board. At this point this functionality is disabled.

5.2.1.6 Over Temperature Protection

Together with all the features above, there is an extra feature of temperature protection provided by the evaluation board. This protection system needs to be configured to specific parameters of the temperature sensor and for the sensor type, either PTC or NTC. The evaluation board uses the external input error to put the driver in HALT mode if the set temperature limit is exceeded.

This feature is disabled because the power hardware does not provide any temperature sensor, but can easily be added in the future.

5.3 Interface board

It is common to the inputs of driver circuits waiting to receive signals with a value of $0/15V$, especially in industrial drivers. This is not the typical voltage level supplied by the output pins of any control platform whether it is based MCU, DSP or FPGA. The commonly used values are $0/3,3V$ or $0/5V$ either for specific internal PWM generator pins or any other general purpose pins.

Thus it is then necessary in most cases using an auxiliary circuit that makes this adaptation of voltage levels, which in this case is $0/5 V$ to $0/15 V$. This circuit should be as simple as possible not to add complexity to the project and to facilitate the hardware debugging process. The circuit should also be designed to have minimal rise and fall times and also low propagation delay.

The solution has to use a low-power bipolar transistor, operated always in switch mode. The collector and base resistors are calculated in order to ensure that is in saturation mode when turned on. This solution allows to obtain a waveform that switches between the desired values ($-0/15 V$) but with an inverted logic. In addition the output values are not exactly 0 or

exactly 15V, which cannot be well interpreted by the driver circuit. To solve these two problems was put forward an inverted buffer, which thus returns to signal a non-inverted logic and switches between values very close to 0 and 15 V, which will be interpreted correctly by the driver.

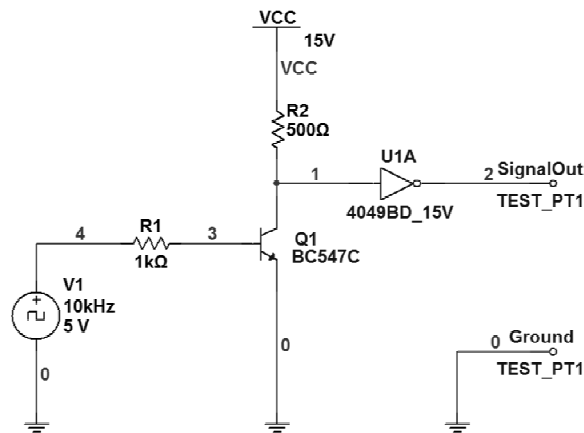


Figure 5.2 5 to 15V circuit

This driver also includes a signal with particular characteristics that is the HALT signal. This signal is active low and both can be activated internally by the driver and forced externally by another circuit. The control system is also of interest to monitor the value of this signal, to have information about the state of operation of the driver. These characteristics imply the need for a bidirectional 5 <-> 15 V circuit.

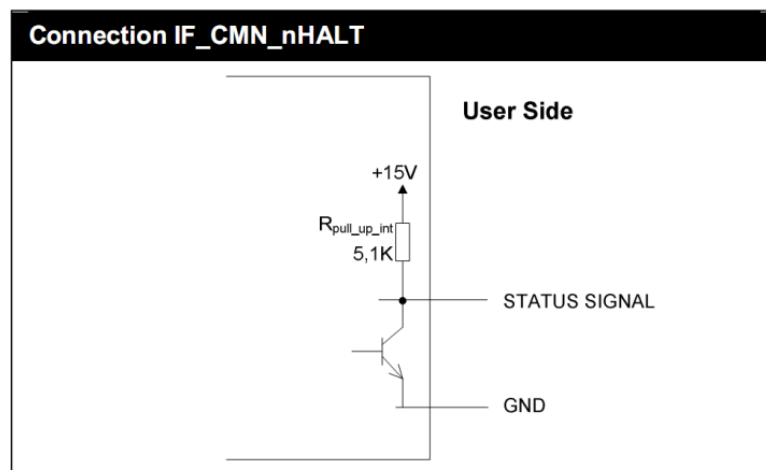


Figure 5.3 Internal equivalent circuit of HALT signal

The solution to handle this signal is to implement the two functions separately. The function of forcing the driver to enter the HALT state is made by a bipolar transistor placed in parallel with the internal one, represented in Figure 5.4, so that when turned on will trigger the protection by forcing the signal to a logic low level. The signal reading is done through a buffer or voltage follower in order to provide access to this value without interfering with

their behavior. In the buffer output a resistive divider is placed to convert the signal voltage from 15 V to 5 V.

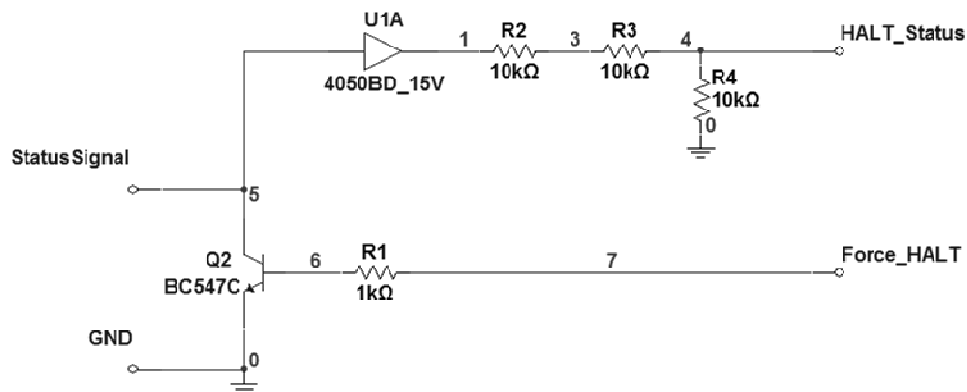


Figure 5.4 HALT signal interface circuit

5.4 Capacitors

Capacitors are passive components of high importance in this design. Its function is to stabilize the voltage at the two DC buses to prevent the DC sources to be operated under a high voltage ripple. In the preliminary design of the converter and for the simulation purpose they can be considered as ideal components, i.e. simply specifying the value of its capacity.

In fact they are not ideal components as any other. Unlike the inductors or transformers which are often designed specifically for a particular converter, the capacitors are available on the market in wide ranges of capacities and rated voltages.

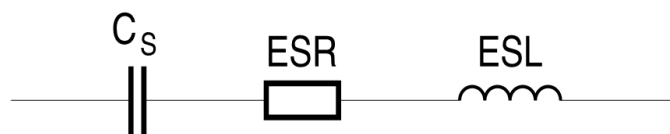


Figure 5.5 Simplified equivalent circuit diagram of an electrolytic capacitor [49]

At this stage the focus will not be projecting any component but to establish the minimum specifications to match the converter needs and identify performance measures that will allow choosing the most adequate component.

The types of capacitors with interest for this work are aluminum electrolytic capacitors and metalized polypropylene film capacitors. The electrolytic capacitors are with high capacity per unit of volume and unit of weight and are best suited to stabilize voltage within large time constants. The other type, Metalized Polypropylene Film Capacitors (MKP) are especially suited to handle high dv/dt , i.e. they provide or absorb large amounts of energy

during very short periods of time without opposing great resistance. When used in DC bus of a switch-mode converter they attenuate the oscillations generated by switching.

5.4.1 Electrolytic capacitors

The minimum values of capacity and rated voltage for electrolytic capacitors were defined in simulation (Table 5.10). Afterwards it was considered important list the parameters that influence its performance and discuss their influence in the converter operation.

Table 5.10 Electrolytic capacitors minimum requirements

Parameter	Value
Capacity (value from simulation)	$\geq 1000 \mu F$
Rated Voltage	$\geq 400 V$

Equivalent Series Resistance (ESR) - Extreme importance in a careful design. This value should be as low as possible since it represents on capacitor terminals a voltage ripple that is a fraction of current. On the other hand also have a direct influence on the power dissipated by the capacitor.

Self-inductance (L_{ESL}) - With particular importance especially when dealing with high current gradients, as this generates parasitic voltage variations proportional to the variation of the current, which is undesirable in a DC bus.

Maximum RMS current - Related to previous is also of great importance. Safe capacitor operation within the nominal voltage rating is only valid in limited temperature range so that the power dissipation is also limited. Maximum power dissipation can be approached as the product of ESR by the square of maximum RMS current.

Operating temperature - The nominal voltage is typically set to a certain maximum temperature. The higher the lower the thermal management concerns of the component. Yet the lower the temperature at which the capacitor can be better maintained since its lifetime increases and can be operated safely with higher voltages.

Useful life - It is generally referred to a specific temperature. In this case it comes as a prototype is not of critical importance but a final product is always a factor to be taken into account. This may become significantly longer operating the capacitor at lower temperatures by decreasing its RMS current or using a cooling method.

Protection - An important detail especially in bench top equipment. This type of capacitor is polarized and when connected in the wrong way there is a risk of explosion. In large components can be interesting the existence of a protection system that avoids the consequences of neglect.

Considering all these aspects was a choice of a component to use. Attempt to be a solution with an acceptable volume compared to the size of the converter and with screw-

type terminals, so as to ease the cabling for connection to the buses. The selected part is B43456A9158M from Epcos®.

Table 5.11 Epcos B43456A9158M Electrolytic capacitor specifications [50]

Parameter	Value
Rated Capacity	1500 μ F
Rated Voltage	400 V
Typical ESR (100 Hz 20 °C)	45 m Ω
(10 kHz 20°C)	$-0.6 \times \text{ESR}_{100\text{Hz}}$ 27 m Ω
Maximum ESR (100 Hz 20 °C)	67 m Ω
Self-inductance L_{ESL}	20 nH
Maximum Impedance (10 kHz 20 °C)	46 m Ω
Maximum RMS current (100 Hz 40 °C)	17 A
Rated RMS current (100 Hz 85 °C)	6.0 A
Useful life	> 12000 h @ 85° > 250000 h @ 40°

5.4.2 Metalized Polypropylene Film Capacitors (MKP)

These capacitors are considered as of great importance for good performance of the converter, especially with high power levels.

As for the electrolytic, before proceeding to the selection of a specific component it was considered useful to establish performance measures and their influence on the converter.

Rated DC Voltage - Must be at least equal to the maximum rated voltage of the bus because they have to withstand this voltage during most of the time.

Rated AC Voltage - A very important parameter. As already mentioned these capacitors are designed to withstand the oscillations (spikes) generated by switching on the bus. This way is so important that they be prepared to deal with voltages above the nominal value. The particular value of this voltage depends on several factors such as the nature of the load or the speed of switching and at this stage is difficult to determine accurately.

RMS current - Another important parameter as in the electrolytic. In this case the values are generally referred to the high frequencies in the range of kHz. The limitations are set not only by thermal aspects but also by the terminals used, which are usually large. It is understood that a modest value of RMS current values may correspond to very high peak current, due to the high crest factor that the current waveform have in these capacitors.

Equivalent Series Resistance (ESR) - In this type of capacitors this parameter is of utmost importance, together with the self inductance. In an ideal situation these capacitors should provide or absorb any current without any voltage change. In fact this assumption is limited by the existence of such parasitic effects. The commercially available components have very

low ESR values (only a few mΩ) due to the materials used and the high contact area of the terminals especially in large capacitors.

Some cases are specially designed for the power modules to be used in this prototype and will be given preference to such devices. Thus it is possible to put in contact the entire area of the terminal from the power module with the capacitor terminals ensuring a minimum added equivalent series resistance.

Self-inductance (L_{ESL}) - Indeed the major quality characteristic of this type of capacitors since they will be subject to surges of high amplitude but also with high variation rates. As the ESR inserts a voltage drop proportional to current value, this parasitic inserts a drop proportional to the derivative of the current.

Maximum permissible voltage change per unit of time $\left(\frac{dv}{dt}\right) = \frac{i_{pk}}{C}$ - Of great importance because the capacities are generally low in this type of capacitors and the current peaks are expected to fairly high which will result in high voltage gradients. The higher was the ability of capacitor to support them better.

Table 5.12 Epcos B32656S8155 MKP capacitor specifications

Parameter	Value
Rated Capacity	1500 nF
Rated DC Voltage	850 V
Rated AC Voltage ($f \leq 1$ kHz)	450 V
RMS current (100 kHz)	13 A
ESR (100 kHz)	5.0 mΩ
Self-inductance L_{ESL}	17 nH (5.5)
Maximum dv/dt	400 V/μs
Maximum k_0	680 000 V ² / μs

As can be seen on Figure 5.5 a realistic model of a capacitor can be represented by four components. At this step the parallel resistance will be neglected since it has a large value. The reactive components form a LC series circuit that has a particular resonance frequency given by:

$$f_{res} = \frac{1}{2\pi\sqrt{CL_s}} \quad (5.4)$$

The manufacturer provides information for this range of products about the resonance frequency vs. the capacity of the component.

For the selected capacity (1500 nF) the natural resonance frequency has a typical value of 1 MHz [51].

$$L_s = \frac{1}{C} \left(\frac{1}{2\pi f_{res}} \right)^2 = \frac{1}{1.5 \times 10^{-9}} \left(\frac{1}{2\pi \times 10^6} \right)^2 = 1,7 \times 10^{-8} H \quad (5.5)$$

5.5 Transformer design

The transformers are widely used components in all areas of electrical engineering. Its function is to transmit energy from one circuit to another through a magnetic circuit. For this discussion the transformers with special interest are the high frequency component that distinguishes the isolated conversion topologies. This type of transformers is usually operated in the area of large kHz to few MHz and with a non-sinusoidal voltage waveform, which leads to the use of specific materials, especially for the core.

Unlike the low-frequency transformers used in electrical network for which many manufacturers offer full commercial ranges, those for power electronics typically have very specific requirements for each proposed converter, implying the need for skills in the project magnetic components such as transformers and inductors.

The most common material in the transformer core for low frequencies is magnetic steel, most the times laminated to reduce eddy currents due to high electrical conductivity. It is for this fact that is not suitable for use at high frequencies.

For use in power electronics are another type of material being ferrite the most common core for these applications [37, 52].

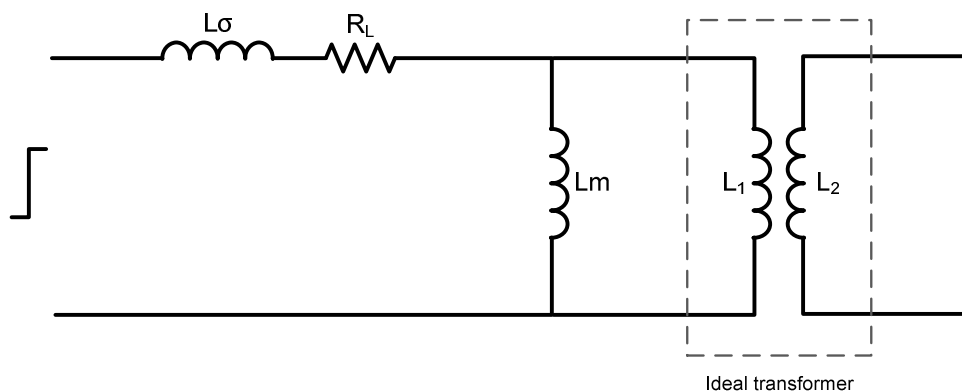


Figure 5.6 Transformer simplified equivalent model (primary referred)

Several approaches to the design of such transformers are presented in the literature [37, 52-53], some with the aim of being fast and other supposed to be more accurate. In fact, like in any other design some simplifications have to be made because of input data that may not be complete and certain parameters can be neglected for a given application.

The considered transformer model is presented in Figure 5.6. To make clearer the design procedure followed, a flow chart is presented in Figure 5.7.

The transformer models are discussed in section 6.4, where the parameterization of such component is performed.

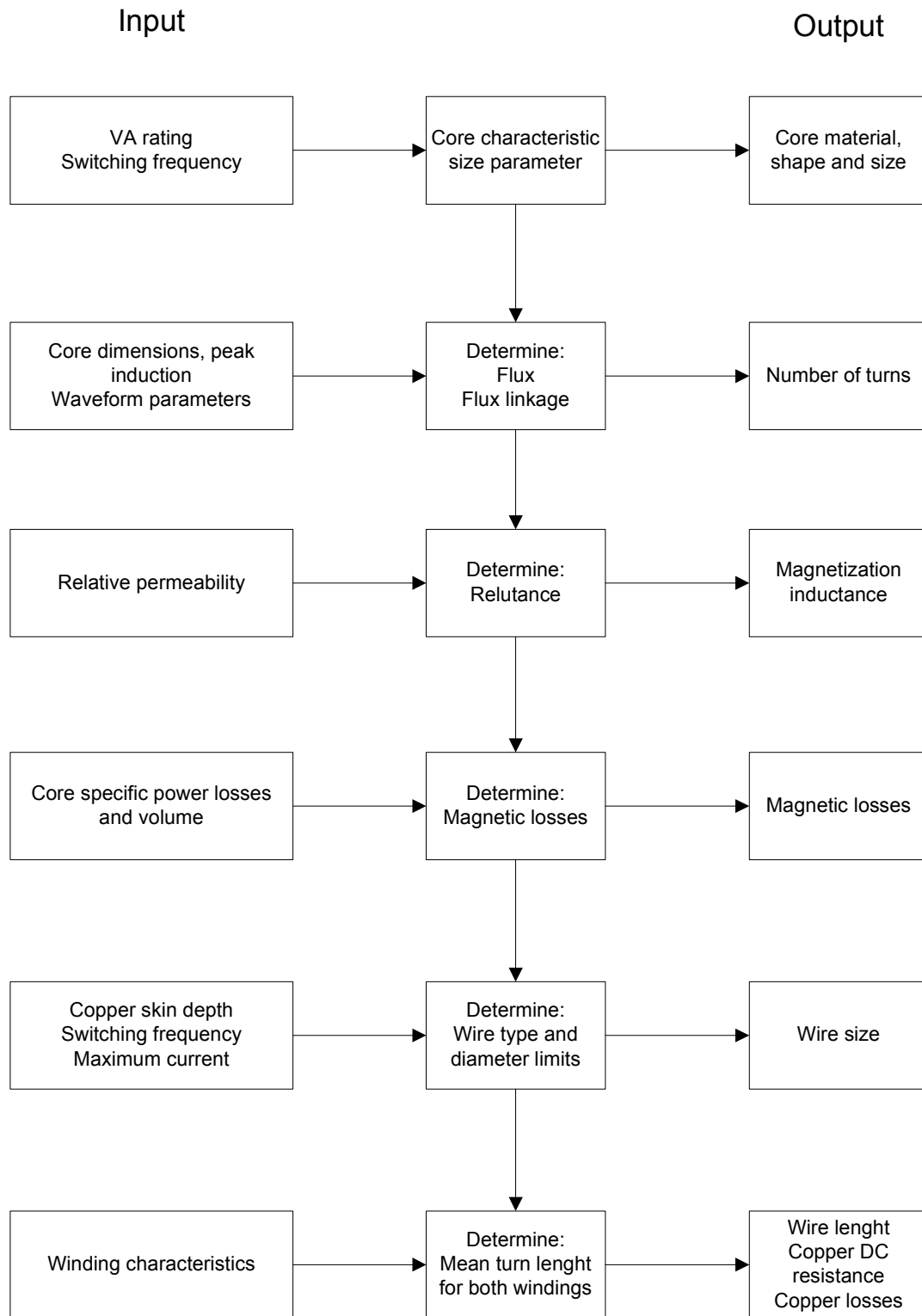


Figure 5.7 Transformer design flowchart

5.5.1 Core selection

As mentioned this type of transformer usually has to be built specifically for a particular application. Yet there is an extensive range of cores, coil formers and all kinds of accessories for this purpose.

The ferrite cores can be found in many different shapes and types of material. The most common formats are toroids, pot cores, and U, I and E cores, all of them in several different sizes. The designations and frequency ranges of the different types of materials suitable for power transformers are presented in Table 5.13.

Table 5.13 Core selection guide for a specific usage [54]

Usage	Frequency range	Material	Shapes
Power transformers, Chokes	1 to 100 kHz	N 27	E, EC, ETD, U, RM, PM
		N 41	Pot cores, RM
		N 61	Small ring, E cores
	up to 200 kHz	N 62	E, U, UR, ETD, ER
		N 67	
	up to 500 kHz	N 72	E, ETD
		N 87	ETD, EFD, RM, ER
		0,3 - 1 Mhz	N 49
0,5 - 1 Mhz	N 59		

So far we can conclude that most of the materials are perfectly suited to the desired frequency (10 kHz). In fact they usually have limitations on maximum frequency or in other cases are optimized for a certain range (e.g. N 49 and N 59).

The selected material is then type N 27 because fits the desired frequency. Their wide availability of shapes and sizes and the ease with which can be found on the market are also factors in favor.

Once selected the material is now necessary to find the appropriate shape and size to handle the power level of this converter. The size is generally select by the core characteristic size a_{ch} that is directly connected with the sum of VA ratings, i.e. the sum of apparent power from all windings.

In this specific case this quantity can be expressed as [52]:

$$S_{tot} = \sum_{all\ windings} V_{rms} I_{rms} = 400 \times 10 + 400 \times 10 = 8000\ VA \quad (5.6)$$

In accord with [52] the relationship between this sum of powers and the characteristic size can be expressed by:

$$a_{ch} = \left(\frac{S_{tot}}{A} \right)^{1/\gamma} \quad (5.7)$$

Where:

γ is an exponent, characterizing the material and shape of the core, $\gamma = 3$

A is a coefficient; for ferrites, A is in the range $A = 5-25$ if a_{ch} is in cm

In remarks concerning to prior expression is noted that for low-frequency design (20-30 kHz) and low-frequency materials or presence of high DC current components, low values of A (5-20) are applicable.

In this case the frequency is low (10 kHz) as well as N 27 material type is also for low frequency, but a continuous component isn't present. Balancing these factors was pointed out a A coefficient with a value of 10.

$$a_{ch} = 9,28 \text{ cm} = 92,8 \text{ mm} \quad (5.8)$$

So is necessary to find a core which characteristic size is at least 92.8 mm. The U-shape 93/76/30 core with a characteristic size of 93 mm is a correct choice for the design.

Due to high availability and adequate power rating a UU 93/152/30 (mm) N27 ferrite core set, composed by two U 93/76/30 cores, will be used. According to datasheet this set is designed for power transformers above one kW, considering a 20 kHz switching frequency.

The magnetic characteristics of this core are presented in Table 5.14.

Table 5.14 N27 UU 93/152/30 core magnetic characteristics [54]

Effective magnetic path length l_e	354 mm
Effective magnetic cross section A_e	840 mm ²
Effective magnetic volume V_e	297 000 mm ³
Core mass m	1500 g
Relative effective permeability μ_e	1800
Peak flux density $B_{p,g}$	370 mT @ 100°C

5.5.2 Number of turns

After selecting a core is important to determine the most appropriate number of turns to be wound. This calculation is usually made for the primary and the number of turns of the secondary then determined by the transformation ratio, which in this case is 1:1. The method

of calculation used is commonly found in the literature, and starts from the integration of a half period of the maximum voltage applied to the primary. These data are presented in Table 5.15 and Figure 5.8.

Table 5.15 Primary voltage parameters

Waveform	Square bipolar
Negative peak	-400 V
Positive peak	+400 V
Duty cycle	50 % (fixed)
Frequency	10 kHz
Period	100 μ s

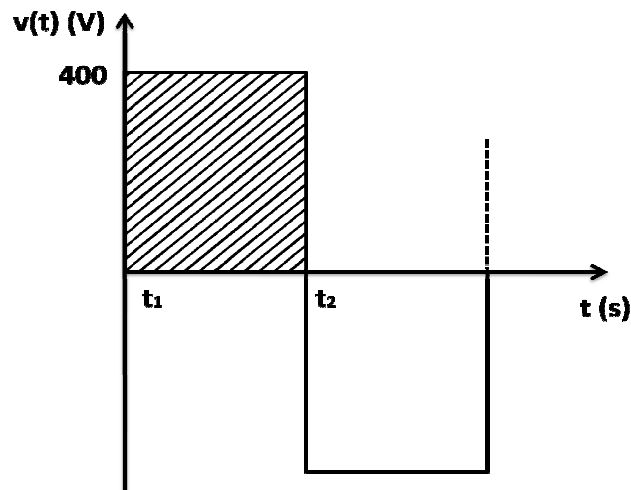


Figure 5.8 Voltage waveform applied to the transformer

Flux linkage:

$$\Psi_{pp} = \int_{t_1}^{t_2} v(t) dt = 20 \times 10^{-3} (V - s) \quad (5.9)$$

Peak-to-peak induction:

$$B_{pp} = 2 \times B_{p,g} = 740 \times 10^{-3} (T) \quad (5.10)$$

Peak-to-peak magnetic flux:

$$\Phi_{pp} = A_e \times B_{pp} = 621,6 \times 10^{-6} \text{ (Wb)} \quad (5.11)$$

Number of turns:

$$N = \frac{\Psi_{pp}}{\Phi_{pp}} \cong 33 \text{ Turns} \quad (5.12)$$

To achieve a turns-ratio of 1:1 the primary and secondary windings must have the same number of turns. After the known number of turns and the core to be used it is possible to estimate the magnetization inductance. The first step is to determine a value for the reluctance of the magnetic circuit.

$$\mu_0 = 4\pi \times 10^{-7} \text{ H/m} \quad (5.13)$$

$$\mathfrak{R} = \frac{l_e}{\mu_0 \mu_r A_e} = \frac{354 \times 10^{-3}}{4\pi \times 10^{-7} \times 3400 \times 840 \times 10^{-6}} = 98,6 \times 10^3 \text{ Turns/H} \quad (5.14)$$

Once determined the value of the magnetic circuit reluctance is possible to obtain a value for the magnetization inductance.

$$L_m = \frac{N^2}{\mathfrak{R}} = \frac{33^2}{186,3 \times 10^3} = 11,04 \times 10^{-3} \text{ H} \quad (5.15)$$

5.5.3 Core losses

The estimation of the total core losses are based on two parameters from the component technical data. These parameters are the specific core power losses that is given for two different temperatures and the effective volume of the core. The total core losses are calculated for the two different temperatures (Table 5.16).

Table 5.16 Core losses estimation [54]

Specific core power losses (P_s)	150 kW/m ³ @ 20 °C ; 100 kW/m ³ @ 100 °C
Effective magnetic volume (V_e)	297 x 10 ⁻⁶ m ³
Total core power losses (P_T)	44,5 W @ 20 °C ; 29,7 W @ 100 °C

5.5.4 Wire

Once completed the design of the magnetic circuit the windings must now be specified. One of the most important factors in this phase is to select the most suitable type of

electrical conductor for the windings. The main types used are solid copper conductor, with round or rectangular cross section, and Litz wire.

The round solid copper conductor is widely used in transformers and coils for frequencies up to some kHz. Its high availability in the market along with the ease to be wound makes it the best choice for most applications. For windings with very large cross section the rectangular conductors are a good option even for frequencies of a few kHz.

The stranded conductors, such as Litz wire, are of particular interest especially for high frequencies above 100 kHz where the skin effect causes a poor use of the copper section.

Table 5.17 Skin depth for Copper at 100°C [37]

Frequency (Hz)	Skin depth δ (mm)
50	10,6
5 k	1,06
10 k	0,750
20 k	0,530
500 k	0,106

In this project the frequency is fixed and was set at 10 kHz. Since it will be used a copper conductor with solid round in section an estimate of the maximum value for its diameter should be made in order to take advantage of the whole cross-section.

$$\delta_{10 \text{ kHz}} = 0,75 \text{ mm} \quad (5.16)$$

$$\phi_{\text{máx}} = 2 \times \delta_{10 \text{ kHz}} = 1,5 \text{ mm} \quad (5.17)$$

$$S_{\text{máx}} = \pi \times \delta_{10 \text{ kHz}}^2 = 1,8 \text{ mm}^2 \quad (5.18)$$

The values found correspond to the maximum diameter / cross section that the driver must have to be totally negligible skin effect. The use of a larger conductor should take into consideration that the resistance will be different for alternating current to DC resistance.

Considering the AWG measurement system, the driver who best fits this application is the AWG14, which makes a diameter of 1.63 mm and a cross section of 2.05 mm².

From the data available for this section we can determine that is enough for the maximum current in the circuit (10 A).

5.5.5 Windings

After choosing the type and diameter of the electrical conductor to be used will be important to determine how and where it will be wound. Since the core has been selected previously is now necessary to define the coil former to be used. The manufacturer of ferrite core (EPCOS) suggests the use of B67345 former together with UU 93/152/30 core, which drawing and available characteristics are presented in Figure 5.9 and Table 5.18 respectively.

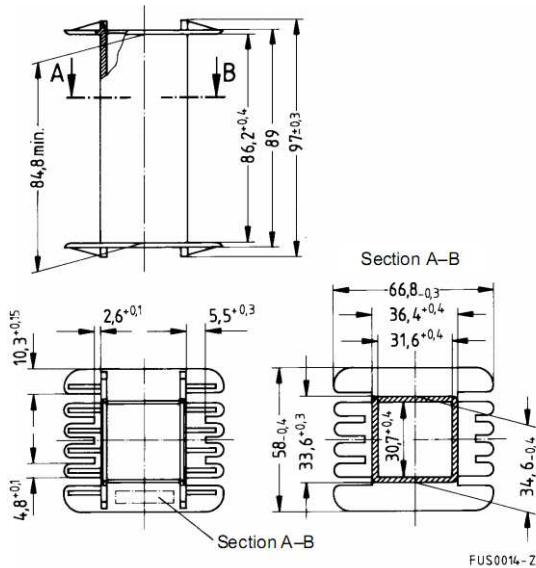


Figure 5.9 Coil former drawing

Table 5.18 Coil former characteristics [54]

Material	GFR 6-polyamide
Number of sections	1
Winding cross section AN (mm ²)	1052
Average turn length lN (mm)	195
Resistance factor; AR = RCu/N2 (μΩ)	6,4

At this stage are already selected the number of turns, the wire used for winding and the coil former. Considering these data it is possible to determine how many layers of winding are necessary, to determine the mean turn length and therefore the required length of wire and finally estimate its resistance.

Winding length (Figure 5.9):

$$W_{length} = 86,2 \text{ mm} \quad (5.19)$$

Wire overall diameter:

$$\Phi_T = 1,63 + 2 \times I_{tck} = 1,83 \text{ mm} \quad (5.20)$$

$$I_{tck} - \text{Insulating layer thickness} \approx 0,1 \text{ mm} \quad (5.21)$$

Maximum number of turns per layer (considering close wound assembly):

$$N_{max} = \frac{W_{length}}{\Phi_T} = \frac{86,2}{1,83} \approx 47 \text{ turns} \quad (5.22)$$

Considering the number of turns previously calculated - 33 turns - is found that only one layer is enough to achieve the desired winding.

At this stage it is already determined all the physical structure of the windings of the transformer. As was done for the magnetic circuit is now necessary to estimate the power losses for the electrical circuit. For this it is necessary to know the maximum rms current and have an accurate estimate of the resistance of the windings.

Known the conductive material to be used (copper) and its cross-section becomes necessary to know also the total length to determine its resistance.

The first step is to determine the mean turn length which is represented in Figure 5.10.

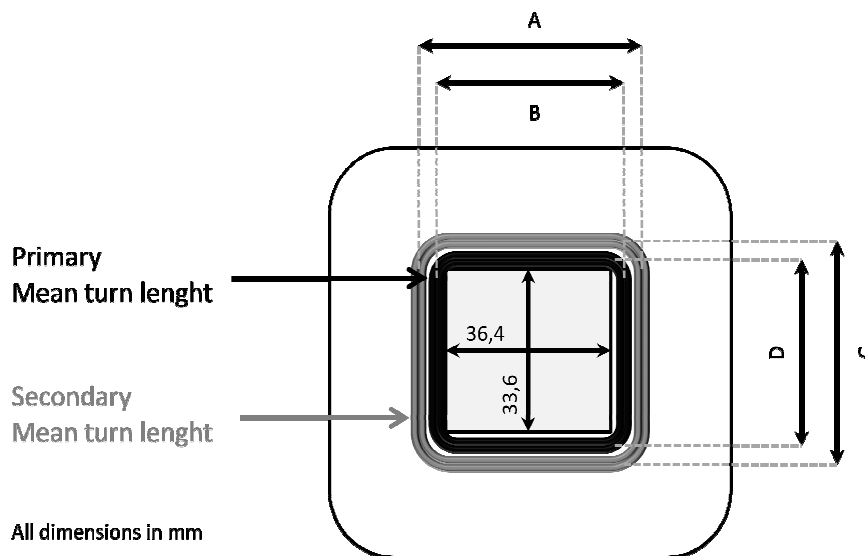


Figure 5.10 Mean turn length identification

Table 5.19 Turn segment dimensions

Segment	Dimension
A	$36,4 + 2 \times \varnothing_T + 2 \times \frac{\varnothing_T}{2} = 36,4 + 3 \times 1,83 = 41,89 \text{ mm}$
B	$36,4 + 2 \times \frac{\varnothing_T}{2} = 36,4 + 1,83 = 38,23 \text{ mm}$
C	$33,6 + 2 \times \varnothing_T + 2 \times \frac{\varnothing_T}{2} = 33,6 + 3 \times 1,83 = 39,09 \text{ mm}$
D	$33,6 + 2 \times \frac{\varnothing_T}{2} = 33,6 + 1,83 = 35,43 \text{ mm}$

5.5.6 Mean turn length

Primary winding

$$l_{avg(p)} = 2 \times B + 2 \times D = 147,32 \text{ mm} = 0,14732 \text{ m} \quad (5.23)$$

Secondary winding

$$l_{avg(s)} = 2 \times A + 2 \times C = 161,96 \text{ mm} = 0,16196 \text{ m} \quad (5.24)$$

5.5.7 Total wire length

Number of turns

$$N = 33 \quad (5.25)$$

Primary winding

$$l_{T(p)} = l_{avg(p)} \times N = 0,14732 \times 33 = 4,86 \text{ m} \quad (5.26)$$

Secondary winding

$$l_{T(s)} = l_{avg(s)} \times N = 0,16196 \times 33 = 5,34 \text{ m} \quad (5.27)$$

5.5.8 Wire resistance

Copper resistivity at 20°C

$$\rho_{20^\circ\text{C}} = 1,68 \times 10^{-8} \Omega \cdot \text{m} \quad (5.28)$$

Wire cross section

$$S = 2,05 \text{ mm}^2 = 2,05 \times 10^{-6} \text{ m}^2 \quad (5.29)$$

Total resistance for primary winding

$$R_{wind.(p)} = \rho \times \frac{l_{T(p)}}{S} = 1,68 \times 10^{-8} \times \frac{4,86}{2,05 \times 10^{-6}} = 39,8 \text{ m}\Omega \quad (5.30)$$

Total resistance for secondary winding

$$R_{wind.(s)} = \rho \times \frac{l_{T(s)}}{S} = 1,68 \times 10^{-8} \times \frac{5,34}{2,05 \times 10^{-6}} = 43,8 \text{ m}\Omega \quad (5.31)$$

Once estimated the resistance of the windings and knowing the maximum rms current that will circulate in the conductors is possible to estimate the losses by Joule effect.

$$P_{Cu(p)} = I_{RMS}^2 \times R_{wind.(p)} = 10^2 \times 39,8 \times 10^{-3} = 3,98 \text{ W} \quad (5.32)$$

$$P_{Cu(s)} = I_{RMS}^2 \times R_{wind.(s)} = 10^2 \times 43,8 \times 10^{-3} = 4,38 \text{ W} \quad (5.33)$$

$$P_{Cu(T)} = P_{Cu(p)} + P_{Cu(s)} = 3,98 + 4,38 = 8,36 \text{ W} \quad (5.34)$$

In fact, the losses in the windings should be somewhat higher than calculated, due to skin effect mentioned above. Once completed the transformer design their main characteristics will be gathered and presented in Table 5.20.

Table 5.20 Designed transformer full specifications

Parameter	Value	
Core material	N27	
Core shape	UU 93/152/30	
Peak-to-peak induction	$740 \times 10^{-3} \text{ (T)}$	
Magnetization inductance	$5,85 \times 10^{-3} \text{ H}$	
Number of turns	Primary	33
	Secondary	33
Transformation ratio	1:1	
Wire type	Round solid copper	
Wire gauge	AWG14	
Core losses	44,5 W @ 20 °C	
	29,7 W @ 100 °C	
Copper losses	8,36 W @ 20 °C	
Total losses	52,86 W @ 20 °C	
Frequency	10 kHz	

5.6 Summary

The details of the prototype development were presented in this chapter. Switches were selected and parameter setting of the hybrid driver was described in detail as it was the first contact with such components.

For the passive components is also given special attention, particularly in the transformer design. The transformer design was made taking into consideration the most important aspects, resulting in the Table 5.20.

Chapter 6

Control system and results

In the previous chapter were designed the main components comprising the power stage of the conversion system. Now it's time to design the command and acquisition system to correctly interact with the converter. The first step was to correctly identify the functional modules and how they are interconnected with the power stage previously designed.

The modules defined as essential were voltage and current transducers, the acquisition system, and the mechanism to generate phase-shifted square waves. Initially will be chosen the current and voltage transducers to be used for the measurements. It is now a precondition that is electrically isolated, as this is a bench top prototype and safety of the experiments must be guaranteed. The other selection parameters are described at the time of choice. Then will be studied the acquisition system already available in the laboratory. In the end, it should be possible combining the characteristics of the transducers and this acquisition system to characterize all of the measurement system in terms of ranges, resolution and error analysis. A mechanism for generating phase shifted square waves with high resolution will be described in detail and its resolution in degrees will be assessed.

The parameterization of the transformer will be performed based on a simplified model and finally the first experimental results of the dual active bridge converter were presented.

In Figure 6.1 are diagramed the basic architecture of the system for better understanding. The modules to develop and whose design is reported in this chapter are in the shaded region.

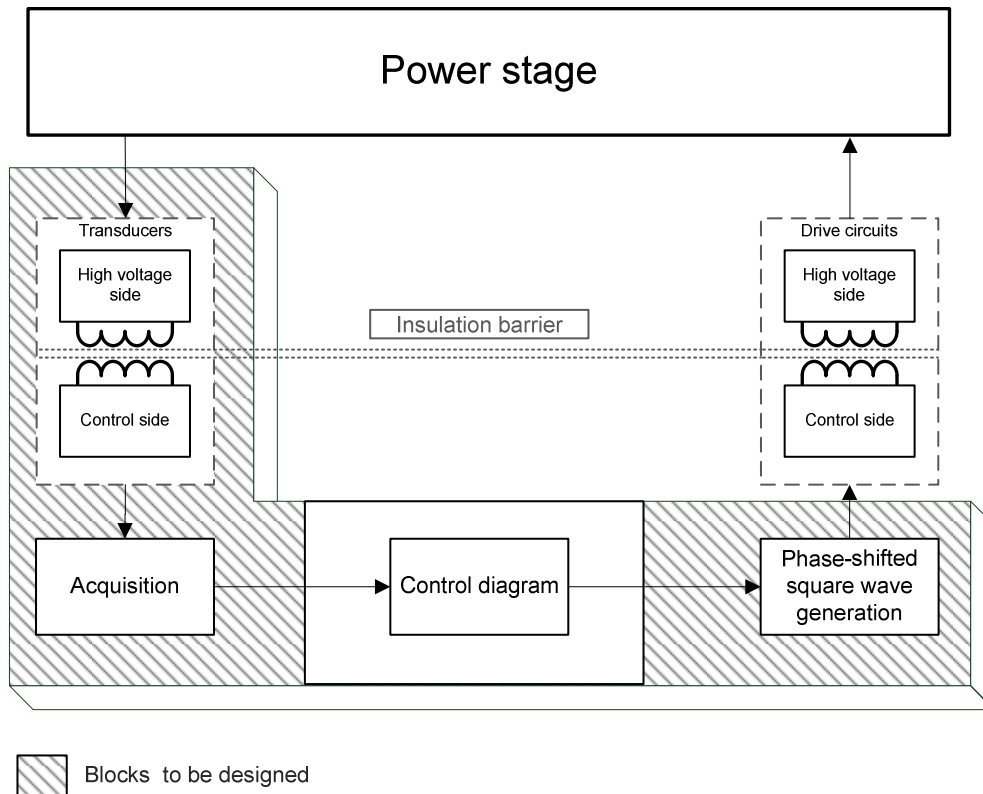


Figure 6.1 Power converter modules

6.1 Measurements

The measures are of central importance in the design of a digitally controlled conversion system. Most of the time signals with high bandwidth have to be measured under good conditions, without affecting the operation of the converter and for many applications the insulation is also a key requirement. With the growth of power electronics manufacturers designed particular components with these characteristics and nowadays they are adapted to perform this function.

Before choosing a specific component is important to understand what distinguishes them, i.e. their performance measures. It is also necessary at this time to establish the characteristics desired for these transducers.

Bandwidth - should be as high as possible. Even when it comes to measure DC signals, the rapid variations in the measured signal should have an effect on the output of a transducer without significant delay. The transducers to be used should also provide the correct measurement of DC signals.

Insulation voltage - even with electrically isolated transducers, the dielectric strength has limits. In the selected transducers this value should be above the maximum voltage that can be found in the power stage (400 V neglecting transient overvoltages).

Measurement range - this range should include the whole range of variables to measure, at least. A reasonable extra range can be added for greater flexibility and also providing a possible operation of the converter in overload conditions for short periods.

Table 6.1 Measured variables and nominal ranges

#	Variable	Range
1	Input current	-10 to + 10 A
2	Output current	-10 to + 10 A
3	Transformer primary current	-10 to + 10 A
4	Input voltage	0 to + 400 V
5	Output voltage	0 to + 400 V

Sensibility - Represents the relationship between the physical quantity measured and sensor output. It is one of the basic characteristics of any transducer. Must be large to measure small variations in the measured quantity with ease.

Linearity - It means that the transducer output varies linearly with the measured quantity. If the sensor has a good linearity is reasonable to relate the input and output through a gain. This is a very desirable feature because it avoids adding complexity to a possible signal conditioning circuit.

Offset - represents the presence of a constant component in the output of the transducer, regardless of what exists at the entrance. In most cases it is too low since the component was designed so that this value was zero. If not negligible, should at least be a well-known value. Some components with internal signal conditioning insert a specific value to adapt the output range to typical input ranges found in common analog to digital converters.

Power consumption - Here it is necessary to refer to two types of transducers and they were the active and the passive. Passive transducers extract energy only from the measured quantity and in such cases it is necessary to assess whether the extracted energy is negligible compared to the magnitude of the variable. In Active transducers the energy extracted from the measured quantity, tends to be smaller, since there is a second power source. The components with internal processing or conditioning are of this type preferentially. For this case it is also important to assess if the total energy consumed by the transducer is low compared with the magnitude of the power stage variables.

Taking into account all these parameters were then defined the current and voltage transducers to be used.

Table 6.2 LEM® LV 25-P voltage transducer data [55]

Parameter	Value
Bandwidth	DC to 10 kHz
Insulation voltage	4,1 kV
Measurement range	Configurable from $\pm 10V$ to $\pm 1500V$
Output range	up to $\pm 12V$
Sensibility	Depending on range from 5,72 mV/V to 858 mV/V
Linearity error	< 0,2 %
Offset	< 0,15 mA
Power consumption	1,05 W

The range of input voltages and output of this component needs to be set by two resistors placed on the outside, one in series with the primary and another in series with the secondary.

The calculation of the resistance of the primary will be done already, since the maximum voltage to be measured it is already known. From [55] is found that the maximum rms current for the primary side is 10 mA.

So, this resistor will be determined in order to pass this current or less when the variable being measured is at its maximum rms value.

$$R_1 \geq \frac{V_{rms(max)}}{I_{PN}} = \frac{400}{0,01} = 40 \text{ k}\Omega \quad (6.1)$$

Considering the most common range of resistor values (E12) the resistor selected will be the first option above the minimum value determined, being that value 47 k Ω .

The resistor to put in series with secondary will be determined in the next step, as it is necessary to know the input range of analog to digital converter.

Table 6.3 LEM® HY 15-P current transducer data [56]

Parameter	Value
Bandwidth	DC to 50 kHz
Insulation voltage	2,5 kV
Measurement range	$\pm 15 A_{rms}$; $\pm 45 A_{pk}$
Output range	$\pm 4V$
Sensibility	$S = \frac{4}{15} mV/A \cong 266 mV/A$
Linearity error	$< \pm 1 \% \text{ of } I_{PN}$
Offset	$< \pm 40 mV$
Power consumption	0,3 W

Unlike the voltage transducer, current transducer has all its parameters fixed. Therefore there is no need for any calculation. If the output range is not suitable for the input range of the acquisition system will be designed later a conditioning circuit.

Both components are to mount on printed circuit boards. Because this is a prototype was considered appropriate to make a board for each transducer. Thus it is possible to easily reconfigure the system of measures to completely match any control scheme.

The developed boards have the same form factor, so they can be mounted on the same holders.

Each one also has three extractable connectors. In the high voltage side connector the conductors are fixed with screws to ease future modification, for the transducers supply there is a three way connector with voltages of (-15, 0, +15 V) and for the output signal was placed a BNC type connector. These features ensure a truly modular measurement system. The resistors needed for the operation of the voltage transducer are also mounted on the voltage measurement boards.

6.2 Acquisition

In closed loop digitally controlled systems the quantification of the signals is the first essential procedure. In fact for the control mechanism have a proper operation and a good performance implies that the acquisition system is well implemented.

In the laboratory where it was developed this prototype there is a platform for rapid prototyping which is already equipped with a analog signal acquisition system. The main characteristics of this system are in Table 6.4.

After known these characteristics and selected the transducers, it is now appropriate to determine whether it is possible a direct connection of signals. Given that all the necessary data is available at this stage is important to assess if the resolution is enough to perform the desired functions and how much the acquisition error represents in absolute terms of the variables measured.

The platform has four parallel channels of analog to digital converters that can be sampled simultaneously, and four groups of multiplexed acquisition each with four input channels and one analog to digital converter. The system allows acquiring up to 8 channels simultaneously, thus not being necessary to use the analog multiplexers since the measured variables are five.

Table 6.4 Analog to digital converters specifications

Parameter	Specification	
	Muxed ADCs (Figure 6.2)	Parallel ADCs (Figure 6.3)
Number of Channels	16	4
Resolution	16 bit	16 bit
Input voltage range	± 10 V	± 10 V
Overvoltage protection	± 15 V	± 15 V
Conversion time	1 μ s	800 ns
Offset error	± 5 mV	± 5 mV
Gain error	$\pm 0,25$ %	$\pm 0,25$ %
Offset drift	40 μ v/K	40 μ v/K
Gain drift	50 ppm/K	50 ppm/K
Signal-to-noise ratio	> 83 dB	> 83 dB

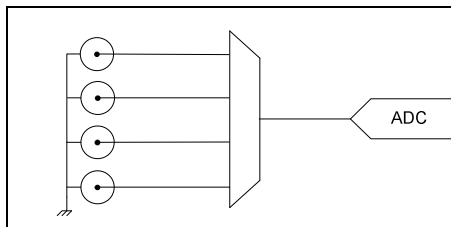


Figure 6.2 Multiplexed analog inputs

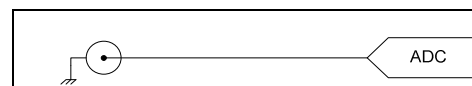


Figure 6.3 Parallel analog inputs

Table 6.5 Current acquisition parameterization

	Parameter	Value
ADC	Resolution	16 bit
	Input voltage range	$\pm 10 V$
	Quantum	$Q = \frac{V_{max} - V_{min}}{2^n - 1} = \frac{20}{65535} = 305,18 \mu V$
Current transducer	Sensibility	$S = \frac{4}{15} mV/A \cong 266 mV/A$
	Current "Quantum"	$Q_I = \frac{Q}{S} = \frac{\frac{20}{65535}}{\frac{4}{15}} = 1,14 mA$
	Output range	$\pm 4 V (\leq \pm 10 V)$

Table 6.6 Voltage acquisition parameterization

	Parameter	Value
ADC	Resolution	16 bit
	Input voltage range	$\pm 10 V$
	Quantum	$Q = \frac{V_{max} - V_{min}}{2^n - 1} = \frac{20}{65535} = 305,18 \mu V$
Voltage transducer	Maximum voltage to measure	$V_{rms(max)} = 400 V$
	Primary series resistor	$R_1 = 47 k\Omega$
	Primary current	$I_{PN(max)} = \frac{400}{47 \times 10^3} = 8,51 mA$
	Secondary current	$I_{SN(max)} = \frac{2500}{1000} \times I_{PN(max)} = 21,3 mA$
	Maximum measuring resistance	$10 \geq R_M \times I_{SN(max)}$ $R_M \leq \frac{10}{I_{SN(max)}}; R_M \leq 469,5 \Omega *$
	Sensibility	$S = \frac{1}{47 \times 10^3} \times \frac{2500}{1000} \times 330; S = 17,55 mV/V$
	Voltage "Quantum"	$Q_V = \frac{Q}{S} = \frac{\frac{20}{65535}}{17,55 \times 10^{-3}} = 17,4 mV$
	Output range	$+ 7,03 V (\leq + 10 V)$

* The selected value is 330 Ω due to sensor restrictions referred on respective datasheet

As expected the resolution of analog to digital converters (16 bit) is quite enough to acquire these signals. This can be proved by quantum obtained in absolute value of the measured variable, both for the current or voltage transducer (Q_I and Q_V).

Finished this procedure can be concluded that the performance of this measurement system is enough to perform the desired functions.

6.2.1 Error analysis

This section will analyze the measurement error of the set composed by the transducer and the sample & hold ADC. The main objective of this analysis is to evaluate if the error value is acceptable for this application and thus decide if this acquisition system is suitable. For this purpose it was collected all available information about the errors of both transducers and the ADC's and estimated a total value. It was found important to also refer this value in absolute units of variables to measure in order to make values more intuitive to be related to the values really measured.

Table 6.7 Voltage measurement error

Parameter		Value
Voltage transducer	Linearity error	0,2 %
	Offset	$\pm 0,15 \text{ mA}$
	Offset in Volt	$\pm R_M \times 0,15 \text{ mA} = \pm 49,5 \text{ mV}$
Multiplexed ADCs	Offset error	$\pm 5 \text{ mV}$
	Gain error	$\pm 0,25 \%$
Total	Offset error	$(\pm 49,5) + (\pm 5) = \pm 54,5 \text{ mV}$
	Linearity + gain error	$(0,2 + (\pm 0,25)) = 0,45 \%$
	All errors	$\pm (54,5 \text{ mV} + 0,45\%)$
	Error referred to measured variable	$\pm (3,1 + 0,45\%) \text{ V}$

Table 6.8 Current measurement error

Parameter		Value
Current transducer	Linearity error	$< \pm 1 \% \text{ of } I_{PN}$
	Offset	$< \pm 40 \text{ mV}$
Parallel ADCs	Offset error	$\pm 5 \text{ mV}$
	Gain error	$\pm 0,25 \%$
Total	Offset error	$< \pm 45 \text{ mV}$
	Linearity + gain error	$< \pm 1,25 \%$
	All errors	$\pm (40 \text{ mV} + 1,25 \%)$
	Error referred to measured variable	$\pm (0,15 + 1,25\%) \text{ A}$

The error obtained in absolute value of the measures has a reasonable value and it is understood that should not compromise a reliable reading of variables.

Nevertheless some conclusions can be made. The voltage transducer has a significant offset error, although its influence is weakened as the absolute value of the variable increases and approaches the nominal value (400 V), which represent less than 1% error at that point. The proportional component of the error has a rather low value (for 400 V is less than 2 V). The main error in the gain of this transducer is not in the component itself, but in the resistors mounted externally. In fact if common resistors with 5% tolerance were used is essential that at least one of them has fine adjustment to calibrate the transducer before use.

In relation to the current transducer offset error can be neglected since the sensor is used in its entire measurement range. Otherwise if it is used to measure very low currents there is a component of uncertainty that can make the measure meaningless. The error in proportion is higher than for the voltage sensor. Considering that the component has a nominal current rating of 15A, the error when measuring the nominal value should represent equal parts, i.e.

the offset error and gain linearity error should have identical values. In this case there are no external components that can insert error.

6.3 Phase-Shifted square wave generation

The control method to be used in this system is phase shifting the two bridges. Thus it is necessary to create a precise mechanism for passing an absolute value of phase-shift in the range of -90° to $+90^\circ$ generated in the digital control system to control logic signals that will act on the drivers of the power stage. When the simulation was introduced was presented a basic method of generating two square waves with control over the phase-shift. As stated at that time the method was not feasible for practical implementation.

The method created at this stage combines internal components (in Slave DSP) and minimal external components. The main component is the internal PWM generator of four independent channels. Outside the logic is implemented by two XOR gates. The method benefits from a low complexity and also from the high time resolution of internal PWM generator. The operation of the phase-shift generator will then be explained separately for direct and reverse power transfer modes (Figure 6.4).

In direct power flow mode the phase shift angle can range from 0 to 90° . The “Power flow mode” bit is set at FALSE. The PWM A channel generates a left-aligned square wave with 50% of duty cycle. The signal for Bridge 1 produced by first XOR gate is exactly the same as PWM A. The switch is set at top position and the phase shift angle is directly converted to a duty cycle, with 360° corresponding to 100%. The computed duty cycle is connected to channel B and in channel C is inserted the duty cycle from B plus 50%. The XOR logic operation results in a square wave for Bridge 2, with a phase-shift referred to channel A. That phase shift is equal to “Phase-Shift Angle” input.

For reverse flow the operation is similar. The “Power flow mode” bit is set at TRUE. The waveform generated by PWM channel A is now inverted due to the constant TRUE value on the other XOR input. The switch changes from bottom position and in this position the “Phase-Shift Angle” input is subtracted to an offset of 180° . This way with an input of 0° the output is 180° degrees offset is null, since the channel is constantly shifted by 180 degrees. When the “Phase-Shift Angle” input value increases, the angle used to calculate the duty cycles B and C decreases, so that there is a negative phase-shift between Bridge 1 and Bridge 2 outputs.

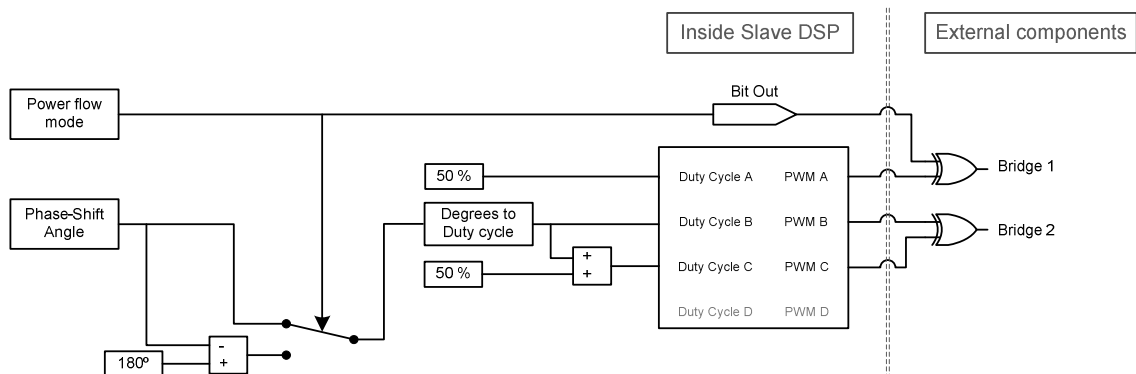


Figure 6.4 Phase-shift generator

Once designed and validated, the system showed a correct operation. Since the characteristics of the PWM generation module are known including their temporal resolution will then be given the resolution of this system in degrees.

Table 6.9 Phase-shift generator resolution

Parameter	Value
Switching period	100 μs
PWM module time resolution	50 ns
Phase-shift generator resolution in degrees	for periods lower than 3,2 ms $\frac{50 \times 10^{-9}}{100 \times 10^{-6}} \times 360 = 0,18^\circ$

As was mentioned at the beginning, it was expected a high resolution of this system. This way we can have increments as small as 0.18 degrees. For example, considering a phase shift range of 0 to 90 degrees and a current range of 0 to 10 A, the minimum increment for regulation will be just 0.02 A.

6.4 Transformer parameterization

As already mentioned, the transformer is of critical importance in this converter. During the project the main characteristics were specified in order to have a component functional and appropriate to this application. Yet some parameters are difficult to calculate accurately because it depends on many factors.

At this stage the other components of the converter are ready to operate. The phase-shift mechanism and the measurement system are also built and validated, and allow to measure the main variables with isolation.

A transformer set was then mounted respecting as closely as possible the specifications resulting from the project. With this transformer were performed several tests with the aim of extracting critical parameters for the operation of the converter, especially the leakage inductance which has a direct influence on the operation of the converter.

With these tests will be possible to determine a fairly realistic model of the transformer to better characterize it and use the parameters for simulation upgrades.

6.4.1 Transformer model

Prior to start the tests in order to find the transformer parameters and create a model is important to understand the considered model and what each parameter represents in fact. At this stage, only three parasitic will be considered: the magnetization inductance, the leakage inductance and the copper resistance.

The immediate model that represents such non-idealities is presented in Figure 6.5.

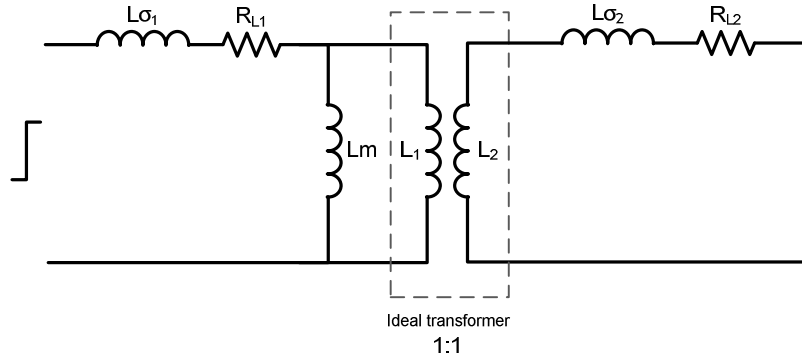


Figure 6.5 Practical transformer equivalent circuit (adapted from [57])

The achieved model has parameters in primary side and secondary side. Using the transformation ratio is possible to place all of them on primary or secondary side. In this work was defined that a primary referred model will be used.

Table 6.10 Transformer secondary to primary modification

Parameter	Value
Secondary leakage inductance (primary referred) $L_{\sigma_{2,1}}$	$L_{\sigma_{2,1}} = L_{\sigma_2} \times \left(\frac{1}{1}\right)^2$
Secondary resistance (primary referred) $R_{L_{2,1}}$	$R_{L_{2,1}} = R_{L_2} \times \left(\frac{1}{1}\right)^2$

The conversion expressions of Table 6.10 result in a primary referred “T” model. This model is presented in Figure 6.6.

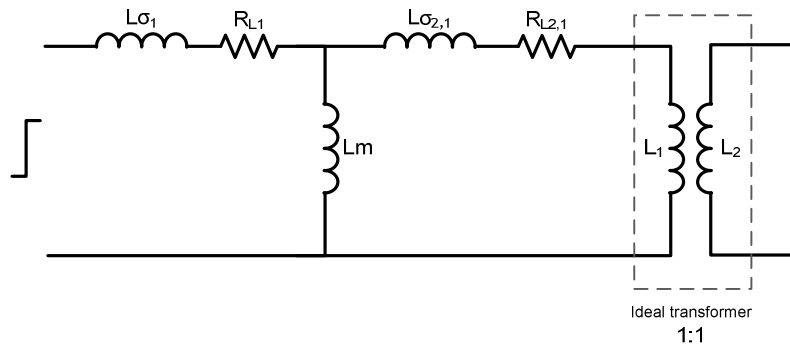


Figure 6.6 Practical transformer equivalent circuit (primary referred) (adapted from [57])

Using a simplified model with combined parameters for the leakage impedance is possible to achieve the model used for transformer parameterization (Figure 6.7). The expressions for the combined parameters are presented in Table 6.11.

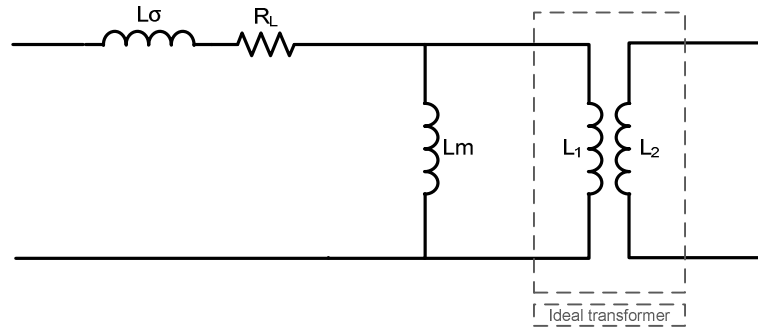


Figure 6.7 Simplified transformer equivalent circuit (primary referred) (adapted from [57])

Table 6.11 Simplified transformer equivalent circuit parameters

Parameter	Value
Total equivalent leakage inductance (primary referred) $L\sigma$	$L\sigma = L\sigma_1 + L\sigma_{2,1}$
Total equivalent resistance (primary referred) R_L	$R_L = R_{L1} + R_{L2,1}$

Considering this model is very simple to determine a s-domain transfer function for the transformer. From Figure 6.7 can be concluded that the voltage applied to primary winding is equal to the sum of voltage drops across $L\sigma$, R_L and Lm . The component of input voltage transferred to secondary winding is the voltage drop across Lm .

$$H(s) = \frac{1}{1} \times \frac{X_{Lm}(s)}{X_{Lm}(s) + X_{L\sigma}(s) + R_L(s)} \quad (6.2)$$

$$H(s) = \frac{sLm}{s(Lm + L\sigma) + R_L} \quad (6.3)$$

6.4.2 DC winding resistance measurement

The first test performed was to determine the resistance value of the copper windings, with the aim to estimate the losses by Joule effect and extract this parameter to the model. Due to its extremely low value would not be possible to measure with a common multimeter or ohmmeter. The solution found is to put a DC source in series with a resistance of 5 ohms and raise the test voltage so that the circuit current reaches 10 A. This value of current was measured with an ammeter and was simultaneously measured the voltage drop of the transformer winding. The resistance value is thus obtained simply by Ohm's law. The test was performed for both windings.

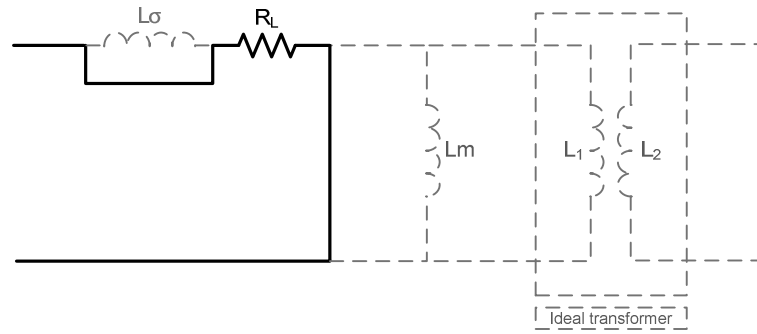


Figure 6.8 Equivalent circuit for DC resistance measurement

Table 6.12 Results from DC winding resistance measurement

	Parameter	Value
	Test current	10 A
Primary	Voltage drop	295 mV
	Calculated DC resistance	29,5 mΩ
	R_{L1}	
Secondary	Voltage drop	386 mV
	Calculated DC resistance	38,6 mΩ
	R_{L2}	
	Primary referred	38,6 mΩ
	$R_{L2,1}$	
Total equivalent resistance (Table 6.11)		68,1 mΩ
	R_L	

Such values do not correspond closely with the value of the ohmic resistance of the wire only, since the transformer was mounted on an experimental board and should be inserted the values of the solder and connectors used.

The estimated power losses based of these values should be seen as representative of the whole experimental set and not just of the transformer.

6.4.3 Short circuit test

The second test performed was with the secondary short circuited. Considering the approximate model of the transformer when the secondary is short circuited the equivalent circuit of the primary is a RL series circuit (Figure 6.9). The step response of this circuit must determine its time constant and thus determine the value of leakage inductance, knowing a priori the value of the resistance.

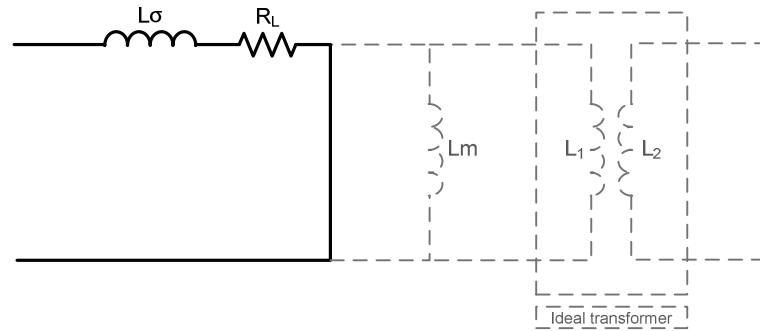


Figure 6.9 Equivalent circuit for shorted secondary

In fact this test cannot be done by directly connecting the power supply to the transformer primary. This limitation is due to the fact that in the current in steady state is limited only by the winding resistance, whose value is just some $m\Omega$. Moreover using this very low resistance value could insert large errors in the inductance value determined; because it is difficult to measure the resistance accurately. The test was then performed with an external testing resistor (R_T).

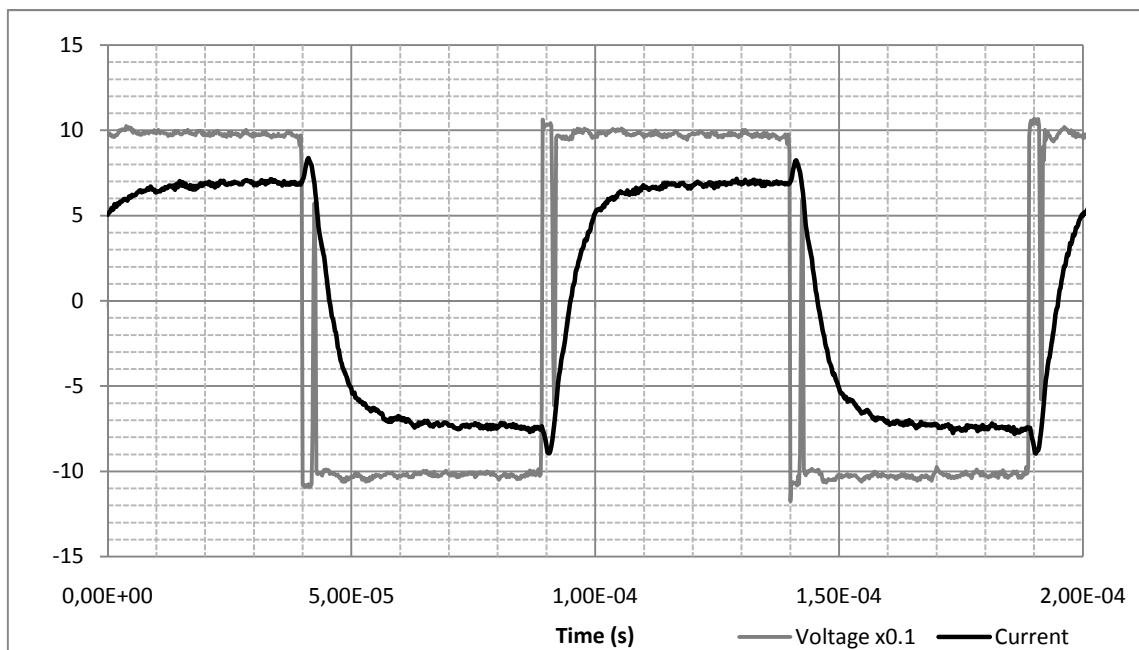


Figure 6.10 Primary winding voltage and current with sorted secondary

Processing data from Figure 6.10 to get one of the rising edges so that the exponential shape can start from $t=0$ and $I=0$, it's possible to perform a curve fitting. This result is presented in Figure 6.11. The expression of current vs. time for a series RL circuit is given in (6.4).

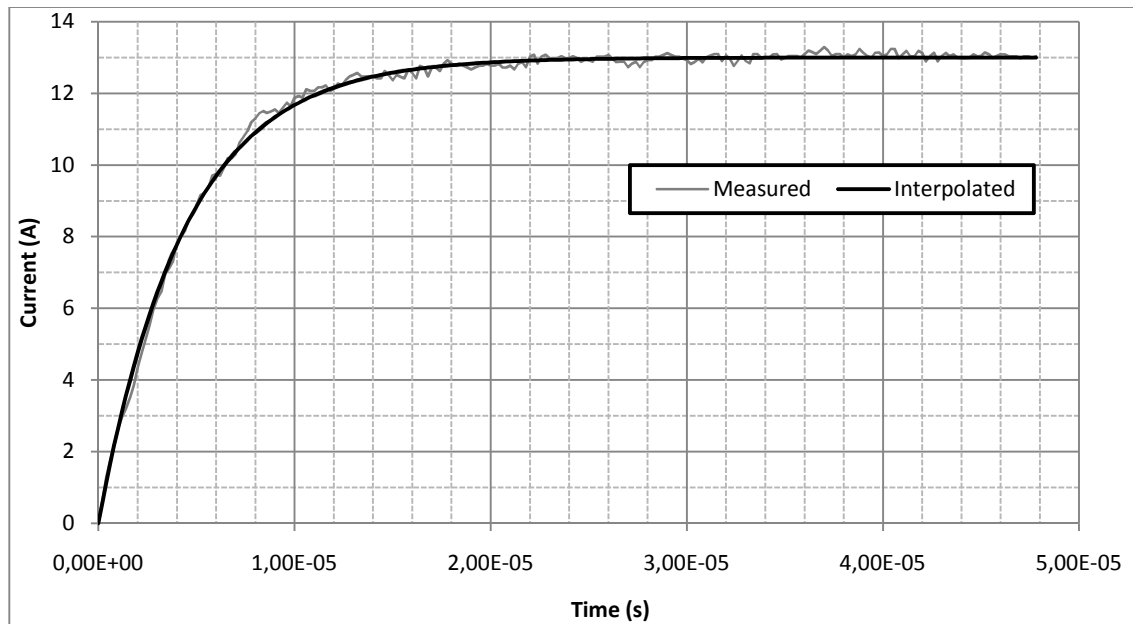


Figure 6.11 Step response with shorted secondary.

$$i(t) = i[\infty] \times \left(1 - e^{-\left(\frac{R}{L}\right)t}\right) \quad (6.4)$$

This interpolation was performed by a solver with the aim of minimizing the absolute difference in relation to the set of points obtained from measurement, adjusting for this the L parameter of (6.1). This can only be done if $i[\infty]$ and R are known parameters. The current for steady state is determined by the average current value after considered steady (20 to 48 μ s). It is important to report that the voltage step applied to the winding have a small drop with the increase of the current. Thus, consider magnitude of the square wave equal to the DC bus voltage inserts an error on the measurement.

For the resistance value estimation was used a method consisting in apply a DC current to all the circuit and measure the voltage drop across the used components (winding resistance, external resistor, wires, etc.). This method is described and used in the next section. The results obtained by this numerical method for the leakage inductance are presented in Table 6.13.

Table 6.13 Parameters from the step response experiment

Parameter	Value
Measured resistance $R = R_t + R_L$	12,26 Ω
Current final value $i[\infty]$	13,0 A
Equivalent Leakage inductance	53,7 μ H

At this time the transformer leakage impedance, referred to the primary, is already determined.

6.4.4 Open circuit test

After determined the series impedance of the transformer, i.e. the leakage inductance and the winding resistance, is now important to determine the magnetization inductance. This test can be performed applying a square wave of considerable magnitude to primary winding, and measure the current on the same winding.

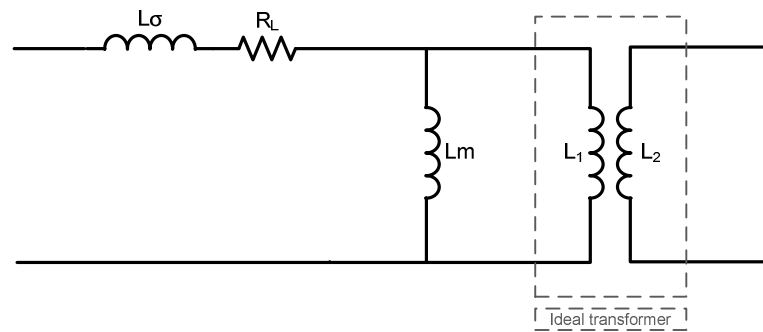


Figure 6.12 Equivalent circuit for open secondary

In this case is expected that current have a small value and with a triangular shape, which means that for the selected frequency the transformer is away from saturation. This experiment should allow the estimation of the magnetization inductance.

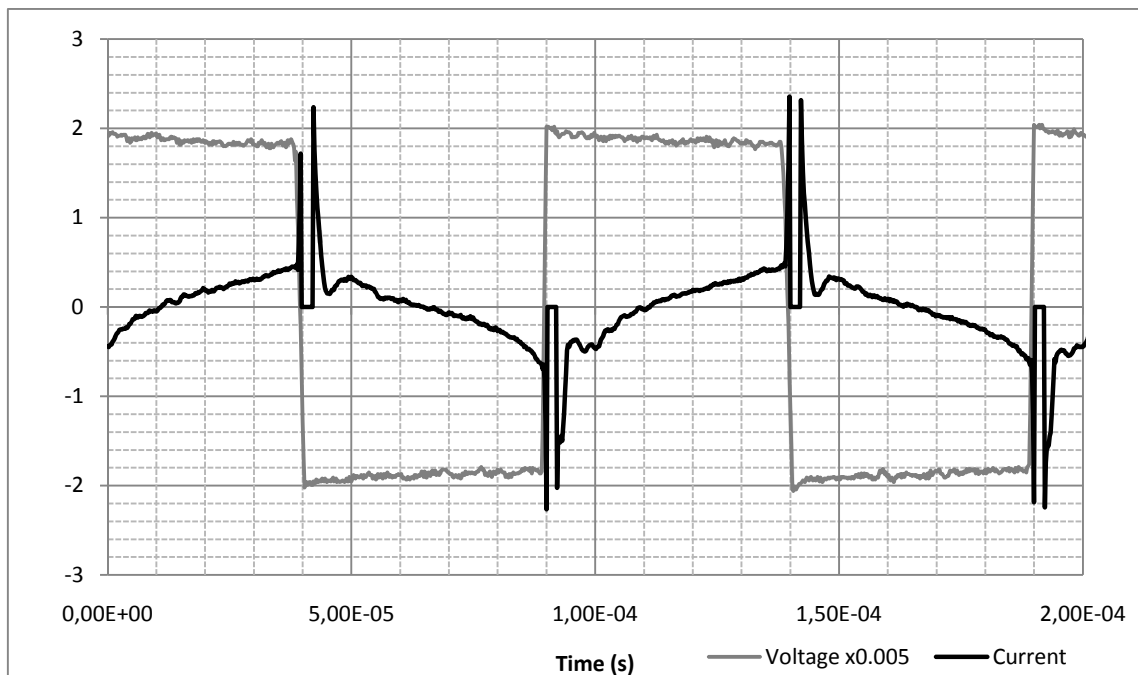


Figure 6.13 Input voltage and current with open circuit secondary

In fact, not only the magnetization current appears on primary waveform. Considerable oscillations after switching are visible and difficult the direct reading of the peak current values. For this purpose some segments were added to Figure 6.14 to identify the magnetization current and allow the estimation of the peak values.

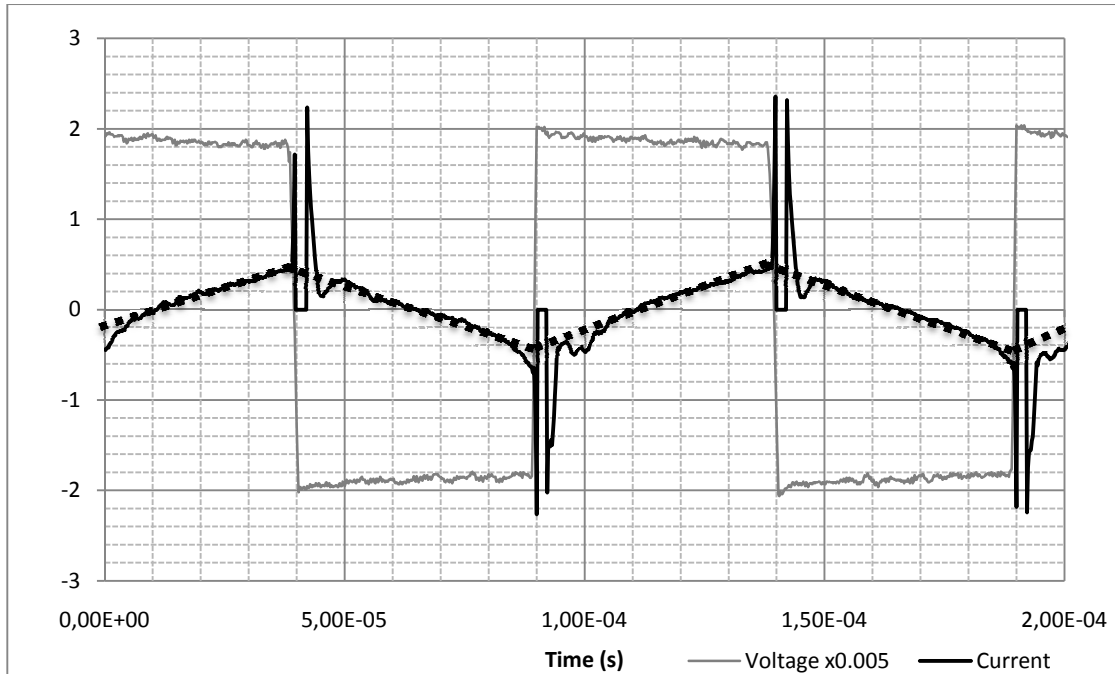


Figure 6.14 Magnetization current identification (dashed)

After identified the magnetization current is important to find a method to estimate the peak values of the triangular waveform. An average method consisting in overlap several segments and fit the curve with a linear function was used.

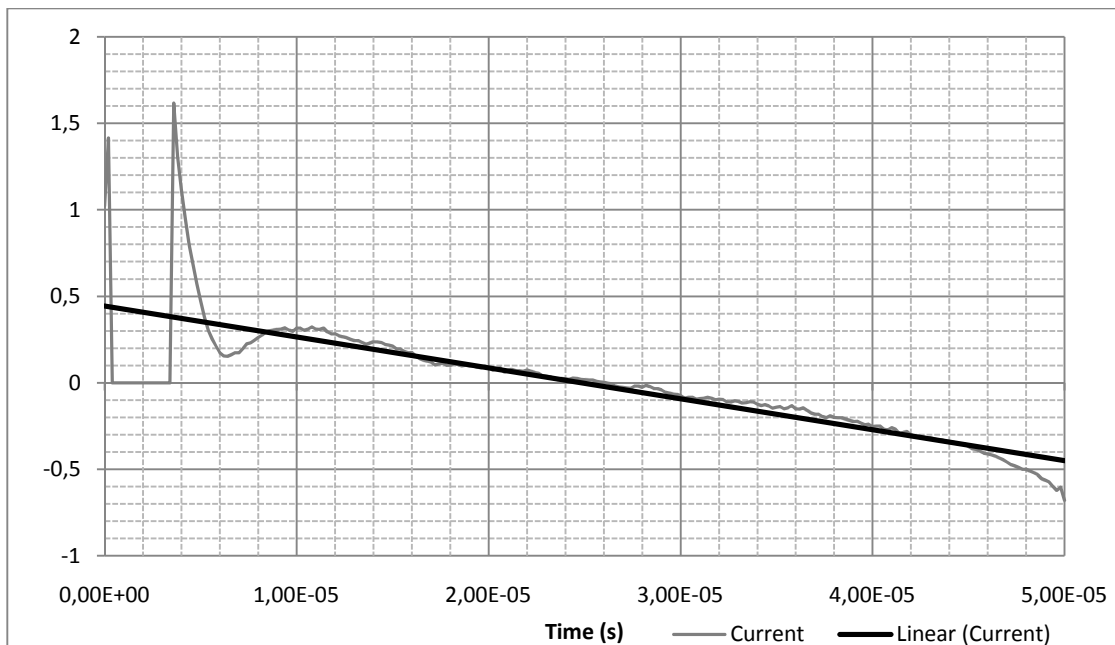


Figure 6.15 Slope estimation of magnetization current

Table 6.14 Peak values of magnetization current

Parameter	Value
Positive peak	+ 0,5 A
Negative peak	- 0,5 A

Once determined the value of the peak-to-peak current is possible to estimate the primary inductance, as it has a direct relationship with the slope of the line.

$$v_L(t) = L \frac{di(t)}{dt} \quad (6.5)$$

$$V_L = L \frac{\Delta i}{\Delta t} \quad (6.6)$$

$$L_1 = \frac{\Delta t \times V_L}{\Delta i} = \frac{50 \times 10^{-6} \times 375}{(500 \times 10^{-3}) - (-500 \times 10^{-3})} = 18,75 \times 10^{-3} H \quad (6.7)$$

This value stands for the total inductance of the primary circuit, i.e. the sum of leakage and magnetization inductances. Since the leakage inductance is previously determined, the difference can be calculated to determine a value for L_m .

$$L_m = L_1 - L_\sigma \quad (6.8)$$

$$L_m = 18,75 \times 10^{-3} - 53,7 \times 10^{-6} = 18,70 \times 10^{-3} H \quad (6.9)$$

As can be seen the leakage inductance has a value negligible compared to the magnetizing inductance. This means that the transformer makes a good magnetic coupling between primary and secondary.

The C_w capacity was not determined in these tests. Completed this process and thus we can consider transformer parameterized in its three main components, the leakage inductance, winding resistance and magnetization inductance.

6.4.5 Model and validation

After determined an approximate model the parameters should be inserted on a simulation model so the tests can be performed and results compared. This way the model can be validated and subsequently used in other simulations.

The parameterized model is presented in Figure 6.16 and was implemented in Simulink® to validate results. Those waveforms obtained are very similar to the measures in reality using the oscilloscope.

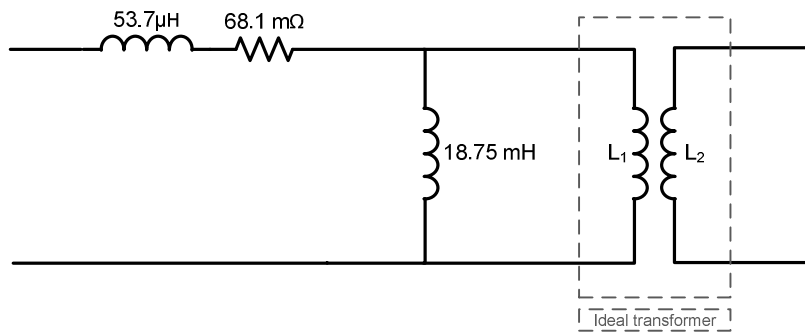


Figure 6.16 Transformer model with parameters

$$H(s) = \frac{s18,75 \times 10^{-3}}{s(18,75 \times 10^{-3} + 53,7 \times 10^{-6}) + 68,1 \times 10^{-3}} \quad (6.10)$$

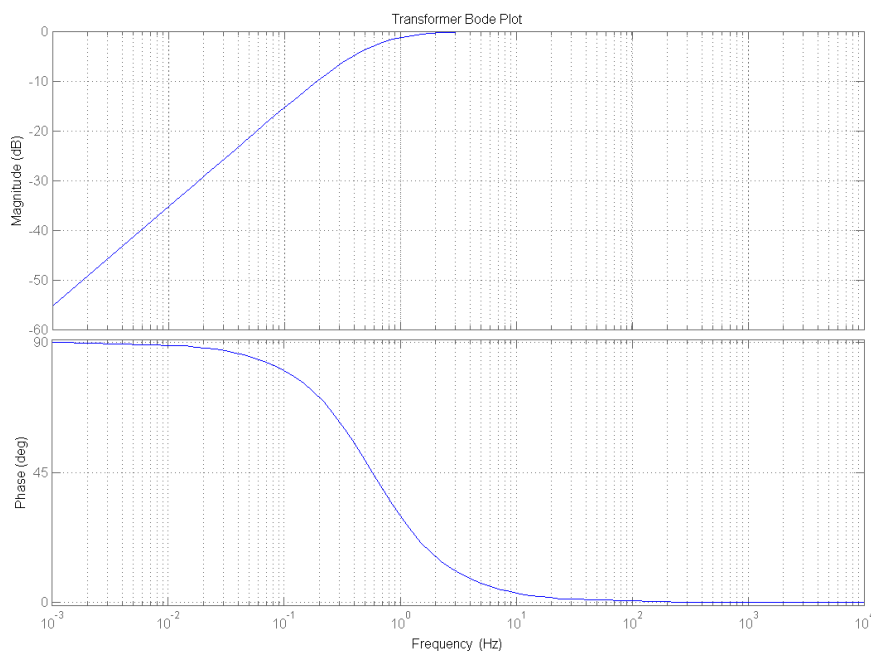


Figure 6.17 Transformer transfer function

The first simulation was to be held with the secondary shorted. The waveform has the same format, same time constant and an approximate saturation value. The current magnitude difference is due to voltage drop present on laboratory DC power supply, which is not present in simulation because an ideal DC voltage source was used. The test was performed in conditions as close as possible from the practical test. Obviously the oscillations are not present because in simulation was not considered any capacity.

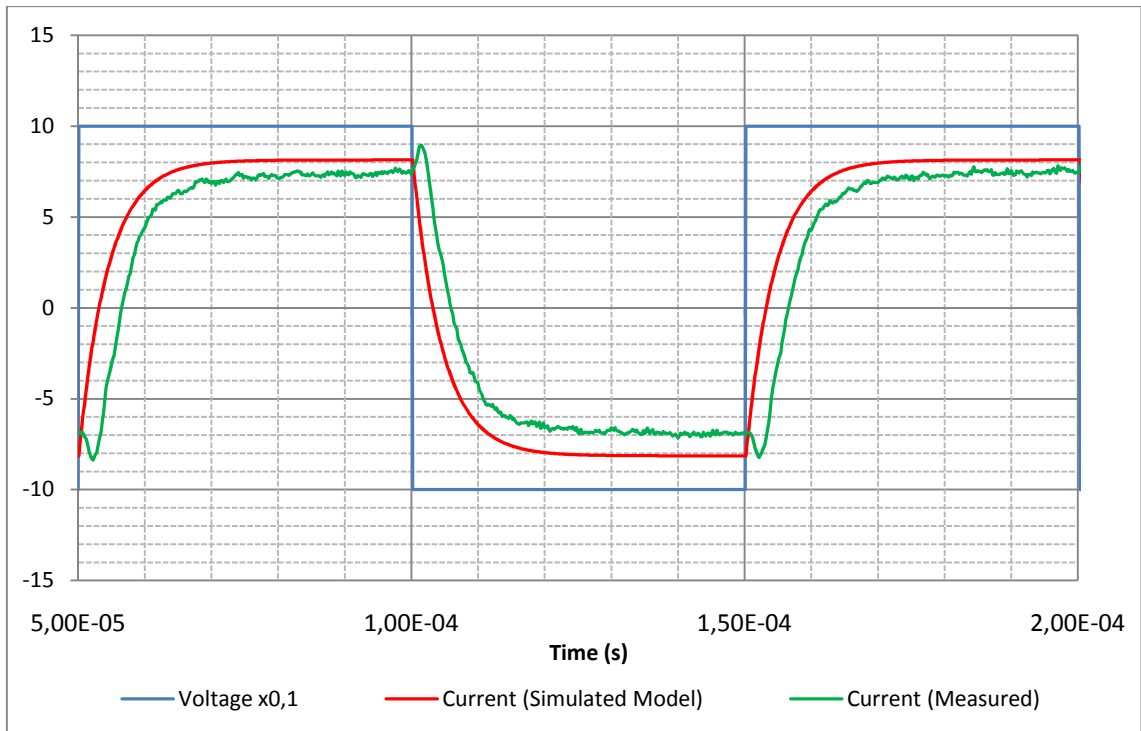


Figure 6.18 Simulated current with shorted secondary

Once verified the waveform for the short circuit test will then observed the waveform for open circuit. The waveform is expected to be a triangular shape without oscillation as before. The values of current peak to peak amplitude should be identical to a practical test. Oscillations are related to winding capacitive effects and are not represented in the considered model. The test was performed with an identical voltage ($\pm 375V$).

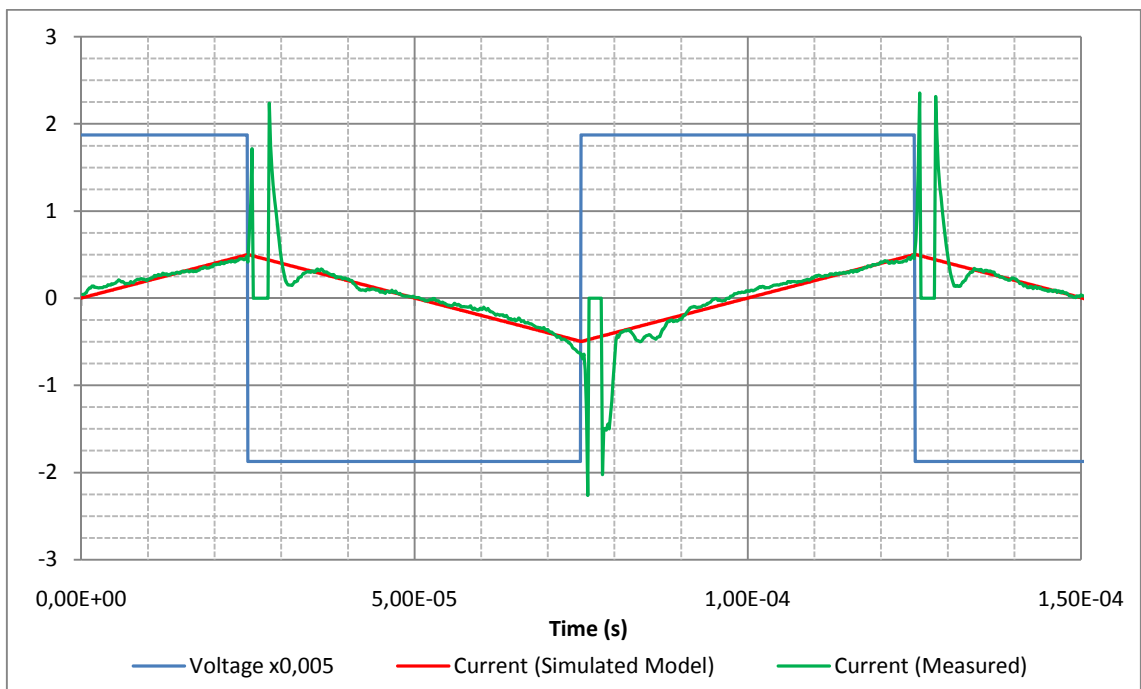


Figure 6.19 Simulated magnetization current

Completing this process is concluded that the model used for the transformer is not very far from reality and that the selected tests allow getting valuable data. From the verification through simulation it is possible to say that this model adds a high value to the development process of the converter.

6.5 Experimental results

The experimental results are considered the ultimate aim of this work. The state of development at this stage allowed the converter to extract some relevant waveforms. The first to be presented are not related to the converter as dual active bridge, and are only for testing the power transformer.

In the second section the command signals and the transformer primary current are presented and analyzed, this turn operating as dual active bridge.

6.5.1 Transformer load tests

At this stage it's time to check how transformer responds to power levels for which it was designed. The power of 4kW cannot be achieved due to limitations of the power supply, which can only provide up to half of that power. The test was performed with a DC power supply connected to one of the full bridges. The AC terminals of the bridge were connected to the transformer primary and secondary to a resistive load (Figure 6.20). The tests were performed for various input voltage levels, because it was considered interesting to see the operation under light and heavy load conditions.

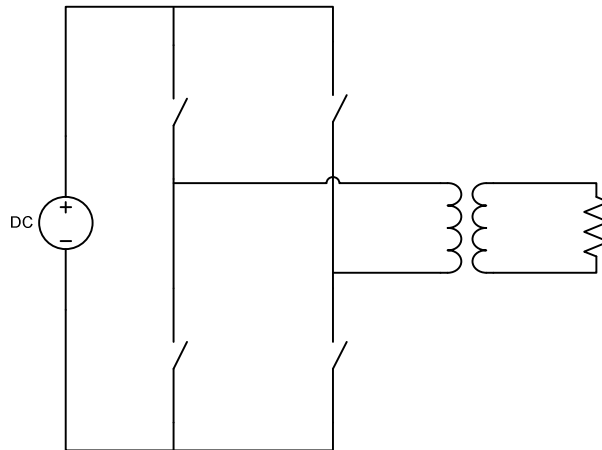


Figure 6.20 Experimental setup for load tests

The first test was performed with a voltage of ± 80 V and a resistance of 48.8Ω which means a current with amplitude of 1.6 A. Resulting waveforms of the voltage and current in the transformer primary are shown in Figure 6.21.

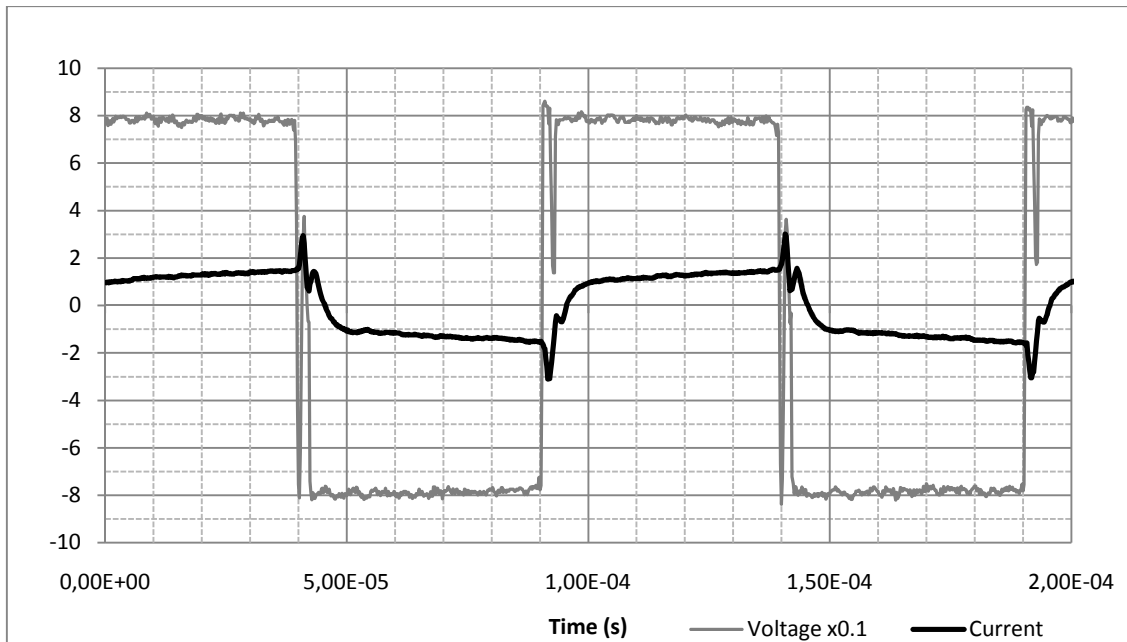


Figure 6.21 Light load test (120 W)

The oscillations observed during the parameterization procedures are still present in these tests. This phenomenon should lead to a further study since its influence on the converter is not properly evaluated. At this point it is important to observe if this phenomenon remains limited for high power levels.

Several tests were then performed with different input voltages and the same load, resulting in a quadratic increase of power. The waveforms obtained in all these tests are obviously not presented since they not contain any additional information.

The waveform shown in Figure 6.22 is for the maximum power level for which the tests were performed.

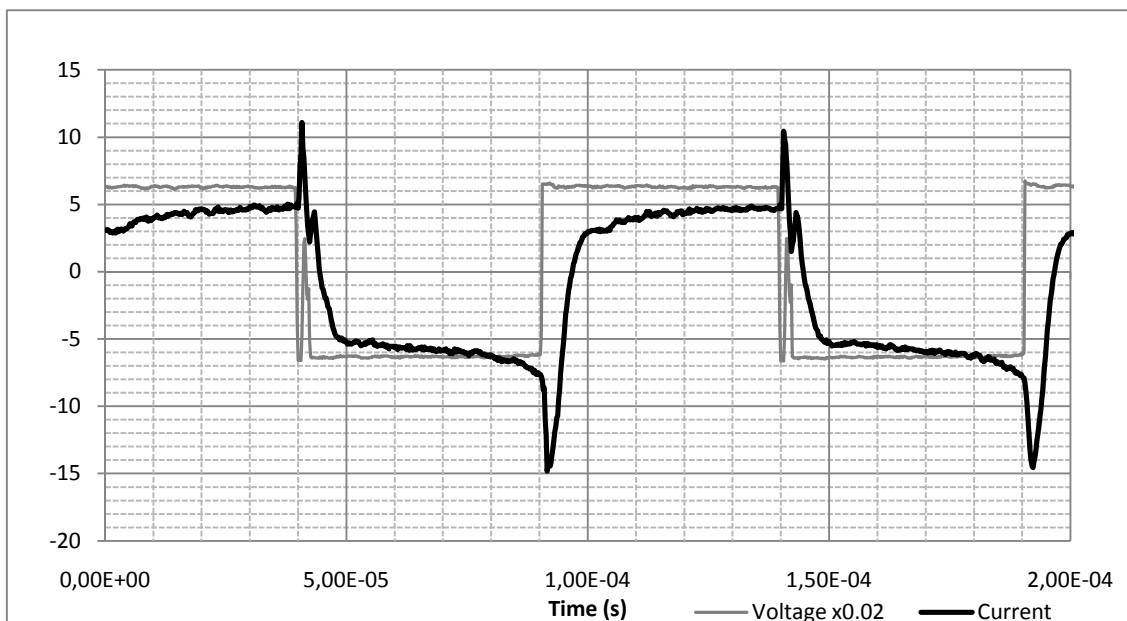


Figure 6.22 Heavy load test (1.5 kW)

This time the oscillations appear with higher amplitude. In fact during the tests it was found that their value has a variation proportional to the amplitude of the current and with a limited value.

From these tests can be concluded that the transformer has a proper operation and can operate on high power range and with high power values. Some critical aspects such as vibration, noise and overheating have been verified as being stable and reasonable for a laboratory assembly.

Some improvements especially in fixing the two core parts may be of interest to reduce the vibration of the transformer.

6.5.2 Converter operation

Once determined the correct operation of all components constituting the converter is the first time to carry out tests for its operation as phase-shifted dual active bridge. These tests were performed with one of the bridges powered by a DC power supply and the other one delivering power to a battery pack (load).

The tests might be performed not only putting the transformer between the bridges (Figure 6.23). In reality, the leakage inductance of only a few μH would result in very large growth rates of the current every time there was a phase-shift between bridges. An inductance was added in series with the transformer primary to increase the value of the equivalent inductance. The inductor used is air-core and was placed far away enough to not have mutual influence with the transformer.

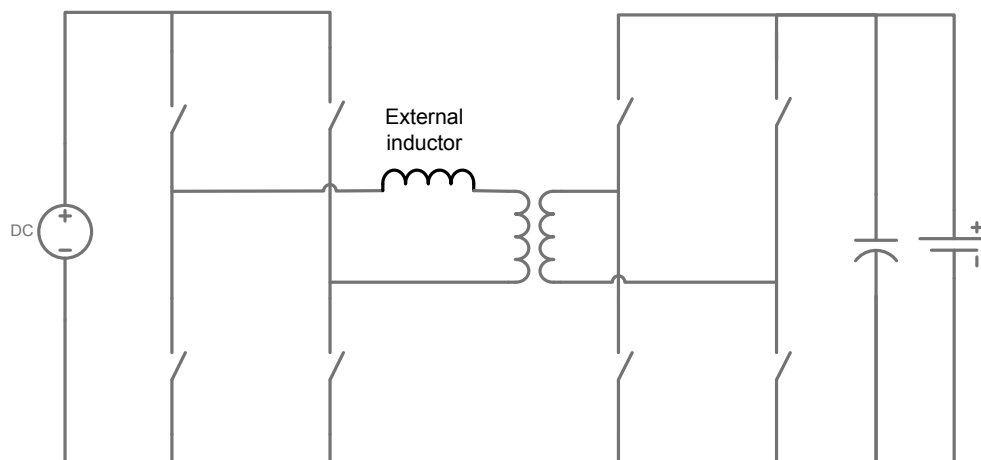


Figure 6.23 Converter schematic with external inductor

The inductor value added was measured and has an inductance of $327,9 \mu\text{H}$. Recalling model value for the leakage inductance can now be determined the total equivalent leakage inductance. This component was used for having an inductance value and a proper current rating, due to limited availability of these components in the laboratory.

$$L_{\sigma total} = L_{\sigma} + L_{\sigma ext.} = 53,7 \times 10^{-6} + 327,9 \times 10^{-6} = 381,6 \times 10^{-6} H \quad (6.11)$$

This value is still below the maximum value determined for the leakage inductance which was 1 mH . On the other hand isn't too low, not allowing the current slope to be very high.

This test was intended to observe the operation in buck and boost modes. This observation is easily made if the input voltage is slightly above the output, since the voltage drops due to current flow rapidly make the converter passing from buck mode to boost mode. The tests were performed for various values of phase-shift.

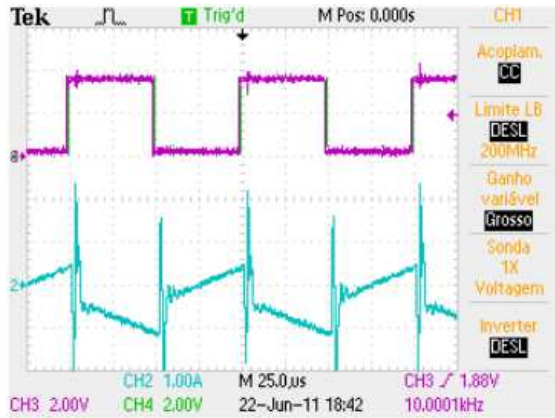


Figure 6.24 Transformer primary current $\phi=5^\circ$

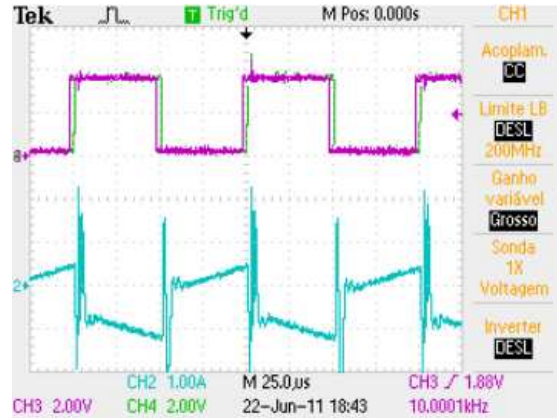


Figure 6.25 Transformer primary current $\phi=10^\circ$

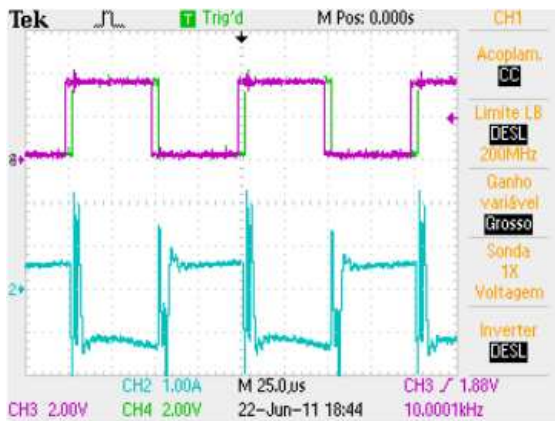


Figure 6.26 Transformer primary current $\phi=15^\circ$

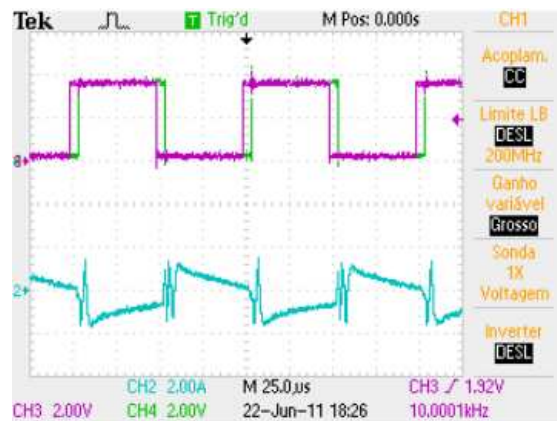


Figure 6.27 Transformer primary current $\phi=20^\circ$

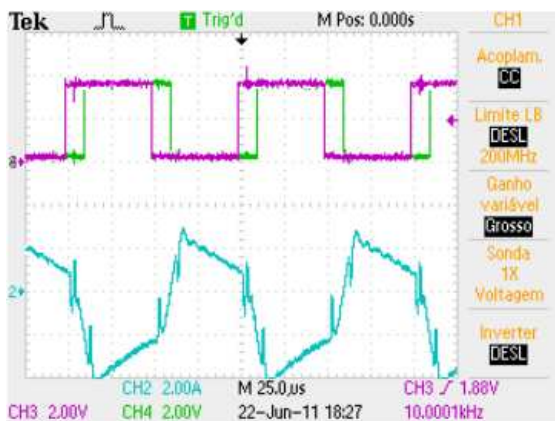


Figure 6.28 Transformer primary current $\phi=40^\circ$

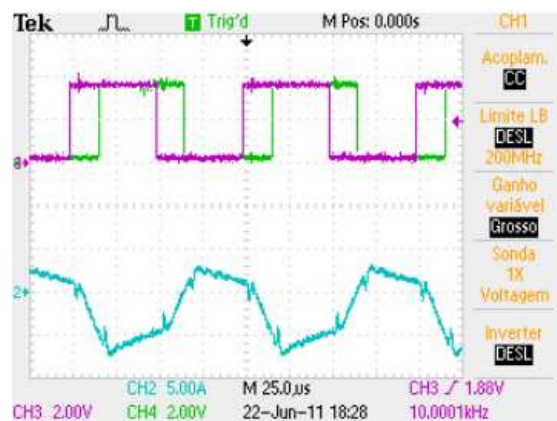


Figure 6.29 Transformer primary current $\phi=60^\circ$

In Figure 6.24 to Figure 6.29 are presented the waveforms collected from the experimental tasks performed. In the first two plots we can see that the converter is in buck mode, i.e. the input voltage is greater than the output voltage. The transformer has no influence in this relationship since it has a transformation ratio of 1:1.

With 15 degrees voltages are very close to each other. This obviously results in a zero slope instants when the bridges are not phase-shifted.

In the following plots (Figure 6.26 to Figure 6.29) the converter is already operating in boost mode, since the high current flow dropped the power supply voltage that is not regulated. Due to the higher values of phase-shift is now easy to observe these periods and see the current varying fast. Another important observation is that amplitude of the oscillations does not increase proportionally to the current. This way can be considered that this phenomenon loses its meaning as the power level increases.

We can then conclude that the converter works correctly in the way of buck and boost operation and high power levels.

6.6 Summary

In this chapter are designed the phase-shift control system and the measurement system. After validated were used to control the converter. Therefore tests were then conducted, first for parameterization and load testing of the transformer and ultimately to operate as dual active bridge converter.

Chapter 7

Conclusions and future work

7.1 Conclusions

From an analysis of the converter has been concluded that provides interesting features for the implementation of this application. The simulations allowed viewing the main waveforms and having the first contact with the operation of the converter. Features such as the current output does not depend on the output voltage (ideally) and its symmetry in terms of phase-shift vs. power transferred in both directions make the same control algorithm can be used to control the converter in the whole power range and both directions. The ripple observed in the batteries is perfectly reasonable and enables the usage of a small filter giving the converter possibility of being a compact device. The comparison of results of the average current output between simulation and analytical expression showed that the simulation model correctly implements the topology.

The design procedure followed for the power stage was found to be a simplified approach, but not compromising the final results. The option for a ready to use IGBT drives was a good solution, considering that the process of develop new devices can be difficult and is out of the scope of this work. The power switches have not been analyzed in depth in this design. During operation of the converter was not observed any negative impact associated with this approach. The main conclusions that can be taken from the power hardware project are about the transformer. In fact during the parameterization is concluded that the project should be even more careful because there is influence of many parameters during operation. The capacity between turns should have been considered during this project in order to be minimized. All other parameters that were designed revealed a correct specification, which was confirmed by experimental results.

The selected physical structure consisting of a double-U core and two concentric single layer windings offer good magnetic coupling, with the leakage inductance having a small value. This way can be added an external inductor in series to perform a desired total equivalent inductance.

The measurement system has been used at this stage to measure the main variables of interest of the prototype and revealed an adequate bandwidth and sensitivity. The estimated offset error of the transducers has been verified in practice. The acquisition system has not yet been used but will be of great interest to implement a closed-loop control system.

The command system for the phase-shift generation was shown to have a very good resolution for the regulation of the converter. Although manually operated allows smooth and precise variations of the power transferred by the converter. The simplified solution which has been developed has proven to be a great choice to implement this type of control using PWM generator module, which are commonly available in DSPs and MCUs.

Regarding the tests utilized for the transformer, those selected was shown to be adequate and able to collect valuable data for the parameterization of the transformer. They require minimal additional equipment/components and allow for a parameterization with sufficient accuracy for this stage of development. This allowed the development of a simplified simulation model in Simulink® which validate the parameters obtained. The model to match the reality should include parasitic capacitance with the aim of modeling the oscillations.

The experimental results obtained during the transformer load tests had the expected results demonstrating proper operation within a wide range of power. Finally the test done with the converter operating as dual active bridge, using the batteries as load and an inductor in series with the transformer primary, demonstrated an operation in accordance with the theory described and the results verified in simulation. The buck and boost operation modes are observed with the expected changes on transformer primary current waveform.

Finally, this converter offers key advantages to the vehicle-to-grid system with a reasonable complexity, implementing at least two of the critical requirements - insulation between grid and vehicle, and power bidirectionality. The potential to have a very high efficiency allows it to be compact, which is extremely important for an on-board charger. This feature can also be used to allow very high switching frequencies (hundreds of kHz) to reduce the ripple in the batteries, which is of great interest. The functionality of current control for battery charging can be implemented by this converter, since the relationship between the control variable and the average current in the batteries it is simple and deeply studied.

7.2 Future work

Although the converter is already functional, is not yet ready to be used for the purpose which is designed for. Some issues like evaluate the efficiency and further study of certain phenomena should be performed.

Related to transformer, the study of its oscillations during the switching should be considered to optimize the design. Regarding the output current to the batteries, it still has a very high oscillation component, which should lead to the study of the factors that influence this parameter and possibly demand for new filter solutions. The relationship between the phase-shift and the ripple should be studied, as was observed in simulation that this influence exists.

Once solved the previous problems related to the operation of the power stage, the converter dynamics must be studied in deep and a closed-loop control should be developed to regulate the output according to a given reference. The interface of this control algorithm with the converter is already implemented by the measurement and acquisition system and the command system.

References

1. Abbott, D., *Keeping the Energy Debate Clean: How Do We Supply the World's Energy Needs?* Proceedings of the IEEE, 2010. **98**(1): p. 42-66.
2. Zhu, Z.Q. and C.C. Chan. *Electrical machine topologies and technologies for electric, hybrid, and fuel cell vehicles.* in *Vehicle Power and Propulsion Conference, 2008. VPPC '08. IEEE.* 2008.
3. Pecas Lopes, J.A., P.M. Rocha Almeida, and F.J. Soares. *Using vehicle-to-grid to maximize the integration of intermittent renewable energy resources in islanded electric grids.* in *Clean Electrical Power, 2009 International Conference on.* 2009.
4. Lopes, J.A.P., F.J. Soares, and P.M.R. Almeida, *Integration of Electric Vehicles in the Electric Power System.* Proceedings of the IEEE, 2011. **99**(1): p. 168-183.
5. Kisacikoglu, M.C., B. Ozpineci, and L.M. Tolbert. *Examination of a PHEV bidirectional charger system for V2G reactive power compensation.* in *Applied Power Electronics Conference and Exposition (APEC), 2010 Twenty-Fifth Annual IEEE.* 2010.
6. Markel, T., M. Kuss, and M. Simpson. *Value of plug-in vehicle grid support operation.* in *Innovative Technologies for an Efficient and Reliable Electricity Supply (CITRES), 2010 IEEE Conference on.* 2010.
7. Cvetkovic, I., et al. *Future home uninterruptible renewable energy system with vehicle-to-grid technology.* in *Energy Conversion Congress and Exposition, 2009. ECCE 2009. IEEE.* 2009.
8. Larminie, J. and J. Lowry, *Electric Vehicle Technology Explained.* 2003: John Wiley & Sons.
9. Valsera-Naranjo, E., et al. *Electrical vehicles: State of art and issues for their connection to the network.* in *Electrical Power Quality and Utilisation, 2009. EPQU 2009. 10th International Conference on.* 2009.
10. Agency, I.E., *Technology Roadmap - Electric and plug-in hybrid electric vehicles.* 2009.

11. Zpryme, *Smart Grid Insights*. 2010.
12. Interoperability, O.o.t.N.C.f.S.G., *NIST Framework and Roadmap for Smart Grid Interoperability Standards, Release 1.0*. January 2010, National Institute of Standards and Technology.
13. SAE. *SAE Automotive Standards*. 2011 [cited 2011 January 27]; Available from: <http://standards.sae.org/automotive/>.
14. UL. *Underwriters Laboratories | Standards for Safety*. 2011 [cited 2011 January 27]; Available from: <http://www.ul.com/global/eng/pages/corporate/standards/>.
15. IEC, *IEC 61851-1 Electric vehicle conductive charging system - Part 1: General Requirements*. 2010.
16. IEC, *IEC 61851-21 Electric vehicle conductive charging system - Part 21: Electric vehicle requirements for conductive connection to an a.c./d.c. supply*. 2010.
17. IEC, *IEC 61851-22 Electric vehicle conductive charging system - Part 22: AC electric vehicle charging station*. 2010.
18. IEC, *IEC 62196-1 Plugs, socket-outlets, vehicle couplers and vehicle inlets - Conductive charging of electric vehicles - Part 1: Charging of electric vehicles up to 250 A a.c. and 400 A d.c.* 2010.
19. Commission, I.E., *IEC 61851-1 Electric vehicle conductive charging system - Part 1: General Requirements*. 2010.
20. MENNEKES, *MENNEKES and electric vehicle*.
21. REMA, *Charger Connectors for Electric Vehicles (EV's)*.
22. Yazaki. *Charging connectors | Charging connectors of the Yazaki Group*. 2011 [cited 2011 15-01-2011]; Available from: <http://charge.yazaki-group.com/english/product/>.
23. CHAdeMO. *CHAdeMO Association Website*. 2011 [cited 2011 February 10]; Available from: <http://www.chademo.com/>.
24. GE. *Electric Vehicle Equipment from GE*. 2011 [cited 2011 February 10]; Available from: <http://www.geindustrial.com/products/static/ecomagination-electric-vehicles/ge-wattstation.html>.
25. GE, *WattStation TM - Fact Sheet*. 2010.
26. AV, *AeroVironment™ EV Solutions™ Fleet Fast Charging Station, 50kW DC Secure, Safe, Fast Charging For Your Hardworking Fleet Model EV50-FS*. 2010.

27. Weise, N.D., K.K. Mohapatra, and N. Mohan. *Universal utility interface for Plug-in Hybrid electric vehicles with vehicle-to-grid functionality*. in *Power and Energy Society General Meeting, 2010 IEEE*. 2010.
28. Bilgin, B., A. Emadi, and M. Krishnamurthy. *Design considerations for a universal input battery charger circuit for PHEV applications*. in *Industrial Electronics (ISIE), 2010 IEEE International Symposium on*. 2010.
29. Rei, R.J., et al. *Grid interactive charging control for plug-in electric vehicles*. in *Intelligent Transportation Systems (ITSC), 2010 13th International IEEE Conference on*. 2010.
30. Grenier, M., M.G. Hosseini Aghdam, and T. Thiringer. *Design of on-board charger for plug-in hybrid electric vehicle*. in *Power Electronics, Machines and Drives (PEMD 2010), 5th IET International Conference on*. 2010.
31. Zhou, X., et al. *Design and control of grid-connected converter in bi-directional battery charger for Plug-in hybrid electric vehicle application*. in *Vehicle Power and Propulsion Conference, 2009. VPPC '09. IEEE*. 2009.
32. Xiaohuz, Z., et al. *Multi-function bi-directional battery charger for plug-in hybrid electric vehicle application*. in *Energy Conversion Congress and Exposition, 2009. ECCE 2009. IEEE*. 2009.
33. Jaganathan, S. and G. Wenzhong. *Battery charging power electronics converter and control for plug-in hybrid electric vehicle*. in *Vehicle Power and Propulsion Conference, 2009. VPPC '09. IEEE*. 2009.
34. Erb, D.C., O.C. Onar, and A. Khaligh. *Bi-directional charging topologies for plug-in hybrid electric vehicles*. in *Applied Power Electronics Conference and Exposition (APEC), 2010 Twenty-Fifth Annual IEEE*. 2010.
35. Haghbin, S., et al. *Integrated chargers for EV's and PHEV's: examples and new solutions*. in *Electrical Machines (ICEM), 2010 XIX International Conference on*. 2010.
36. Lisheng, S., A. Meintz, and M. Ferdowsi. *Single-phase bidirectional AC-DC converters for plug-in hybrid electric vehicle applications*. in *Vehicle Power and Propulsion Conference, 2008. VPPC '08. IEEE*. 2008.
37. Mohan, N., T.M. Undeland, and W.P. Robbins, *Power Electronics - Converters, Applications, and Design (3rd Edition)*. 2003: John Wiley & Sons.
38. Rashid, M.H., *Power Electronics Handbook*. 2001: Academic Press.
39. Kheraluwala, M.N., et al., *Performance characterization of a high-power dual active bridge*. *Industry Applications, IEEE Transactions on*, 1992. **28**(6): p. 1294-1301.
40. Kheraluwala, M.H., et al. *Performance characterization of a high power dual active bridge DC/DC converter*. in *Industry Applications Society Annual Meeting, 1990., Conference Record of the 1990 IEEE*. 1990.

41. Alonso, A.R., et al. *An overall study of a Dual Active Bridge for bidirectional DC/DC conversion*. in *Energy Conversion Congress and Exposition (ECCE), 2010 IEEE*. 2010.
42. Demetriades, G.D., *On small-signal analysis and control of the single and the dual active bridge topologies*. 2005, KTH, Sweden: Stockholm.
43. Blake, C. and C. Bull *IGBT or MOSFET: Choose Wisely*.
44. SEMIKRON, *SK100GB12V SEMITRANS 2*. 2010.
45. Herzer, R., et al. (2010) *Integrated Gate Driver Circuit Solutions*.
46. SEMIKRON, *SKYPER® 52 R Driver Core - Technical Explanations* 2010.
47. SEMIKRON, *SKYPER® 32PRO R Driver Core - Technical Explanations* 2007.
48. SEMIKRON, *Evaluation Board 1 SKYPER® 32PRO R - Technical Explanations* 2008.
49. EPCOS, *Aluminum electrolytic capacitors - General technical information*. 2010.
50. EPCOS, *Aluminum electrolytic capacitors with screw terminals - Series/Type: B43456, B43458*. 2010.
51. EPCOS, *Film Capacitors - General technical information*. 2009.
52. Bossche, A.V.d. and V.C. Valchev, *Inductors and Transformers For Power Electronics*. 2005: CRC Press.
53. Erickson, R.W. and D. Maksimovic, *Fundamentals of Power Electronics (Second Edition)*. 2001: Springer.
54. SIEMENS, *Ferrites and Accessories*. p. 610.
55. LEM, *Voltage Transducer LV 25-P*.
56. LEM, *Current Transducers HY 5 to 25-P*.
57. Mora, J.F., *Máquinas eléctricas (Quinta Edición)*. 2003: McGRAW-HILL.

Annex A - Workplan

Number	Task	Resource	Start	End	Duration	% Complete	15/11	22/11	29/11	6/12
1	Análise dos requisitos do projecto. Selecção da estrutura de potência e modos de funcionamento		15/11/2010	31/12/2010	35					
1.1	Pesquisa e selecção bibliográfica para a tarefa 1		15/11/2010	25/11/2010	9					
1.2	Análise e especificação dos requisitos base do projecto.		15/11/2010	26/11/2010	10					
1.3	Estudo de alternativas e selecção da estrutura de potência		19/11/2010	13/12/2010	17					
1.4	Selecção de modos de funcionamento do conversor		22/11/2010	14/12/2010	17					
1.5	Elaboração do documento respectivo à tarefa 1		17/12/2010	31/12/2010	11					
2	Estudo, projecto e implementação dos circuitos de interface para comando e protecção dos semicondutores de potência. Estudo das diferentes tecnologias disponíveis para implementar o isolamento eléctrico.		14/2/2011	10/3/2011	19					
2.1	Estudo		14/2/2011	22/2/2011	7					
2.2	Projecto		18/2/2011	28/2/2011	7					
2.3	Implementação		1/3/2011	7/3/2011	5					
2.4	Teste e validação		7/3/2011	10/3/2011	4					
3	Estudo, projecto e implementação das diversas cadeias de medida das grandezas eléctricas e módulo de interface.		14/2/2011	18/3/2011	25					
3.1	Estudo		14/2/2011	22/2/2011	7					
3.2	Projecto		21/2/2011	2/3/2011	8					
3.3	Implementação		3/3/2011	11/3/2011	7					
3.4	Teste e validação		11/3/2011	18/3/2011	6					
4	Montagem e teste do conversor de potência.		14/2/2011	10/3/2011	19					
5	Estudo e implementação de um sistema de controlo baseada num sistema com processadores digitais de sinais, para funcionamento em tempo real.		3/3/2011	4/4/2011	23					
5.1	Estudo		3/3/2011	9/3/2011	5					
5.2	Simulação		7/3/2011	16/3/2011	8					
5.3	Programação		13/3/2011	23/3/2011	8					
5.4	Implementação		24/3/2011	28/3/2011	3					
5.5	Teste e validação		27/3/2011	4/4/2011	6					
6	Exercitar e aprofundar os algoritmos escolhidos com base em simulações numéricas.		5/4/2011	21/4/2011	13					
7	Realização de testes comparativos entre os algoritmos desenvolvidos e outras soluções técnicas baseadas em metodologias convencionais.		22/4/2011	6/5/2011	11					
8	Redacção da dissertação.		17/1/2011	1/7/2011	120					
8.1	Pesquisa bibliográfica aprofundada e redacção do estado da arte		17/1/2011	11/2/2011	20					
8.2	Redacção do documento final primeira versão		9/5/2011	7/6/2011	22					
8.3	Redacção do documento final versão para entrega		14/6/2011	1/7/2011	14					

